

2022-12-01

Exploring the Anticancer Mechanism of Thienopyrazole Derivative Tpz-1 in Acute Myeloid Leukemia

Jessica Dyanne Hess
University of Texas at El Paso

Follow this and additional works at: https://scholarworks.utep.edu/open_etd



Part of the [Biology Commons](#), [Cell Biology Commons](#), and the [Molecular Biology Commons](#)

Recommended Citation

Hess, Jessica Dyanne, "Exploring the Anticancer Mechanism of Thienopyrazole Derivative Tpz-1 in Acute Myeloid Leukemia" (2022). *Open Access Theses & Dissertations*. 3687.
https://scholarworks.utep.edu/open_etd/3687

This is brought to you for free and open access by ScholarWorks@UTEP. It has been accepted for inclusion in Open Access Theses & Dissertations by an authorized administrator of ScholarWorks@UTEP. For more information, please contact lweber@utep.edu.

EXPLORING THE ANTICANCER MECHANISM OF THIENOPYRAZOLE DERIVATIVE
TPZ-1 IN ACUTE MYELOID LEUKEMIA

JESSICA DYANNE HESS
Doctoral Program in Biosciences

APPROVED:

Renato J. Aguilera, Ph.D., Chair

Manuel Llano, M.D., Ph.D.

Sourav Roy, Ph.D.

Md Nurunnabi, Ph.D.

Charles T. Spencer, Ph.D.

Stephen L. Crites, Jr., Ph.D.
Dean of the Graduate School

Copyright ©

by

Jessica D. Hess

2022

DEDICATION

This dissertation is dedicated to my mother Dyanna Hess-Miller, my grandmother Guadalupe E. Faz, my other half David A. Camacho, and my beloved writing buddies Samson, Callí, and Tony. Thank you for the endless love and support.

EXPLORING THE ANTICANCER MECHANISM OF THIENOPYRAZOLE DERIVATIVE
TPZ-1 IN ACUTE MYELOID LEUKEMIA

by

JESSICA DYANNE HESS

DISSERTATION

Presented to the Faculty of the Graduate School of

The University of Texas at El Paso

in Partial Fulfillment

of the Requirements

for the Degree of

DOCTOR OF PHILOSOPHY

Department of Biological Sciences

THE UNIVERSITY OF TEXAS AT EL PASO

December 2022

ACKNOWLEDGEMENTS

This dissertation would not have been possible without the support of my mentor, committee members, professors, research colleagues, family, and friends. There are not enough words to express my sincere gratitude for your relentless encouragement and belief in my ability to succeed as a scientist.

First, I would like to thank Dr. Aguilera for taking a chance on me despite my low undergraduate grades, and for giving me the opportunity to pursue my childhood dream of researching cancer. You afforded me the freedom to learn, fail, and flourish without fear of harsh judgement. I will forever be indebted to you for the kindness you have shown me along the way — and I promise to pay it forward. I couldn't have asked for a better mentor for this journey, and I am SO proud to be your student. You've truly instilled in me what it takes to be a compassionate and independent scientist. I hope we stay in touch forever. Soy güerita, pero morenita en la corazón!

To my past and present committee members: Dr. Suman Sirimulla, Dr. Manuel Llano, Dr. Sourav Roy, Dr. Md Nurunnabi, and Dr. Charles Spencer. I appreciate the time and effort you have put into helping me achieve this milestone. Your kind and thoughtful feedback has encouraged me to think more philosophically, recognize the limitations of my research, and overcome my fear of criticism (and public speaking). Your unique perspectives and expertise were instrumental in teaching me how to approach and view my work from many angles, which is a skill I will cherish throughout my career.

To all my Aguilera lab friends: Lisett, Paulina, Edgar, Mia, Luca, Becca, Adolfo, Alexa, Stephanie, Manny, Laura, Gaby, and Karol, thank you for helping me grow and learn. Your patience, kindness, and help made the lab feel more like home than work. I'll

never forget the conversations about science and life that we shared! I wish you all the best in your careers and know that you are all destined to do great things.

To the Cellular Characterization and Biorepository core staff: Dr. Varela, Gladys, and Denisse. I'm so honored to have had the opportunity to work alongside such an amazing team! I looked forward to each time we had the chance to chat about life, experiments, and share delicious food. I am so very grateful for the personal and professional support you have given me over the years. I will miss you incredibly.

To my mom Dyanna, my #1 supporter and fan, it goes without saying that this achievement would not have been possible with your love. WE did this! There's no instruction manual for parenting, but honestly, I think you really nailed it. You've shown me that anything is possible with persistence. Thank you for seeing me through every high and low with grace and compassion. You are the reason I am resilient, relentless, and will never quit when things get hard. I'm so proud to be your daughter and your friend – I love you more than anything, forever.

To my grandma, Lupe, I know I can always count on you to cheer me on. You were, and continue to be, my inspiration for pursuing a career in cancer research. El Paso holds such a special place in my heart because of you; it's my very own "city of hope". Thank you for all your help throughout my time in graduate school. I'll always remember how easy you made the transition to El Paso in those first few months. I'm happy we got to share the time together visiting family, tidying the house, watching our shows, laughing, and getting to know each other as adults. I already miss living so close!

Last but not least, my David, I love you so much. You're the best friend and partner I could ask for. Our relationship is a fairytale, and I am obsessed with the life and family

we have built. I've never felt so loved, secure, and free to be myself. You're also the best dad to our fur babies. I knew you were meant to be mine from the moment I saw you in Dr. Vines' class — I haven't been able to take my eyes off you since. There's no one in the galaxy that could ever compare to you. Thank you so much for all the advice and encouragement you've given me over the years, babe. You've seen me through some of my lowest and stressful points, and because of that I am certain we can make it through absolutely anything together. I can't wait to start this new journey with you in California.

ABSTRACT

Anticancer drug discovery is a time and resource-consuming process for which exceedingly reliable and efficient modern approaches are needed. Phenotypic drug screenings can generate highly potent and innovative drug candidates; however, deconvolution of the drug's target often presents significant barriers to drug development. To overcome this hurdle, we have originally combined *in vitro* and *in silico* analyses to uncover the molecular mechanism(s) driving the anticancer activity of the uniquely structured small molecule drug candidate, Tpz-1. Our study revealed that Tpz-1 is a multitargeted agent which induces the programmed death of HL-60 acute myeloid leukemia cells primarily through disruption of microtubule organization. Additionally, structural analysis and medical text mining revealed a functional relationship between Tpz-1 and the understudied thienopyrazole chemical group. This dissertation therefore offers our colleagues in anticancer drug discovery an innovative methodology and class of molecules to drive future small molecule screening initiatives.

TABLE OF CONTENTS

DEDICATION	iii
ACKNOWLEDGEMENTS	v
ABSTRACT	viii
TABLE OF CONTENTS	ix
LIST OF TABLES.....	xiii
LIST OF FIGURES.....	xiv
ABBREVIATIONS	xvi
CHAPTER 1: INTRODUCTION	1
1.1. General Introduction.....	1
1.1.1. Cancer Incidence and Treatment Disparities in the United States	1
1.1.2. How Cancer Develops	1
1.1.3. Standard Cancer Treatments.....	2
1.1.4. Anticancer Drug Discovery	2
1.1.5. Apoptosis in Cancer Development and Treatment Response	2
1.2. Significance.....	5
1.3. Specific Aims.....	6
CHAPTER 2: IDENTIFICATION OF A UNIQUE CYTOTOXIC THIENO[2,3- C]PYRAZOLE DERIVATIVE WITH POTENT AND SELECTIVE ANTICANCER EFFECTS IN VITRO	8
2.1. Objective	8
2.2. Simple Summary.....	9
2.3. Abstract.....	9
2.4. Introduction	10
2.5. Materials and Methods.....	12
2.5.1. Cell Lines and Culture Conditions.....	12
2.5.2. Preparation of Compounds	14
2.5.3. Initial Library Screening and Compound Selection	14
2.5.4. Differential Nuclear Staining Assay.....	14

2.5.5. Cytotoxic Concentration 50% and Selective Cytotoxicity Index Values	16
2.5.6. AnnexinV-FITC/PI Assay	16
2.5.7. Caspase Activation Assays	17
2.5.8. Reactive Oxygen Species Assay	18
2.5.9. Mitochondrial Depolarization Assay	19
2.5.10. Cell Cycle Analysis	20
2.5.11. Phospho-Kinase Arrays	21
2.5.12. Confocal Microscopy	21
2.5.13. Statistical Analysis	23
2.6. Results	23
2.6.1. Drug Screening Identified a Thienopyrazole Derivative (Tpz-1) with Potent Cytotoxicity against Several Cancer Cell Lines	23
2.6.2. Tpz-1 Displays Highly Selective Cytotoxicity against Leukemia and Lymphoma Cell Lines	24
2.6.3. Tpz-1 Triggers Movement of Phosphatidylserine to the Outer Plasma Membrane	27
2.6.4. Tpz-1 Induces Caspase-Dependent Apoptosis	29
2.6.5. Tpz-1 Causes Cell Stress through an Accumulation of Reactive Oxygen Species	30
2.6.6. Tpz-1 Treatment Disrupts Mitochondrial Function	30
2.6.7. Tpz-1 Cell Death Is Restricted to Cells in the G2/M Phase	31
2.6.8. Tpz-1 Interferes with Src and MAP Kinase Function	33
2.6.9. Tpz-1 Treatment Impedes Microtubule Organization	35
2.7. Discussion	38
2.8. Open Access	42
CHAPTER 3: THE USE OF WEB-BASED BIOINFORMATIC PLATFORMS TO DISTINGUISH POTENTIAL TARGETS OF TPZ-1	43
3.1. Objective	43
3.2. Abstract	43
3.3. Introduction	44
3.4. Materials and Methods	46
3.4.1. Morphology of Tpz-1-treated cancer cells	46
3.4.1.1. Timelapse Microscopy	46

3.4.2. Tpz-1 target identification by transcriptomics.....	47
3.4.2.1. RNA Extraction	47
3.4.2.2. Whole Transcriptome and CuffDiff Analysis	47
3.4.2.3. Database for Annotation, Visualization, and Integrated Discovery (DAVID).....	47
3.4.2.4. KEGG PATHWAY Database	48
3.4.2.5. ConnectivityMap	48
3.4.2.6. Ingenuity Pathway Analysis (IPA).....	50
3.4.3. Tpz-1 target identification by chemical structure.....	51
3.4.3.1. SMILES Chemical Notation	51
3.4.3.2. ChEMBL.....	52
3.4.3.3. SwissDrugDesign.....	52
3.4.3.4. COREMINE Medical Text Mining.....	53
3.5. Results	54
3.5.1. Timelapse microscopy revealed morphological changes associated with Tpz-1 treatment	54
3.5.2. Tpz-1 mechanistic analysis <i>via</i> transcriptomics revealed extensive alterations to gene expression	57
3.5.2.1. Differential Gene Expression and KEGG Pathway Analysis.....	57
3.5.2.2. ConnectivityMap	61
3.5.2.3. Ingenuity Pathway Analysis	64
3.5.3. Tpz-1 structural analysis indicated key functional groups with potential to drive anticancer activity and <i>in vivo</i> toxicities	69
3.5.3.1. SwissTargetPrediction	69
3.5.3.2. SwissSimilarity	70
3.5.3.3 ChEMBL Database	72
3.5.3.4. SwissADME	73
3.5.3.5. COREMINE query of pyrazole compounds, thiophenes, and neoplasms	75
3.6. Discussion.....	80
3.6.1. Tpz-1-treated cells lose cytoskeletal integrity within hours of treatment.....	80
3.6.2. Transcriptome analysis revealed a network of cancer-related pathways downregulated by Tpz-1	81
3.6.2.1. Cell-ECM and Cell-Cell Interaction Mechanisms	81

3.6.2.2. Axon guidance molecules in cancer	84
3.6.2.3. Hippo signaling	85
3.6.2.4. Regulation of actin cytoskeleton	85
3.6.2.5. Small cell lung and bladder cancers	86
3.6.2.6. Transcriptome analysis also identified the upregulation of several cellular pathways by Tpz-1	86
3.6.2.7. Tpz-1 induced gene expression changes that influence the cell cycle	87
3.6.2.8. Tpz-1-treated cells appear to be primed for programmed cell death	87
3.6.2.9. ConnectivityMap analysis supports an effect of Tpz-1 on the cytoskeleton	88
3.6.2.10. Ingenuity Pathway Analysis further connects Tpz-1 cytotoxicity to cytoskeleton-associated signaling pathways	94
3.6.3. Structural analysis revealed hypothetical molecular targets of Tpz-1 ..	97
3.6.3.1. Evaluation of Tpz-1's drug-likeness via SwissDrugDesign tools and ChEMBL	97
3.6.3.2. COREMINE medical text mining exposed the probable contribution of the thienopyrazole moiety to Tpz-1 function	98
3.6.4. Similarities exist between experimental and predicted targets of Tpz-1	101
CHAPTER 4: CONCLUSIONS	104
4.1. Final Discussion	104
4.2. Limitations	106
4.3. Future Directions	106
4.4. Final Conclusions	107
REFERENCES	108
APPENDIX	129
A.1. Supplementary Figures	129
CURRICULUM VITA	152

LIST OF TABLES

Table 2.1. Cytotoxic concentration 50% (CC ₅₀) of Tpz-1 in a panel of 17 cancer and 1 non-cancerous cell line at 24 h (top), 48 h, and 72 h (bottom) of exposure.	24
Table 2.2. Selective cytotoxicity index (SCI) values of Tpz-1 in 17 cancer cell lines at 48 h (top) and 72 h (bottom) of exposure.	26
Table 3.1. Relevant KEGG pathways downregulated by Tpz-1.	58
Table 3.2. KEGG pathways upregulated by Tpz-1.	60
Table 3.3. Perturbagens with similar differential gene expression signatures to Tpz-1.	62
Table 3.4. The top 15 potential targets of Tpz-1 identified by SwissTargetPrediction. ...	69
Table 3.5. ChEMBL target predictions for ChEMBL4441641 (Tpz-1) at 90% confidence.	72
Table 3.6. A comparison of potential targets and cellular pathways affected by Tpz-1.	102

LIST OF FIGURES

Figure 2.1. Chemical structures of pyrazole, thiophene, and thienopyrazoles.....	11
Figure 2.2. Chemical structure of thieno[2,3-c]pyrazole derivative Tpz-1.	12
Figure 2.3. The intrinsic apoptosis pathway mediates Tpz-1-induced cell death.....	28
Figure 2.4. Tpz-1 cytotoxicity is G2-M phase-dependent in HL-60 cells after 72 h of exposure.	33
Figure 2.5. Tpz-1 interferes with Src and MAP pathway signaling in HL-60 cells after 3 h of exposure.	34
Figure 2.6. Tpz-1 (10 μ M) inhibits tubulin polymerization in Hs27 cells after 4 h of exposure.	37
Figure 2.7. Tpz-1 (0.19 μ M) disrupts spindle formation and polarity in HeLa cells undergoing mitosis.	38
Figure 3.1. Morphological changes in HeLa H2B-GFP cells treated with Tpz-1 for 30 hours.	57
Figure 3.2. ConnectivityMap database '1.0' query with the Top 150 upregulated and Top 150 downregulated genes.	62
Figure 3.3. IPA results for top 100 genes downregulated by Tpz-1.	67
Figure 3.4. IPA results for top 100 genes upregulated by Tpz-1.....	68
Figure 3.5. Top 12 bioactive molecules in the ChEMBL database with structural similarity to Tpz-1.	72
Figure 3.6. SwissADME BOILED-Egg (gastrointestinal absorption/blood brain barrier penetrance) and iLOGP (lipophilicity) results for Tpz-1.	74
Figure 3.7. Top 10 biological processes co-mentioned in MEDLINE literature containing the terms 'Pyrazole Compound', 'Thiophenes', and 'Neoplasms'.	77
Figure 3.8. Top 10 genes/proteins co-mentioned in MEDLINE literature containing the terms 'Pyrazole Compound', 'Thiophenes', and 'Neoplasms'.	78
Figure 3.9. Top 10 molecular functions co-mentioned in MEDLINE literature containing the terms 'Pyrazole Compound', 'Thiophenes', and 'Neoplasms'.	79
Figure 3.10. Top 10 drugs co-mentioned in MEDLINE literature containing the terms 'Pyrazole Compound', 'Thiophenes', and 'Neoplasms'.	80
Supplementary Figure S2.1. Tpz-1-induced cell death is mediated by apoptosis in CCRF-CEM cells.	130
Supplementary Figure S2.2. Caspase-3/7 activity is reduced after 8 h exposure to Tpz-1 in CCRF-CEM cells.	132
Supplementary Figure S2.3. Caspase-8 is inactive after 4 h in Tpz-1-treated HL-60 cells.	134
Supplementary Figure S2.4. Tpz-1 causes DNA fragmentation that interferes with evaluation of the CCRF-CEM cell cycle.	136
Supplementary Figure S3.1. KEGG 'Proteoglycans In Cancer' pathway diagram obtained from DAVID analysis of Tpz-1 downregulated genes.....	137
Supplementary Figure S3.2. KEGG 'RAP1 Signaling Pathway' diagram generated by DAVID analysis of genes downregulated by Tpz-1.....	138
Supplementary Figure S3.3. KEGG 'ECM-Receptor Interaction' pathway diagram obtained from DAVID analysis of Tpz-1 downregulated genes.....	139

Supplementary Figure S3.4. KEGG 'Adherens Junction' pathway obtained <i>via</i> DAVID analysis of Tpz-1 downregulated genes.....	140
Supplementary Figure S3.5. KEGG 'Focal Adhesion' pathway generated by DAVID analysis of Tpz-1 downregulated genes.....	141
Supplementary Figure S3.6. KEGG 'Axon Guidance' pathway obtained from DAVID analysis of Tpz-1 downregulated gene list.....	142
Supplementary Figure S3.7. KEGG 'Hippo signaling pathway' obtained from DAVID analysis of genes downregulated by Tpz-1.....	143
Supplementary Figure S3.8. KEGG 'Regulation of Actin Cytoskeleton' pathway obtained by DAVID analysis of Tpz-1 downregulated genes.....	144
Supplementary Figure S3.9. KEGG 'Small Cell Lung Cancer' pathway obtained through DAVID analysis of Tpz-1 downregulated genes.....	145
Supplementary Figure S3.10. KEGG 'Bladder Cancer' pathway obtained from DAVID analysis of genes downregulated after Tpz-1 treatment.....	146
Supplementary Figure S3.11. KEGG 'Cell Cycle' pathway.....	146
Supplementary Figure S3.12. KEGG 'Apoptosis' pathway.....	147
Supplementary Figure S3.13. KEGG 'Autophagy' pathway.....	148
Supplementary Figure S3.14. KEGG 'Necroptosis' pathway.....	149
Supplementary Figure S3.15. Graphical summary of IPA for top 100 genes downregulated by Tpz-1.....	150
Supplementary Figure S3.16. Graphical summary of IPA for top 100 genes upregulated by Tpz-1.....	151

ABBREVIATIONS

°C	Degree(s) Celsius
2D	Two-dimensional
3D	Three-dimensional
ABL	V-Abl Abelson murine leukemia viral oncogene homolog
ADME	Absorption, distribution, metabolism, and excretion
AGRN	Agrin
AGT	Angiotensinogen
AJUBA	Ajuba LIM protein
Akt	V-Akt murine thymoma viral oncogene homolog
AKT3	Akt serine/threonine kinase 3
AKTIP	AKT interacting protein
AML	Acute myeloid leukemia
APAF-1	Apoptotic peptidase activating factor 1
ARHGEF1	Rho guanine nucleotide exchange factor 1
ARHGEF12	Rho guanine nucleotide exchange factor 12

ATCC	American Type Culture Collection
AU	Airy unit
AURK	Aurora kinase
AURKB	Aurora kinase B
BAIAP2	BAR/IMD domain containing adaptor protein 2
BAK	BCL2 antagonist/killer
BAX	BCL2 associated X
BCL2	B-cell lymphoma 2
BID	BH3-interacting domain death agonist
BING	Best inferred gene
Blk	Proto-oncogene Src family tyrosine-protein kinase Blk
BRAF	B-Raf proto-oncogene
BRCA1	Breast cancer type 1 susceptibility protein
BSA	Bovine serum albumin
CAPN2	Calpain 2
Carboxy-H ₂ DCFDA	6-carboxy-2',7'-dichlorodihydrofluorescein diacetate

CASP1	Caspase 1
CC BY	Creative Commons Attribution license
CC ₅₀	Cytotoxic concentration 50%
CCL5	C-C motif chemokine ligand 5 (RANTES)
CCN1	Cellular communication network 1
CCND1	Cyclin D1
CCNE2	Cyclin E2
CDC14B	Cell division cycle 14B
CDH1	Cadherin 1 (E-cadherin)
CDK2	Cyclin-dependent kinase 2
CDKN1A	Cyclin dependent kinase inhibitor 1A
CFL2	Cofilin 2
CID	Compound identifier
CLK1	CDC like kinase 1
CMap	ConnectivityMap
CO ₂	Carbon dioxide

COL4A2	Collagen type IV alpha 2 chain
COX5B	Cytochrome c oxidase subunit Vb
CP	Compound
CREB	Cyclic-AMP responsive element-binding protein
CRK	CRK proto-oncogene (P38)
CSPG	Chondroitin sulfate
CTNNA1	Catenin alpha 1
CTNNB1	Catenin beta 1
CXCL8	C-X-C motif chemokine ligand 8
DAG1	Dystroglycan 1
DAPI	4',6-diamidino-2-phenylindole
DAVID	Database for Annotation, Visualization, and Integrated Discovery
DCF	2',7'-dichlorofluorescein
DDR1	Discoidin domain receptor tyrosine kinase 1
DEG	Differentially expressed gene
DENND1B	DENN/MADD domain containing 1B

DHRS2	Dehydrogenase/reductase SDR family member 2
DIABLO	Direct IAP-binding protein with low pI
DIC	Differential interference contrast
DISC	Death-inducing signaling complex
DMSO	Dimethyl sulfoxide
DNA	Deoxyribonucleic acid
DNS	Differential nuclear staining
DSP	Desmoplakin
DYRK1A/2	Dual specificity tyrosine phosphorylation regulated kinase 1A and 2
ECM	Extracellular matrix
EDN1	Endothelin 1
EFNA3	Ephrin A3
EFNB1/2	Ephrin B1 and B2
EGF	Epidermal growth factor
EGFR	Epidermal growth factor receptor
ENAH	ENAH actin regulator

ENTPD5	Ectonucleoside triphosphate disphosphohydrolase 5
EPHB2/3	Ephrin type-B receptor 2 and 3
ERBB2	Tyrosine kinase-type cell surface receptor Erb-B2 (HER2)
ERK1/2	MAPK1 and 3
ETS1	ETS proto-oncogene 1
F-actin	Filamentous actin
F2	Coagulation factor II (thrombin)
F2R	Coagulation factor II (thrombin) receptor
FADD	Fas-associated via death domain
FBS	Fetal bovine serum
FC	Fold change
FERMT3	FERM domain containing kindlin 3
FGFR1	Fibroblast growth factor receptor 1
FGFR4	Fibroblast growth factor receptor 4
Fgr	Proto-oncogene Src family tyrosine-protein kinase Fgr
FITC	Fluorescein-5-isothiocyanate

FN1	Fibronectin 1
Fyn	Proto-oncogene Src family tyrosine protein kinase Fyn
FZD6/7	Frizzled class receptor 6 and 7
g	Relative centrifugal force (g-force)
g/mol	Grams per mole
G0/G1	Resting phase/growth 1 phase
G2/M	Growth 2/mitotic phase
GATA1	GATA binding protein 1
GFI1	Growth factor independent 1 transcriptional repressor
GFP	Green fluorescent protein
GPCR	G-protein coupled receptor
h	Hour(s)
H2B	Histone H2B
H2B-GFP	Histone H2B–green fluorescent protein
H ₂ O ₂	Hydrogen peroxide
HA	Hyaluronan

Hck	Proto-oncogene Src family tyrosine-protein kinase Hck
HCRTR1/2	Hypocretin receptor 1 and 2
HGNC	HUGO Gene Nomenclature Committee
HIF1A	Hypoxia inducible factor 1 subunit alpha
HLX	H2.0 like homeobox
HMGB1	High mobility group box 1 (amphoterin)
HRAS	Proto-oncogene H-Ras
Hsp90	Heat shock protein 90
HSPG	Heparan sulfate
HUGO	Human Genome Organization
IAP	Inhibitors of apoptosis
IETD-FMK	methyl (4S)-5-[[[(2S,3R)-1-[[[(3S)-5-fluoro-1-methoxy-1,4-dioxopentan-3-yl]amino]-3-hydroxy-1-oxobutan-2-yl]amino]-4-[[[(2S,3S)-3-methyl-2-(phenylmethoxycarbonylamino)pentanoyl]amino]-5-oxopentanoate
Ifn	Interferon
IFNG	Interferon gamma
IGF-1R	Insulin-like growth factor type 1 receptor

IKBKE	Inhibitor of nuclear factor kappa B kinase subunit epsilon
IL1A	Interleukin 1 alpha
IL1B	Interleukin 1 beta
IL2	Interleukin 2
IL33	Interleukin 33
IL4	Interleukin 4
IL5	Interleukin 5
IPA	Ingenuity Pathway Analysis
ITG	Integrin
ITGA2/6/V	Integrin subunit alpha 2/6/V
ITGAL	Integrin subunit alpha L
ITGB4	Integrin subunit beta 4
ITPR1	Inositol 1,4,5-triphosphate receptor 1 (ACV)
IUPAC	International Union of Pure and Applied Chemistry
JC-1	5',6,6'-tetrachloro-1,1',3,3'- tetraethylbenzimidazolylcarbocyanine iodide
JNK	JUN N-terminal kinase

KD	Knockdown
KEGG	Kyoto Encyclopedia of Genes and Genomes
KIF5C	Kinesin family member 5C
KLK3	Kallikrein-related peptidase 3
KRAS	Kirsten rat sarcoma viral oncogene homolog (K-Ras)
KRT17	Keratin 17
KRT19	Keratin 19
KRT7	Keratin 7
KRT8	Keratin 8
KSPG	Keratan sulfate
LAMB1/3	Laminin subunit beta 1 and 3
LAMC1	Laminin subunit gamma 1
LAT2	Linker for activation of T cells family member 2
Lck	Proto-oncogene Src family tyrosine-protein kinase Lck
LCP1	Lymphocyte cytosolic protein 1
LINCS	Library of Integrated Network-Based Cellular Signatures

Log2FC	Log2 fold change
Lyn	Proto-oncogene Src family tyrosine-protein kinase Lyn
LYZ	Lysozyme
MAD1L1	Mitotic arrest deficient 1 like 1
MAP	Mitogen-activated protein
MAPK	Mitogen-activated protein kinase
MAPK12	Mitogen-activated protein kinase 12 (p38 γ)
MDPI	Multidisciplinary Digital Publishing Institute
MFI	Median fluorescence intensity
min	Minute(s)
mM	Millimolar
MMP10	Matrix metalloproteinase 10
mRNA	Messenger ribonucleic acid
MRTFA/B	Myocardin related transcription factor A and B
mTORC1	Mammalian target of rapamycin complex 1
MTPC	N'-(2-methoxybenzylidene)-3-methyl-1-phenyl-1H-thieno[2,3-c]pyrazole-5-carbohydrazide

MW	Molecular weight
MYD88	Myeloid differentiation primary response 88
MYH10	Myosin heavy chain 10
NFATC1/2	Nuclear factor of activated T cells 1 and 2
NFKB1	Nuclear factor kappa B subunit 1
NFκB	Nuclear factor kappa B
NHW	Non-Hispanic white
NIM-DAPI	Nuclear isolation medium-DAPI
NKD1	NKD inhibitor of WNT signaling pathway 1
NOS	Nitric oxide synthase
NR0B1	Nuclear receptor subfamily 0 group B member 1
NS4B	Nonstructural protein 4B
P2X3	Purinergic receptor P2X 3
p38	MAPK14
p70S6k	P70 S6 kinase
PAK4	P21-activated kinase 4

PARD3	Par-3 family cell polarity regulator
PARD6B	Par-6 family cell polarity regulator beta
PBS	Phosphate-buffered saline
PDE7A	Phosphodiesterase 7A
PDL1	Programmed cell death 1 ligand 1 (CD274)
PG	Proteoglycan
pI	Isoelectric point
PI	Propidium iodide
PIK3AP1	Phosphoinositide-3-kinase adaptor protein 1
PIK3C2A	Phosphatidylinositol-4-phosphate 3-kinase catalytic subunit type 2 alpha
PIK3R3	Phosphoinositide-3-kinase regulatory subunit 3
PIM1	Serine/threonine-protein kinase proto-oncogene Pim-1
PLAC8	Placenta associated 8
PLCB2	Phospholipase C beta 2
PLGA-PEG	Poly(lactide-co-glycolide)-poly(ethylene glycol)
PLS3	Plastin 3

PLXNA3	Plexin A3
PLXNB1	Plexin B1
PRKCZ	Protein kinase C zeta
PROM1	Prominin 1
PS	Phosphatidylserine
PXN	Paxillin
PYCARD	Apoptosis-associated speck-like protein containing a CARD
RASGRP2	RAS guanyl releasing protein 2
RNA	Ribonucleic acid
RNASET2	Ribonuclease T2
ROS	Reactive oxygen species
RRAS	Oncogene R-Ras
RTK	Receptor tyrosine kinase
S	Synthesis phase
SCI	Selective cytotoxicity index
SDC4	Syndecan 4

SEMA3C/F	Semaphorin 3C and 3F
SEMA4	Semaphorin 4F
SID	Substance identifier
SMAD1	SMAD family member 1
SMAD4	SMAD family member 4
SMILES	Simplified molecular input line entry system
Src	V-Src avian sarcoma viral oncogene homolog
St. Dev	Standard deviation
STAT3	Signal transducer and activator of transcription 3
STAT4	Signal transducer and activator of transcription 4
STAT5	Signal transducer and activator of transcription 5
STK3	Serine/threonine kinase 3
TBP	TATA-box binding protein
TBS-T	Tris-buffered saline–Tween 20 solution
TCF7L2	Transcription factor 7 like 2
TGFB3	Transforming growth factor beta 3

THBS1	Thrombospondin 1
TICAM1	Toll like receptor adaptor molecule 1
TLR4	Toll like receptor 4
TNF	Tumor necrosis factor
TNFRSF10A	TNF receptor superfamily member 10A
TP53	Tumor protein p53
Tpz-1	N'-(2-methoxybenzylidene)-3-methyl-1-phenyl-1H-thieno[2,3-c]pyrazole-5-carbohydrazide
TRAF4/5	TNF receptor associated factor 4 and 5
TRIP13	Thyroid hormone receptor interactor 13
TSC1	Tuberous sclerosis 1
U/mL	Units per milliliter
UNT	Untreated
UQCRFS1	Ubiquinol-cytochrome c reductase, Rieske iron-sulfur polypeptide 1
USD	U.S. dollar
UTEP	University of Texas at El Paso
v/v	Volume per volume

VAV2	Vav guanine nucleotide exchange factor 2
VEGFA	Vascular endothelial growth factor A
WASL	WASP like actin nucleation promoting factor
WNT6	Wnt family member 6
Yes	Proto-oncogene Src family tyrosine protein kinase Yes
ZNF655	Zinc finger protein 655
µg/mL	Micrograms per milliliter
µL	Microliter
µM	micromolar

CHAPTER 1: INTRODUCTION

1.1. GENERAL INTRODUCTION

1.1.1. Cancer Incidence and Treatment Disparities in the United States

Hispanics are a rapidly growing ethnic group in the United States that are more likely to encounter barriers to high-quality, expedient healthcare due to socioeconomic circumstances and poor characterization of the population's cultural heterogeneity [1–4]. Cancer thus remains the leading cause of death among Hispanics in the U.S., with over 175,000 new cases expected in 2021 [1]. Despite the younger average age of U.S. Hispanics compared to non-Hispanic white (NHW) individuals, advanced-stage diagnosis and poor prognosis are more prevalent in Hispanics and can be attributed to the health disparities they face [1,3,4]. Although significant advancements in treatment have been made, cancer incidence has generally remained stable over the last several decades [5]; therefore, more drugs to combat advanced stages of the disease are needed.

1.1.2. How Cancer Develops

Cancers generally arise from a single cell that has acquired mutations that program its uncontrolled proliferation. As cancer cells continue to abnormally divide, their genetic instability introduces tumor heterogeneity that presents significant challenges to disease management by facilitating the expansion of treatment-resistant subpopulations [6,7]. An individual's unique genetic and epigenetic constitution can also contribute to the success of current cancer treatments.

1.1.3. Standard Cancer Treatments

Surgery, radiation, and chemotherapy are the primary treatments of choice for many cancers, used alone or in combination [8,9]. However, a significant limitation of conventional chemotherapies is their broad destruction of rapidly dividing cells, including normal cells like those in the digestive tract and hair follicles [10]. The toxic side effects of current chemotherapeutics can thus limit an individual's tolerance for the prescribed treatment dose.

1.1.4. Anticancer Drug Discovery

The discovery and development of small molecule anticancer agents is an expensive and time-consuming process, and generally takes over ten years and around 1.8 billion USD to go from hit identification to clinical use [11]. Hit identification and lead discovery involve finding compounds that elicit the desired effect in vitro and optimizing them to generate lead drug candidates [11]. There exist two major approaches in drug discovery: phenotypic and target-based drug screening [12]. Phenotypic screening involves evaluating the effect of novel molecules on whole cells, whereas target-based screening requires identifying disease-associated molecular targets [12]. Phenotypic screening was the mainstay of in vitro drug discovery until advancements in molecular biology and genetics shifted research focus to targeted screenings in the 1990s [12,13].

1.1.5. Apoptosis in Cancer Development and Treatment Response

Apoptosis is essential for normal cell turnover in our tissues and describes the immune-silent process by which old, damaged, or dangerous cells are shed [14]. It is a morphologically distinct event that relies on the proteolytic activity of caspase enzymes to orchestrate the disassembly of cells from the inside out [15]. Some of the

characteristic features of apoptosis include decreased cell volume, condensed chromatin, DNA fragmentation, and membrane blebbing [16,17]. In contrast to necrosis, dead cell components are neatly packaged into small vesicles (apoptotic bodies) and are rapidly engulfed by nearby phagocytes to avoid inflammation [17]. Genetic and epigenetic changes to the apoptotic machinery can confer a considerable survival advantage to cells; thus, evasion of apoptosis is a hallmark of cancer [18–20].

Apoptosis is an innate defense mechanism that programs cell death in response to various stimuli, including DNA damage, cell stress, chemical exposures, immune reactions, and pathogens [21]. A delicate balance of B-cell lymphoma 2 (BCL2) family proteins and tumor necrosis factor (TNF) superfamily transmembrane death receptors ensures a proper cellular response to internal and external apoptotic stimuli [20]. BCL2 family proteins can be pro- or anti-apoptotic, and they control cell sensitivity to internal signals for death at the outer mitochondrial membrane by promoting or inhibiting mitochondrial permeabilization [20,22]. In contrast, the death receptors relay external signals for apoptosis upon ligand binding [20].

There are two major pathways of apoptosis: intrinsic and extrinsic. The intrinsic pathway is stimulated by death signals from within the cell and is also known as the stress-activated pathway. In this process, pro-apoptotic BCL2 proteins BAX and BAK enable mitochondrial permeabilization and release of cytochrome C and direct IAP-binding protein with low isoelectric point (pI) (DIABLO) into the cytoplasm [15,20]. As a result, Cytochrome C forms a complex with apoptotic peptidase activating factor 1 (APAF-1) proteins that is known as the apoptosome [15,20]. The apoptosome recruits and activates caspase-9, which initiates a signaling cascade that leads to the cleavage

of death substrates and execution of apoptosis by caspases-3/6/7 [15,20].

Simultaneously, DIABLO ensures caspases are available by sequestering inhibitors of apoptosis (IAP) proteins [15,20].

In contrast, extrinsic apoptosis is stimulated by ligand binding to transmembrane death receptors, also known as the receptor-activated pathway. In this pathway, TNF superfamily death receptors trimerize upon ligand binding, causing recruitment and formation of a death-inducing signaling complex (DISC) comprised of Fas-associated via death domain (FADD) and caspase-8 or 10 [15,20]. The DISC activates caspase-8 to initiate a signaling cascade that converges with the intrinsic apoptotic pathway at caspases-3/6/7 [15,20]. BH3-interacting domain death agonist (BID) is a pro-apoptotic protein that can also be cleaved by caspase-8 to enable disruption of the outer mitochondrial membrane [15,20].

Cancer cells are infamous for their unstable genome and can acquire resistance to apoptosis through various genetic and epigenetic mutations [7,20]. Often, multiple regulatory pathways become dysregulated in cancer and complement each other to promote tumor growth [23]. Many chemotherapies on the market indirectly trigger apoptosis by targeting proteins involved in cell proliferation or survival [24]. However, the benefit of these drugs is often limited due to off-target effects and how the cancer's apoptotic machinery is dysregulated [18].

Apoptosis pathways canonically interact with many other signaling mechanisms to maintain an appropriate balance of pro- and anti-apoptotic protein activity [19,23,25]. Understanding how cancer cells have tipped the balance of BCL2 family proteins, caspases, death receptors, and other elements of the apoptotic machinery in favor of

survival can help inform which drug(s) will provide the most personalized cancer-specific effect. However, drug resistance can be acquired through secondary changes in gene expression that interfere with drug-to-target binding or downstream signaling. Consequently, exploiting the interactions of apoptosis pathways with less frequently targeted tumor-promoting signaling mechanisms may help to overcome current treatment limitations by sensitizing or resensitizing cells to chemotherapy and reducing off-target effects [7,19,23,24,26,27]. In theory, this benefit can be maximized if non-crossreacting signal transduction pathways with non-overlapping toxicities are targeted.

1.2. SIGNIFICANCE

The specific cancer treatment a patient receives depends on their type of cancer, whether it has spread, and to where. Most often, patients receive chemotherapy in conjunction with other cancer treatments. Unfortunately, many prescribed chemotherapeutics exhibit poor selectivity for cancer cells and highly toxic side effects [10]. Depending on a person's tolerance, these side effects may interfere with clinicians' ability to administer chemotherapy at the most effective dose and frequency to treat their cancer. Thus, there is an ongoing need for novel small molecule chemotherapies which address these challenges by being more potent and targeted toward cancer cells.

Despite the success of target-based screenings over the past few decades, a recent decline in newly approved drugs has prompted the resurgence of phenotypic screenings to revitalize drug discovery [12,13,28]. To contribute to the rejuvenation of anticancer drug discovery, this dissertation describes a modern and innovative approach to phenotypic screening that combined *in vitro* and *in silico* analyses to predict the

molecular mechanism of the uniquely structured and potent small molecule candidate, Tpz-1.

1.3. SPECIFIC AIMS

The goal of this project was to identify a novel small molecule with cytotoxic effects that are specific to cancer in vitro and investigate the molecular pathways involved in compound-induced cell death. To accomplish this, a library of compounds from the ChemBridge DIVERset library were evaluated for cytotoxicity in a high-throughput phenotypic screening, and a variety of in vitro and in silico experiments were performed to distinguish the mode of cell death and probable cellular target of the most potent drug candidate, Tpz-1. Moreover, the unique molecular structure of Tpz-1 prompted our evaluation of the physical features which could play a role in its cytotoxicity. The specific aims for this project are outlined below and detailed in the chapters that follow.

Specific Aim 1: To identify a potential anticancer drug candidate from the ChemBridge DIVERset small molecule library (Chapter 2).

- High-throughput initial screening of compounds against CCRF-CEM leukemia cells
- Cytotoxic evaluation of lead compound candidate Tpz-1 in a variety of tumorigenic and non-tumorigenic human cell lines
- Analysis of the potential of Tpz-1 to induce apoptosis in leukemic cells
- Evaluation of Tpz-1's effect on cell cycle progression

Specific Aim 2: To investigate the cellular mechanisms impacted by Tpz-1 treatment (Chapters 2 and 3).

- Literature review to identify key structural features and prior research on Tpz-1
- Evaluation of Tpz-1-induced changes to MAP and Src family kinase phosphorylation
- Visualization of treated cell morphology using confocal and timelapse microscopy
- Cataloguing of Tpz-1's effect on genome-wide mRNA expression *via* whole transcriptome analysis of treated leukemic cells

Specific Aim 3: To evaluate the drug-likeness of Tpz-1 (Chapter 3).

- Prediction of drug kinetics and based on the chemical structure of Tpz-1
- Identification of structural features that could be optimized to improve the cancer-selectivity and solubility of Tpz-1
- Comparison of in vitro and in silico experimental findings to deconvolute the potential target of Tpz-1

CHAPTER 2: IDENTIFICATION OF A UNIQUE CYTOTOXIC THIENO[2,3-C]PYRAZOLE DERIVATIVE WITH POTENT AND SELECTIVE ANTICANCER EFFECTS IN VITRO¹

2.1. OBJECTIVE

Tpz-1 was identified as the most potent and cytotoxic compound in a high-throughput screening of small drug-like molecules from the Chembridge DIVERset library. This chapter explores the cytotoxic activity of Tpz-1 and its partial mechanism of action.

The material in this chapter was published in *Biology*, an open access journal from Multidisciplinary Digital Publishing Institute (MDPI) (Basel, Switzerland). This article has been permitted for reuse in this dissertation by the Creative Commons Attribution License (CC BY), found here: <https://creativecommons.org/licenses/by/4.0/>. As first author my contributions were the conceptualization, methodology, formal analysis, investigation, data curation, draft preparation, review, and editing of this work. The co-authors are Luca H. Macias (L.H.M.), Denisse A. Gutierrez (D.A.G.), Karla Moran-Santibanez (K.M.-S.), Lisett Contreras (L.C.), Stephanie Medina (S.M.), Paulina J. Villanueva (P.J.V.), Robert A. Kirken (R.A.K.), Armando Varela-Ramirez (A.V.-R.), Manuel L. Penichet (M.L.P.), and Renato J. Aguilera (R.J.A.).

Co-author contributions were as follows: conceptualization, A.V.-R., M.L.P., and R.J.A.; methodology, D.A.G., and A.V.-R.; formal analysis, A.V.-R., and R.J.A.; investigation of cytotoxicity, L.H.M., D.A.G., L.C., S.M., and P.J.V.; investigation of kinase phosphorylation, K.M.-S.; investigation of cytoskeleton, D.A.G., and A.V.-R.; resources,

¹ Published as Hess, J.D.; Macias, L.H.; Gutierrez, D.A.; Moran-Santibanez, K.; Contreras, L.; Medina, S.; Villanueva, P.J.; Kirken, R.A.; Varela-Ramirez, A.; Penichet, M.L.; Aguilera, R.J. Identification of a Unique Cytotoxic Thieno[2,3-c]Pyrazole Derivative with Potent and Selective Anticancer Effects In Vitro. *Biology* **2022**, *11*, 930. <https://doi.org/10.3390/biology11060930>

A.V.-R., R.A.K., M.L.P., and R.J.A.; data curation, A.V.-R.; writing—original draft preparation, A.V.-R.; writing—review and editing, A.V.-R., M.L.P., and R.J.A.; supervision, A.V.-R. and R.J.A. All authors have read and agreed to the published version of the manuscript.

2.2. SIMPLE SUMMARY

Despite their documented antitumor effects, thienopyrazole-based compounds remain an underexplored class of molecules. In this study, a screening of 2000 novel molecules revealed a unique thienopyrazole derivative, Tpz-1, that elicited potent and selective programmed cell death in human blood, breast, colon, and cervical cancer cell lines when compared to non-cancerous human fibroblast (Hs27) cells. Furthermore, in HL-60 leukemia cells, Tpz-1 interfered with components of signaling pathways and the cytoskeleton that are important to cell shape, internal organization, growth, and division. These findings encourage the continued investigation and development of Tpz-1 and other thienopyrazole derivatives to target and treat cancers.

2.3. ABSTRACT

In recent years, the thienopyrazole moiety has emerged as a pharmacologically active scaffold with antitumoral and kinase inhibitory activity. In this study, high-throughput screening of 2000 small molecules obtained from the ChemBridge DIVERset library revealed a unique thieno[2,3-c]pyrazole derivative (Tpz-1) with potent and selective cytotoxic effects on cancer cells. Compound Tpz-1 consistently induced cell death at low micromolar concentrations (0.19 μ M to 2.99 μ M) against a panel of 17 human cancer cell lines after 24 h, 48 h, or 72 h of exposure. Furthermore, an in vitro investigation of Tpz-1's mechanism of action revealed that Tpz-1 interfered with cell cycle progression,

reduced phosphorylation of p38, CREB, Akt, and STAT3 kinases, induced hyperphosphorylation of Fgr, Hck, and ERK 1/2 kinases, and disrupted microtubules and mitotic spindle formation. These findings support the continued exploration of Tpz-1 and other thieno[2,3-c]pyrazole-based compounds as potential small molecule anticancer agents.

Keywords: thienopyrazole; anticancer drug discovery; leukemia; cytotoxicity; differential nuclear staining; apoptosis; kinase activity regulation; microtubule disruption; mitotic spindle organization

2.4. INTRODUCTION

Small molecule agents have become a mainstay of targeted cancer treatment in the past 20 years. Unlike macromolecule drugs, small molecules can penetrate cells and bind a wide array of intra- or extracellular targets; additionally, they can be selective or broad-spectrum agents [29–31].

Pyrazoles and thiophenes are well-studied pharmacophores known for their diverse and remarkable biological activity, particularly in cancer, and are common scaffolds in small molecule drug design [32,33]. Pyrazoles are 5-membered heterocycles that contain three carbon atoms and two adjacent nitrogen (**Figure 2.1**). Pyrazole derivatives have been approved to treat various leukemias, lymphomas, and other cancers in the United States and China [31]. In addition, numerous experimental pyrazoles have shown antiproliferative activity and apoptosis against several cancer types in vitro [34–36]. In contrast, thiophene is a 5-membered heterocycle with four carbon atoms and one sulfur (**Figure 2.1**). Thiophene derivatives are also prominent in

drug design and are indicated to treat a variety of cancers and other conditions in the U.S. and China [31,37].

Thienopyrazoles are a bicyclic combination of the pyrazole and thiophene moieties and have been endorsed as antiproliferative, antiviral, antimicrobial, and anti-inflammatory agents [38–40]. There exist three isomers of thienopyrazole: thieno[2,3-c]pyrazole, thieno[3,2-c]pyrazole, and thieno[3,4-c]pyrazole (**Figure 2.1**) [40].

Thieno[2,3-c]pyrazoles are less-explored than the other isomers, despite growing evidence detailing their significant phosphodiesterase 7A (PDE7A) [41,42], purinergic receptor P2X3 [43], non-receptor tyrosine kinase ABL [44], Aurora kinase (AURK), insulin-like growth factor type 1 receptor (IGF-1R), and cyclin-dependent kinase 2 (CDK2) inhibition [45,46]. Tpz-1 (**Figure 2.2**) is a novel small molecule thieno[2,3-c]pyrazole derivative that we recently discovered after screening 2000 compounds for novel anticancer agents within the ChemBridge DIVERset library.

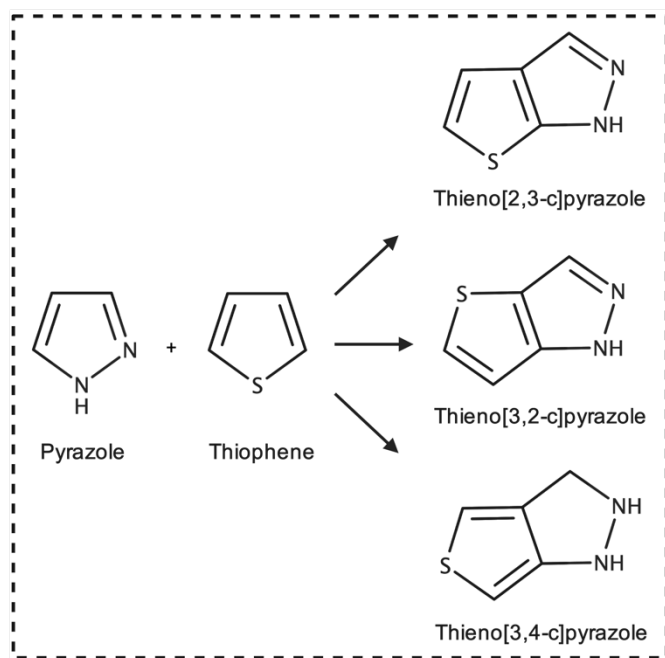


Figure 2.1. Chemical structures of pyrazole, thiophene, and thienopyrazoles.

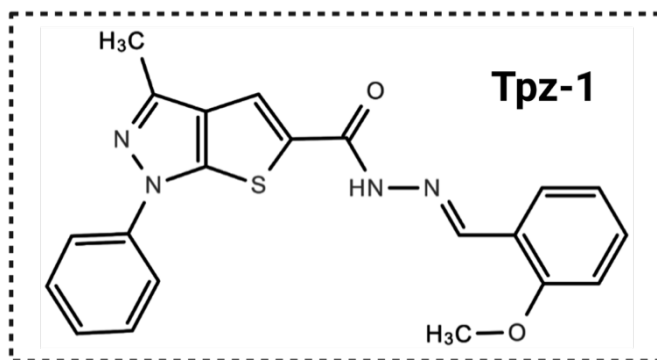


Figure 2.2. Chemical structure of thieno[2,3-c]pyrazole derivative Tpz-1 (N'-(2-methoxybenzylidene)-3-methyl-1-phenyl-1H-thieno[2,3-c]pyrazole-5-carbohydrazide; MW: 390 g/mol).

Formally named N'-(2-methoxybenzylidene)-3-methyl-1-phenyl-1H-thieno[2,3-c]pyrazole-5-carbohydrazide, we found that this compound was also identified as cytotoxic and a mitotic inhibitor in two previous studies under the aliases 5248881 [47] and MTPC [48]. However, the molecular mechanism by which this unique compound induces cell death was not explored.

Leukemias are a leading cancer type in children and adults [5,49]. In addition, secondary and refractory acute leukemias are known to develop from prior exposure to cytotoxic therapies [50–53]. Despite recent advances, a subset of patients continue to die from leukemia or complications resulting from treatment [54]. Consequently, we set out to partially elucidate how Tpz-1 potently induces death in acute leukemia cells in vitro.

2.5. MATERIALS AND METHODS

2.5.1. Cell Lines and Culture Conditions

In this study, the cytotoxicity of Tpz-1 was evaluated against a panel of sixteen cancer cell lines and one non-tumorigenic human cell line. All cell lines were obtained from the American Type Culture Collection (ATCC, Manassas, VA, USA).

Ten of the cell lines were of blood cancer origin: CCRF-CEM (T lymphoblast, ATCC CRL-2265), HL-60 (promyeloblast, ATCC CCL-240), Ramos (B lymphocyte, ATCC CRL-1596), Jurkat (T lymphocyte, ATCC CRL-2899), MOLT-3 (T lymphoblast, ATCC CRL-1552), NALM6 (lymphocyte, ATCC CRL-3273), MM.1S (B lymphoblast, ATCC CRL-2974), MM.1R (B lymphoblast, ATCC CRL-2975), U266 (B lymphocyte, ATCC TIB-196), RPMI 8226 (B lymphocyte, ATCC CRM-CCL-155); and were cultured in RPMI-1640 medium complete with 10% heat-inactivated fetal bovine serum (FBS), 100 U/mL penicillin, and 100 µg/mL streptomycin. An exception was made for HL-60, which required supplementation with an additional 10% FBS. In addition, two colorectal adenocarcinoma cell lines, COLO 205 (ATCC CCL-222) and HT-29 (ATCC HTB-38), were identically maintained in RPMI-1640 complete medium. Two triple-negative breast adenocarcinoma cell lines, MDA-MB-231 (ATCC CRM-HTB-26) and MDA-MB-468 (ATCC HTB-132), and estrogen-receptor-positive (ER+) cell line MCF7 (ATCC HTB-22) were cultured in DMEM medium complete with 10% FBS, 100 U/mL penicillin, and 100 µg/mL streptomycin; cervical adenocarcinoma cell line HeLa (ATCC CRM-CCL-2) and non-tumorigenic foreskin fibroblast Hs27 (ATCC CRL-1634) cells were also maintained in this medium. Lastly, dopaminergic neuroblastoma cell line SH-SY5Y (ATCC CRL-2266) was cultured in DMEM/F12 medium with 10% FBS and antibiotics added as described above. All cells were cultivated in a 5% CO₂ humidified 37 °C environment.

Before use in experiments, the viability of each cell culture was quantified by flow cytometry following propidium iodide (PI) staining or visualized by trypan blue exclusion [55]. Only cell populations with ≥ 95% viability and at 60–75% confluence in the

exponential growth phase were seeded into multiwell plates to minimize baseline cell death.

2.5.2. Preparation of Compounds

All compounds described herein were commercially purchased. Experimental compounds from the ChemBridge DIVERset library were obtained pre-diluted to 10 mM in dimethyl sulfoxide (DMSO). This ChemBridge stock of N'-(2-methoxybenzylidene)-3-methyl-1-phenyl-1H-thieno[2,3-c]pyrazole-5-carbohydrazide (C₂₁H₁₈N₄O₂S; MW 390 g/mol), also known as Tpz-1, was used for the experiments detailed below. Lyophilized reference compounds Paclitaxel and Cytochalasin-D were similarly prepared in DMSO; and hydrogen peroxide (H₂O₂) was alternatively diluted in 1x phosphate-buffered saline (PBS).

Aliquots of Tpz-1 and other compound stocks were thawed and diluted with DMSO, or 1x PBS for H₂O₂, to a 100x or 250x working concentration for use in experiments to achieve a final vehicle concentration of 1% v/v or less.

2.5.3. Initial Library Screening and Compound Selection

Two thousand experimental compounds of the ChemBridge DIVERset library were initially screened against the CCRF-CEM cell line in vitro at a single concentration of 10 μM by differential nuclear staining assay. Any compound which induced > 50% cell death at 10 μM was isolated and additionally screened at concentrations ranging from 0.01 to 10 μM to calculate the dose of compound needed to induce 50% cell death.

2.5.4. Differential Nuclear Staining Assay

Differential nuclear staining (DNS) is a live cell imaging assay that uses two nuclear fluorescent dyes to distinguish between live and dead populations based on cell

permeability [56]. To achieve this, Hoechst 33342 (blue) is used to stain the nuclei of all cells in a sample, whereas PI (red) is used to distinguish only those with damaged membranes. Thus, cells that co-localize both red and blue signals, exhibiting a magenta color, are defined as the dead/dying population.

For DNS analysis, cells were first seeded in 96-well plates at a density of 10,000 cells/well in 100 μ L of complete medium and incubated overnight to facilitate cell attachment and acclimation. The next day, cells were exposed to Tpz-1 concentrations ranging from 0.01 to 10 μ M, 1% v/v DMSO (vehicle control), 1 mM H₂O₂ (positive control), or left untreated (UNT) for 24–72 h. Four independent measurements were used for the samples, except for the vehicle control in which eight DMSO-treated independent measurements were used to ensure the average total cell count was representative for each experiment series. One to two hours before the end of treatment, a 1 μ g/mL final concentration of Hoechst 33342 and PI was quickly added to each well and incubated until the remaining time elapsed. Four contiguous images, taken in 2 \times 2 montages, were captured via GE InCell Analyzer 2000 with a 10x objective from the two fluorescent channels corresponding to Hoechst and PI emission. After analysis, the captured high-content images were segmented using the GE InCell Analyzer Workstation 3.2 software to obtain live and dead cell counts and percentages within each well. Due to technical problems, for the MCF7 cell line, the BD Pathway 855 bioimaging system was used to capture a similar 2 \times 2 montages per well, and images were segmented with its associated AttoVision v1.6.2 software (BD Biosciences, Rockville, MD, USA). To account for the lower total cell count in Tpz-1 or H₂O₂-treated (Treatment) samples caused by cell destruction (disappearance from count) over the course of incubation, cell death

percentages were normalized to the vehicle control (DMSO) average total cell count by the following equation:

$$\frac{(\text{DMSO average total cell count} - \text{Treatment total cell count}) + \text{Treatment dead cell count}}{\text{DMSO average total cell count}} \times 100$$

Normalized percentages of dead cells per treatment replicate were subsequently averaged and used to estimate CC₅₀ values.

2.5.5. Cytotoxic Concentration 50% and Selective Cytotoxicity Index Values

The cytotoxic concentration 50% (CC₅₀) for each cell line indicates the average concentration (μM ± S.D.) needed to kill 50% of the cell population at a given time point. From the percentage of cell death for each technical replicate at a concentration above and below 50% cell death, CC₅₀ for each cell line was calculated via linear interpolation and averaged to obtain the reported values [35,57,58].

To measure Tpz-1's cancer selectivity in vitro, selective cytotoxicity index (SCI) values were calculated by dividing the CC₅₀ of non-tumorigenic control cell line Hs27 by the CC₅₀ of individual cancer cell lines at the same incubation time [59].

2.5.6. AnnexinV-FITC/PI Assay

To determine if Tpz-1 stimulates apoptotic or necrotic cell death, HL-60 acute myeloid leukemia or CCRF-CEM T lymphoblast leukemia cells were transferred to a 24-well plate at a seeding density of 100,000 cells in 1 mL complete culture media. After overnight incubation, cells were treated with the cell line's 24 h CC₅₀ or 2xCC₅₀ of Tpz-1 for 24 h. Also, 0.1% v/v DMSO, 100 μM H₂O₂, and untreated cells were used as the vehicle, positive, and negative controls. All results, experimental points, and corresponding controls represent three independent determinations. Immediately following treatment, cells were pelleted at a centrifuge pre-cooled to 4 °C for 5 min at 500

×g. The resulting supernatant was discarded, and cell pellets were resuspended in 103.5 μL of a cold AnnexinV-FITC/PI/1x binding buffer mixture, then chilled on ice while covered for 30 min. Afterward, 300 μL of ice-cold 1x binding buffer was added to each well immediately prior to flow cytometry. Total apoptosis was calculated by summing early apoptotic (AnnexinV-FITC positive/PI negative signal) and late apoptotic (AnnexinV-FITC positive/PI positive) cell populations. The statistical significance of the apoptosis induced by Tpz-1 was evaluated by comparing experimentally treated samples to those of DMSO by *t*-test ($p = 0.05$). Approximately 20,000 events (cells) were acquired per sample. Data analysis was achieved via the flow cytometer's Kaluza software (Beckman Coulter, Indianapolis, IN, USA).

2.5.7. Caspase Activation Assays

Caspase-3/7 are proteases activated in the execution phase of apoptosis's intrinsic and extrinsic pathways [60]. Therefore, to further validate that apoptosis is the cell death mechanism of Tpz-1, caspase-3/7 activation (NucView 488 Caspase-3/7 Substrate Assay Kit, Biotium) was measured in compound-treated HL-60 acute myeloid leukemia and CCRF-CEM T cell leukemia cells [61]. The substrate provided in the kit consists of a fluorogenic DNA dye with DEVD moiety that is specific for caspase-3/7. When cleaved by caspase-3/7, the substrate forms a high-affinity nuclear dye that emits a bright green signal detectable by flow cytometry. For this assay, cells were seeded in 24-well plates at a density of 100,000 cells per well in 1 mL complete culture medium and incubated overnight. Cells were subsequently treated with the appropriate 24 h CC_{50} or $2xCC_{50}$ of Tpz-1 for 6 h (data shown) or 8 h (in Supplementary Materials). Controls were included as previously described. Three independent measurements were analyzed for each

experimental and control treatment. At the end of treatment, cells were collected and centrifuged at 262 ×g for 5 min. The supernatant was discarded, and pelleted cells were resuspended in 102.5 µL of 1x PBS and NucView 488 Caspase-3/7 substrate mixture (5 µM final concentration), then covered and incubated at room temperature for 45 min. After, 300 µL of 1x PBS was added, and a flow cytometer was used to analyze samples immediately. Cells emitting green fluorescence were defined as apoptotic cells with active caspase-3/7. Approximately 20,000 events (cells) were acquired per sample, and the Beckman Coulter Kaluza software was used for data analysis.

Caspase-8, in contrast, is an initiator of the extrinsic pathway of apoptosis and its activation directly promotes the cleavage of downstream executioner caspase-3/7 [60,62]. Hence, to evaluate if Tpz-1 stimulates extrinsic apoptosis, we assessed the activation of caspase-8 via substrate assay kit following the manufacturer's protocol (Abcam; Ab65614) to stain HL-60 cells after 4 h treatment with the 24 h CC₅₀ or 2xCC₅₀ of our compound. In this experiment, the caspase-8-specific inhibitor IETD-FMK is conjugated to FITC and emits fluorescence that is detectable by flow cytometry when bound to active caspase-8. In addition, cell seeding, controls, data acquisition, and data analysis were performed in a manner consistent with our other cytometric experiments.

2.5.8. Reactive Oxygen Species Assay

Reactive oxygen species (ROS) can be an indicator of mitochondrial dysfunction in intrinsic apoptosis [63]. Thus, we measured the accumulation of ROS was by 6-carboxy-2',7'-dichlorodihydrofluorescein diacetate (carboxy-H₂DCFDA) reagent (Invitrogen, C400) [64]. In this experiment, the acetate groups of nonfluorescent carboxy-H₂DCFDA are cleaved by intracellular esterases and oxidation to form the green

fluorescing product 2',7'-dichlorofluorescein (DCF). HL-60 acute myeloid leukemia or CCRF-CEM T cell leukemia cells were each distributed into 24-well plates at a seeding density of 100,000 cells/well in 1 mL complete medium and treated with the appropriate 24 h CC₅₀ or 2xCC₅₀ of Tpz-1 or controls, as previously mentioned, for 18 h [64]. Three independent measurements were evaluated for all experimental and control treatments. Post-treatment, samples were collected and centrifuged for 5 min at 262× g, then resuspended in a pre-warmed mixture of 1x PBS and carboxy-H₂DCFDA at a final concentration of 10 μM dye. Cells were incubated for 1 h at 37 °C in a 5% CO₂ humidified environment, centrifuged at 262× g for 5 min, then resuspended in 500 μL PBS, and analyzed by flow cytometer after a 30-min recovery period. Approximately 20,000 cell events were obtained and analyzed per sample, and data analysis was achieved as mentioned in the cytometric analyses described above.

2.5.9. Mitochondrial Depolarization Assay

To monitor the mitochondrial integrity of cells exposed to Tpz-1, changes in mitochondrial membrane potential were studied via MitoProbe JC-1 Assay Kit (Molecular Probes, M34152). 5',6,6'-tetrachloro-1,1',3,3'-tetraethylbenzimidazolylcarbocyanine iodide (JC-1) is a fluorescent cationic probe capable of accumulating inside mitochondria. In healthy mitochondria, the JC-1 dye aggregates to spontaneously form red fluorescent complexes, however, in damaged mitochondria, the JC-1 dye cannot accumulate enough for these complexes to develop, and the dye alternatively emits green fluorescence [65,66]. The red/green fluorescence ratio of JC-1 is thus a reliable indicator of mitochondrial integrity. For this assay, HL-60 or CCRF-CEM cells were seeded in 24-well plates at a density of 100,000 cells/well in 1 mL complete culture media and were treated

with the 24 h CC_{50} or $2xCC_{50}$ of Tpz-1 and controls (as previously described) for 5 h. Three independent measurements were analyzed per cell treatment. When the incubation time expired, cells were collected and centrifuged at $262\times$ g for 5 min, then resuspended in 500 μ L 1x PBS containing 2 μ M JC-1 dye. Cells were stored at 37 °C in a 5% CO_2 humidified incubator for 30 min, then washed with warm PBS before analysis by flow cytometer. Green fluorescing cells were an indication of depolarized mitochondria within a given sample. Approximately 20,000 events were acquired per sample, and data analysis was achieved as mentioned for other cytometric analyses.

2.5.10. Cell Cycle Analysis

To determine the effect of Tpz-1 on the cell cycle, the DNA content of individual cells was quantified by nuclear isolation medium (NIM)–DAPI staining (NPE Systems, Inc./Beckman Coulter). The NIM–DAPI reagent simultaneously permeabilizes plasma membranes and stains cellular DNA with a violet-excited DNA-intercalating agent (DAPI). A cell's DAPI signal is directly proportional to the amount of cellular DNA such that $G_0/G_1 < S < G_2/M$, hence DAPI fluorescence intensity was used to quantify the percentage of cells in each phase of the cycle for each sample. For this experiment, asynchronously cultured HL-60 and CCRF-CEM cells were separately seeded in 24-well plates at a density of 50,000 cells/well in 1 mL of complete culture media, incubated overnight, and treated with the appropriate 24 h $\frac{1}{4} CC_{50}$ or $\frac{1}{2} CC_{50}$ of Tpz-1 for 72 h. These concentrations were selected for consistency with our other cytometric analyses. 0.1% v/v DMSO, 100 μ M H_2O_2 , and untreated controls were also included. All treatments were assessed using three independent measurements. After treatment, cells were collected and centrifuged at $262\times$ g for 5 min. The supernatant was discarded, cell pellets were

resuspended in a mixture of 100 μ L 1x PBS and 200 μ L NIM–DAPI solution, then quickly analyzed via flow cytometer. Fluorescent signal was captured using an FL9 detector and a 405 nm laser. Approximately 20,000 events (cells) were analyzed per sample, with data analysis achieved as previously mentioned.

2.5.11. Phospho-Kinase Arrays

The phosphorylation of tyrosine-protein Src family and mitogen-activated protein (MAP) kinases were assessed on Tpz-1 treated vs. untreated cells via Multiplex Luminex assay kits. The phosphorylation status of MAP kinases CREB, JNK, NF κ B, p38, ERK 1/2, Akt, p70S6k, STAT3, and STAT5 were detected via the Milliplex MAP human multi-pathway signaling network kit (Millipore). Similarly, phosphorylation of Src kinases Src, Fyn, Yes, Lck, Lyn, Fgr, Blk, and Hck were detected using the Milliplex MAP 8-Plex human Src family kinase kit (Millipore). In these experiments, 5×10^6 HL-60 cell samples were collected in microcentrifuge tubes and treated with a sub-CC₅₀ dose, 0.01 μ M or 0.1 μ M, of Tpz-1 and incubated for 3 h at 37 °C. The cells in each sample were lysed, their protein concentrations determined, and Multiplex Luminex assays were performed following the same procedure as the experimental compound P3C [35]. Acquisition and data analysis were performed using Luminex xPONENT 3.1 software.

2.5.12. Confocal Microscopy

To assess the effect of Tpz-1 on cytoskeletal architecture, non-tumorigenic Hs27 and cervical adenocarcinoma HeLa cell lines were utilized [58]. Cells were detached from their vessels and separately seeded into thin-bottomed 96-well plates at a density of 2.5×10^3 cells in 100 μ L complete medium and incubated at 37 °C overnight to promote reattachment. The next day, a 10 μ M dose of Tpz-1 was applied to Hs27 cells and a 0.19

μM dose to HeLa cells for 4 h and 24 h, respectively. Additionally, vehicle (1% v/v DMSO), actin polymerization inhibitor (5 $\mu\text{g}/\text{mL}$ Cytochalasin-D), tubulin stabilizer (1 μM Paclitaxel), and untreated controls were included.

After incubation, 100 μL of freshly prepared 8% formaldehyde was added directly to each well as a fixative solution, and the plate was incubated at room temperature for 20 min. Next, the liquid in each well was removed, and 200 μL of 0.1% v/v Tween 20 in 1x PBS was added for washing/permeabilization and then incubated for 10 min at room temperature. After washing cells twice more, the liquid was removed from each well and 200 μL of 5% w/v bovine serum albumin (BSA) dissolved in Tris-buffered saline with 0.5% v/v Tween 20 (TBS-T) was added for blocking purposes. Samples were then incubated at room temperature and on a rocking platform for 1 h with the blocking solution to minimize non-specific binding. Afterward, samples were triple-stained with 50 μL of 0.1% v/v Tween 20 in 1x PBS solution containing 5 $\mu\text{g}/\text{mL}$ DAPI to visualize nuclei, 0.165 μM Alexa Fluor 568-conjugated phalloidin for actin microfilaments (F-actin), and 0.5 $\mu\text{g}/\text{mL}$ Alexa Fluor 488-conjugated anti- α -tubulin monoclonal antibody for microtubules (polymerized tubulin). The stained cells were protected from light and placed on a rocking platform for 1 h at room temperature. Next, samples were washed three times with 200 μL of 0.1% v/v Tween 20 permeabilization solution. After the final wash, cells were kept in a fresh 200 μL of 0.1% v/v Tween 20. Images of stained cells were subsequently captured on three fluorescent channels (DAPI, Alexa-568, and Alexa-488) with a Zeiss LSM-700 confocal microscope equipped with an EC Plan-Neofluar 40x/1.30 oil DIC objective. A 1-Airy Unit (AU) pinhole setting was consistently utilized for each channel.

For image acquisition and analysis, the ZEN 2009 software was used (Zeiss, New York, NY, USA).

2.5.13. Statistical Analysis

All flow cytometry experimental points are representative of three independent measurements, whereas, for differential nuclear staining, four independent measurements were performed. Eight independent measurements were used to obtain the total cell count for vehicle-treated samples in each DNS assay. Experimental values are reported as the average of independent measurements per treatment with corresponding standard deviation. Statistical significance was determined by two-tailed paired Student's *t*-tests ($p = 0.05$) comparing treatment samples to vehicle controls; p -values ≤ 0.05 were considered significant. Significance values are reported as * $p < 0.05$, ** $p < 0.01$, and *** $p < 0.001$.

2.6. RESULTS

2.6.1. Drug Screening Identified a Thienopyrazole Derivative (Tpz-1) with Potent Cytotoxicity against Several Cancer Cell Lines

We initiated a high-throughput screening project of 2000 compounds from the ChemBridge DIVERset chemical library in search of novel cancer-killing compounds. Cytotoxicity of each compound was first explored via DNS assay against the acute lymphoblastic leukemia cell line CCRF-CEM, and compounds that elicited 50% or greater cell death after 48 h of exposure were isolated for further analysis. Tpz-1 (**Figure 2.2**) emerged as the most attractive candidate, with a CC_{50} of 0.25 μ M toward the CCRF-CEM cell line, and was thus retested for its ability to induce cell death in other cell types.

2.6.2. Tpz-1 Displays Highly Selective Cytotoxicity against Leukemia and Lymphoma Cell Lines

To elucidate the potential selectivity of Tpz-1 toward different cell types, cytotoxicity was examined against a panel of human cell lines derived from a variety of cancerous blood and tissues.

The cytotoxicity of Tpz-1 toward individual cell lines was assessed between 24–72 h of exposure through the DNS assay. Cells that grow in suspension were evaluated generally after 48 h, whereas adherent cells were incubated for 72 h due to their slower doubling time. In 14 cancer cell lines, the CC₅₀ of Tpz-1 was below 1 μM (**Table 2.1**). Additionally, Tpz-1 was noticeably less potent toward non-cancerous Hs27 cells.

Table 2.1. Cytotoxic concentration 50% (CC₅₀) of Tpz-1 in a panel of 17 cancer and 1 non-cancerous cell line at 24 h (top), 48 h, and 72 h (bottom) of exposure.

Hematological Cancer Cell Lines		
Cell Line	Origin	CC ₅₀ (μM ± St. Dev) ^a
CCRF-CEM	T-cell leukemia	0.74 ± 0.18 (24 h)
		0.25 ± 0.04 (48 h)
		0.19 ± 0.01 (72 h)
HL-60	Acute myeloid leukemia	0.95 ± 0.03 (24 h)
		0.63 ± 0.03 (48 h)
		0.27 ± 0.03 (72 h)
Ramos	Burkitt's lymphoma	0.30 ± 0.01 (48 h)
Jurkat	T-cell leukemia	0.41 ± 0.004 (48 h)
MOLT-3	T-cell leukemia	2.10 ± 0.14 (48 h)
NALM6	B-cell precursor leukemia	0.24 ± 0.002 (48 h)

MM.1S	Multiple myeloma	0.82 ± 0.08 (48 h)
MM.1R	Dexamethasone-resistant multiple myeloma	0.78 ± 0.02 (48 h)
U266	Multiple myeloma	0.93 ± 0.13 (48 h)
RPMI 8226	Multiple myeloma	0.33 ± 0.01 (48 h)
Non-Tumorigenic Cell Lines		
Hs27 *	Foreskin fibroblast	6.11 ± 0.03 (48 h)
		5.72 ± 2.29 (72 h)
Solid Tumor Cell Lines		
MDA-MB-231	Triple-negative breast adenocarcinoma	1.94 ± 0.19 (72 h)
MDA-MB-468	Triple-negative breast adenocarcinoma	0.80 ± 0.07 (72 h)
MCF7	ER+ breast adenocarcinoma	2.99 ± 0.67 (72 h)
COLO 205	Colorectal adenocarcinoma	0.93 ± 0.03 (72 h)
HT-29	Colorectal adenocarcinoma	0.91 ± 0.06 (72 h)
HeLa	Cervical adenocarcinoma	0.68 ± 0.04 (72 h)
SH-SY5Y	Neuroblastoma	0.21 ± 0.01 (72 h)

^a The CC₅₀ refers to the concentration at which 50% of the cell population dies after 24 h, 48 h, or 72 h Tpz-1 exposure; ± values denote standard deviations; * Indicate non-tumorigenic cell lines.

From the CC₅₀ values calculated at 48 h and 72 h, selective cytotoxicity index (SCI) scores were calculated by dividing the CC₅₀ of Hs27 cells by the CC₅₀ of individual cancer cell lines (**Table 2.2**). Very high selectivity (SCI ≥ 20.37) was observed in CCRF-CEM, Ramos, NALM6, HL-60, and SHSY-5Y cell lines, and scores were also favorable (SCI ≥ 2.0) across the other cancer cell lines we tested. Interestingly, the SCI for hematopoietic cells averaged 13.82; thus, in vitro specificity of Tpz-1 toward blood cancers exists. Of the hematologic cancer cell lines in our panel, Tpz-1 was most sensitive and selective

toward leukemias (SCI = 15.48). As a result of this selectivity, the cytotoxicity of Tpz-1 against HL-60 and CCRF-CEM cells was also evaluated via DNS at 24 h, and these cell lines were chosen as our in vitro models to assess Tpz-1's ability to induce apoptosis.

Table 2.2. Selective cytotoxicity index (SCI) values of Tpz-1 in 17 cancer cell lines at 48 h (top) and 72 h (bottom) of exposure.

Cell Line	SCI 48 h
CCRF-CEM	24.44
HL-60	9.70
Ramos	20.37
Jurkat	14.90
MOLT-3	2.91
NALM6	25.46
MM.1S	7.45
MM.1R	7.83
U266	6.57
RPMI 8226	18.52
Cell Line	SCI 72 h
CCRF-CEM	30.11
HL-60	21.19
MDA-MB-231	2.95
MDA-MB-468	7.15
MCF7	1.91
COLO 205	6.15
HT-29	6.29
HeLa	8.41

2.6.3. Tpz-1 Triggers Movement of Phosphatidylserine to the Outer Plasma Membrane

Tpz-1 treatment caused significant translocation of phosphatidylserine (PS) to the outer leaflet of cell plasma membranes after 24 h, a hallmark event of apoptosis [67]. To distinguish between apoptotic and necrotic cell death, we performed an Annexin V-FITC/PI assay. The Annexin V protein (~36.8 kDa) is a high-affinity ligand of PS, which, when conjugated to the fluorophore fluorescein-5-isothiocyanate (FITC), can be readily detected by flow cytometry when bound to PS. In this experiment, cells in the early stages of apoptosis were distinguished by their emission of FITC signal. In contrast, membrane-compromised late-stage apoptotic and necrotic cells were detected by propidium iodide (PI); those positive for both FITC and PI were considered apoptotic, and those only positive for PI were deemed necrotic. Our results showed significant PS translocation after 24 h of exposure to Tpz-1 at the predicted 24 h CC_{50} and $2xCC_{50}$ concentrations (HL-60 $p < 0.001$, **Figure 2.3a**; CCRF-CEM $CC_{50} p < 0.05$ and $2xCC_{50} p < 0.001$, **Figure S2.1a**), suggesting that the primary mode of cell death for this compound is apoptosis.

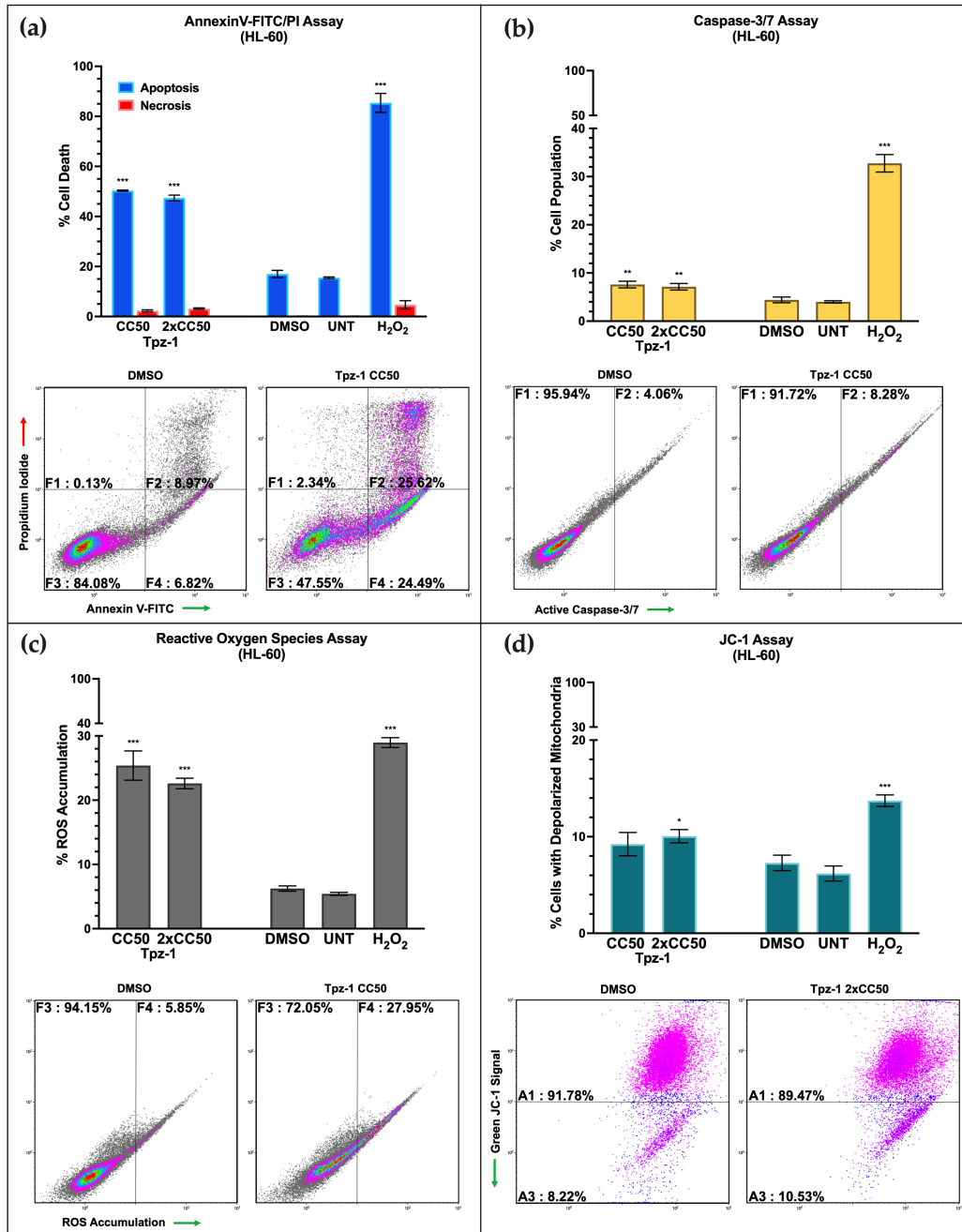


Figure 2.3. The intrinsic apoptosis pathway mediates Tpz-1-induced cell death.

(a) Analysis of phosphatidylserine externalization by flow cytometry showed apoptosis induction in HL-60 cells after 24 h of exposure to CC₅₀ (0.95 μM; $p < 0.00001$) and 2xCC₅₀ (1.9 μM; $p < 0.00001$) concentrations of Tpz-1. The percentages displayed represent total (early and late) apoptosis values. **(b)** Flow cytometry analysis indicated

that Tpz-1 CC_{50} (0.95 μ M; $p = 0.00646$) and $2xCC_{50}$ (1.9 μ M; $p = 0.005941$) concentrations induced significant caspase-3/7 activation after 6 h of incubation in HL-60 cells. Positive fluorescence for NucView 488 Caspase-3/7 substrate indicated caspase-3/7 activation. **(c)** Tpz-1 causes reactive oxygen species accumulation in HL-60 cells at CC_{50} (0.95 μ M; $p = 0.000139$) and $2xCC_{50}$ (1.9 μ M; $p < 0.00001$) concentrations. ROS was quantified using the carboxy- H_2DCFDA reagent. **(d)** Tpz-1 disrupted mitochondrial membrane potential in HL-60 cells after 5 h of incubation. A modest but significant increase in depolarized mitochondria was seen in cells treated with Tpz-1 $2xCC_{50}$ (1.9 μ M; $p = 0.029193$). Mitochondrial depolarization was quantified using the JC-1 dye; an increase in green fluorescent signal denoted loss of membrane potential. **(a–d)** Cells were treated with the 24 h CC_{50} (0.95 μ M) or $2xCC_{50}$ (1.9 μ M) for the HL-60 cell line, and 1% v/v DMSO or 1 mM H_2O_2 as vehicle and positive controls for cytotoxicity, respectively. Untreated (UNT) controls were also included. The percentages and standard deviations represent the average of three technical replicates. Representative density plots for each experiment are shown. Statistical analysis was achieved by two-tailed Student's paired t -test, and the asterisk annotations represent the statistical significance of the treatments against the vehicle control; (*) $p < 0.05$, (**) $p < 0.01$, (***) $p < 0.001$.

2.6.4. Tpz-1 Induces Caspase-Dependent Apoptosis

To support our evidence that Tpz-1 induces apoptosis, caspase-3/7 activation was measured in CCRF-CEM and HL-60 cells by flow cytometry. Caspase-3/7 is an integral part of the intrinsic and extrinsic pathway machinery; therefore, cells were treated with the CC_{50} or $2xCC_{50}$ of Tpz-1 for 6 h (both cell lines) or 8 h (CCRF-CEM only) to sufficiently

stimulate apoptosis before staining for cleaved caspase-3/7 and to optimize fluorophore signal intensity. Our results revealed a modest but significant activation of caspase-3/7 in the two Tpz-1 treatments (HL-60 $p < 0.01$; CCRF-CEM $p < 0.05$) compared to vehicle-treated control samples at 6 h (**Figures 2.3b and S2.1b**). Decreased caspase-3/7 activation was observed at the 8 h time point in CCRF-CEM cells (**Figure S2.2**), indicating that peak caspase-3/7 activation occurs closer to 6 h after treatment. Similarly, to determine if Tpz-1 stimulates extrinsic apoptosis, we evaluated for the activation of the key initiator, caspase-8; however, we did not detect an increase in activity after 4 h of treatment (**Figure S2.3**). Together, this data puts forth intrinsic apoptosis as a probable mode of cell death inflicted by Tpz-1.

2.6.5. Tpz-1 Causes Cell Stress through an Accumulation of Reactive Oxygen

Species

Reactive oxygen species (ROS) indicate cellular homeostatic disturbance, and their accumulation promotes apoptosis [68]. To assess for physiological damage inflicted by Tpz-1, ROS accumulation was quantified with the carboxy-H₂DCFDA reagent and analyzed by flow cytometry. Accumulation of ROS in HL-60 and CCRF-CEM cells was assessed after exposure to the 24 h CC₅₀ or 2xCC₅₀ of Tpz-1 for 18 h. Significant ROS accumulation in Tpz-1 treated samples was evident ($p < 0.001$; **Figures 2.3c and S2.1c**), suggesting the contribution of oxygen radicals to apoptosis.

2.6.6. Tpz-1 Treatment Disrupts Mitochondrial Function

The intrinsic apoptosis pathway is associated with mitochondrial outer membrane permeabilization that drives the release of ROS and pro-apoptotic proteins from mitochondria [63,69]. Therefore, we investigated the loss of mitochondrial membrane

integrity using the JC-1 reagent. The JC-1 dye enters and accumulates in functional mitochondria to form red fluorescent complexes. In contrast, in mitochondria that have lost membrane potential, the dye can no longer accumulate and emits green fluorescence. An increase in green emission signal can therefore distinguish compound-induced mitochondrial de-polarization. Our analysis revealed a slight but significant depolarization of mitochondria in HL-60 and CCRF-CEM cells after treatment with Tpz-1 ($p < 0.05$) for 5 h (**Figures 2.3d and S2.1d**). This data additionally supports the involvement of the intrinsic pathway of apoptosis.

2.6.7. Tpz-1 Cell Death Is Restricted to Cells in the G2/M Phase

To assess the dependence of Tpz-1 activity on the cell cycle, phase distribution was evaluated in HL-60 and CCRF-CEM cells after treatment with the 24 h $\frac{1}{4}\times\text{CC}_{50}$ or $\frac{1}{2}\times\text{CC}_{50}$ Tpz-1 for 72 h. Low concentrations of Tpz-1 were used to minimize the interference of fragmented DNA in our assessment. Samples were stained with a nuclear isolation medium containing the fluorophore DAPI (NIM-DAPI) post-incubation. In this assay, the DAPI signal is proportional to the amount of cellular DNA at each phase. Thus, its emission was used to quantify the DNA content in each sample by flow cytometry. As predicted, a significant increase in DNA fragmentation (represented by the sub-G0/G1 phase) was evident in both HL-60 and CCRF-CEM and denoted the apoptotic population in each sample ($\frac{1}{4}\times\text{CC}_{50}$ $p < 0.05$; $\frac{1}{2}\times\text{CC}_{50}$ $p < 0.001$). Although DNA fragmentation was successfully attenuated in HL-60 cells (~10% of the population), the sub-G0/G1 population was twice as large in CCRF-CEM (~20%). A decrease in the G2/M phase was seen in HL-60 cells treated with Tpz-1, revealing an inverse relationship between Tpz-1 treated cells in the sub-G0/G1 and G2/M stages of cell division (**Figure 2.4**). These results

establish a potential connection between Tpz-1 activity and cells as they prepare for mitosis. However, the overabundant DNA fragmentation in the CCRF-CEM cell line made it difficult to distinguish the different cell populations (**Figure S2.4**), and so it remains unclear if this phenomenon is shared or unique to HL-60 cells.

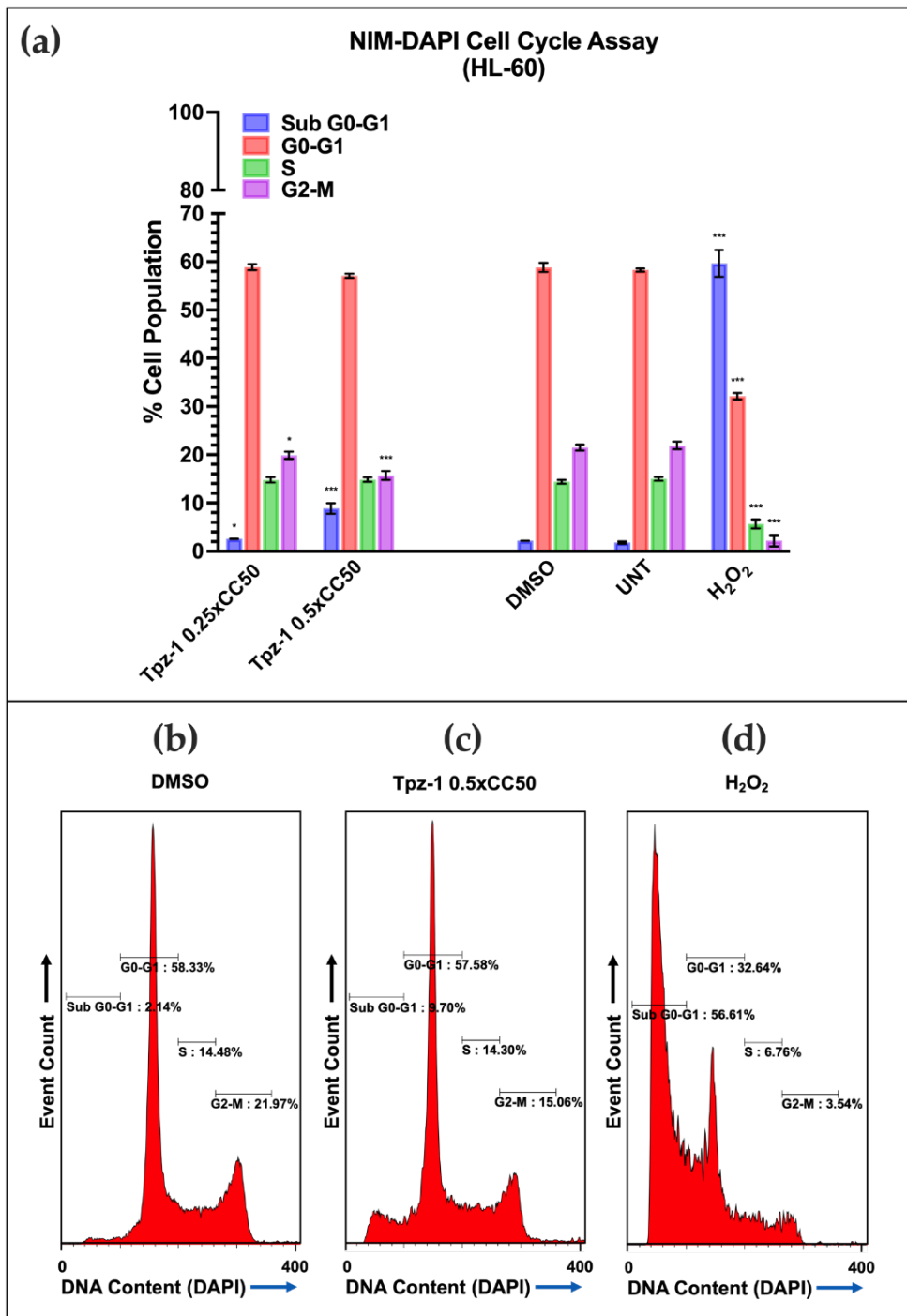


Figure 2.4. Tpz-1 cytotoxicity is G2-M phase-dependent in HL-60 cells after 72 h of exposure.

(a) Cells were treated with the 24 h 0.25xCC₅₀ (0.24 μM; Sub G0-G1 $p = 0.047421$; G2-M $p = 0.046939$) or 0.5xCC₅₀ (0.48 μM; Sub G0-G1 $p = 0.000484$; G2-M $p = 0.000873$). NIM–DAPI was used to stain and quantify the DNA content of each sample. Tpz-1-treated cells displayed DNA fragmentation, denoted by an increase of cells in sub G0-G1, that was concurrent with a loss of cells in G2/M. 0.1% v/v DMSO and 100 μM H₂O₂ were utilized as vehicle and positive controls for cytotoxicity, respectively. Untreated (UNT) controls were also included. The percentages and standard deviations represent the average of three technical replicates. **(b–d)** Representative histograms for DMSO, 0.5xCC₅₀ Tpz-1, and H₂O₂ treated samples. Statistical analysis was achieved by two-tailed Student's paired *t*-test, and the asterisk annotations in each graph represent the statistical significance of the treatments against the vehicle control; (*) $p < 0.05$, (***) $p < 0.001$.

2.6.8. Tpz-1 Interferes with Src and MAP Kinase Function

Protein kinases regulate many cellular functions, including proliferation, mitosis, apoptosis, and metabolism. Dysregulation of these processes is frequently oncogenic. Thus, there have been considerable efforts to develop small molecule kinase inhibitors to treat a variety of cancers. Kinase inhibitors remain a popular target in anticancer drug discovery today, and several have been approved for clinical use in recent years. Studies with other thienopyrazole-derivatives have also shown substantial kinase inhibition [41,44–46] prompting the need to assess Tpz-1's effect on a multi-pathway panel of human kinases. Changes in phosphorylation of Src and MAP kinases were assessed by

Multiplex Luminex assay using 0.01 μM or 0.1 μM Tpz-1-treated HL-60 cell lysates. Decreased median fluorescence intensity (MFI) was observed in MAP family kinases p38 (0.01 μM $p < 0.05$, 0.1 μM $p < 0.01$; **Figure 2.5**), CREB (0.01 μM $p < 0.05$, 0.1 μM $p < 0.01$; **Figure 2.5**), Akt (0.01 μM $p < 0.05$, 0.1 μM $p < 0.01$; **Figure 2.5**), and STAT3 (0.01 μM $p < 0.05$, 0.1 μM $p < 0.01$; **Figure 2.5**) and implies kinase hypophosphorylation; whereas increased MFI/hyperphosphorylation was evident in Src family kinases Fgr (0.01 μM and 0.1 μM $p < 0.05$; **Figure 2.5**), Hck (0.1 μM $p < 0.05$; **Figure 2.5**), and MAP kinase ERK 1/2 (0.01 μM and 0.1 μM $p < 0.05$; **Figure 2.5**).

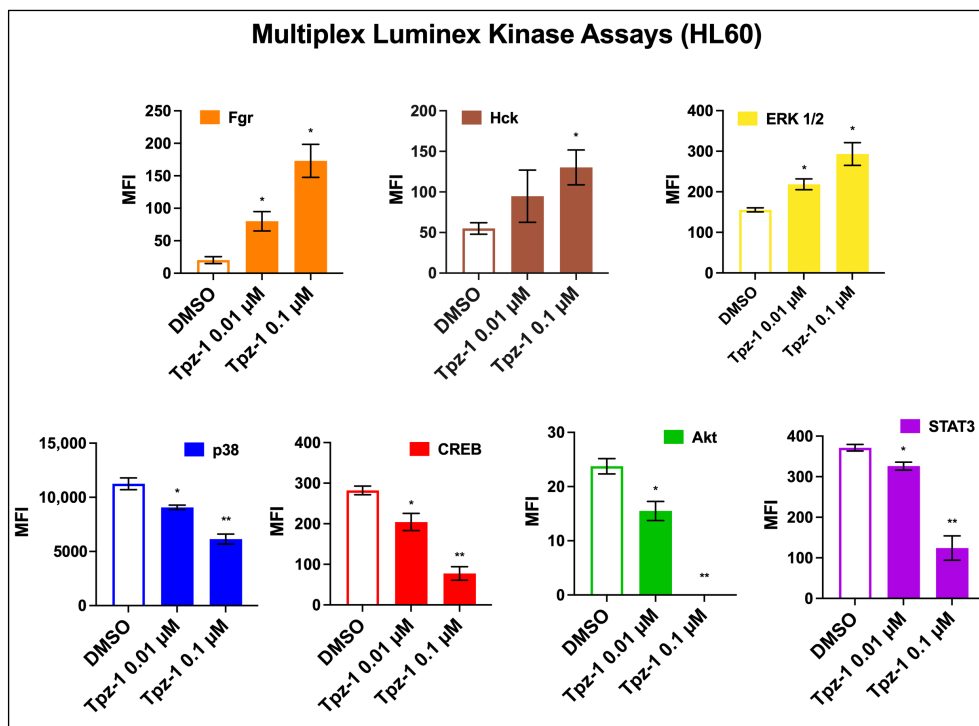


Figure 2.5. Tpz-1 interferes with Src and MAP pathway signaling in HL-60 cells after 3 h of exposure.

Cellular extracts from cells exposed to 0.01 μM Tpz-1, 0.1 μM Tpz-1, or 0.2% v/v DMSO were analyzed for changes in kinase phosphorylation via antibody/bead-based Luminex xMAP technology. The y-axis indicates median fluorescence intensity (MFI) and error

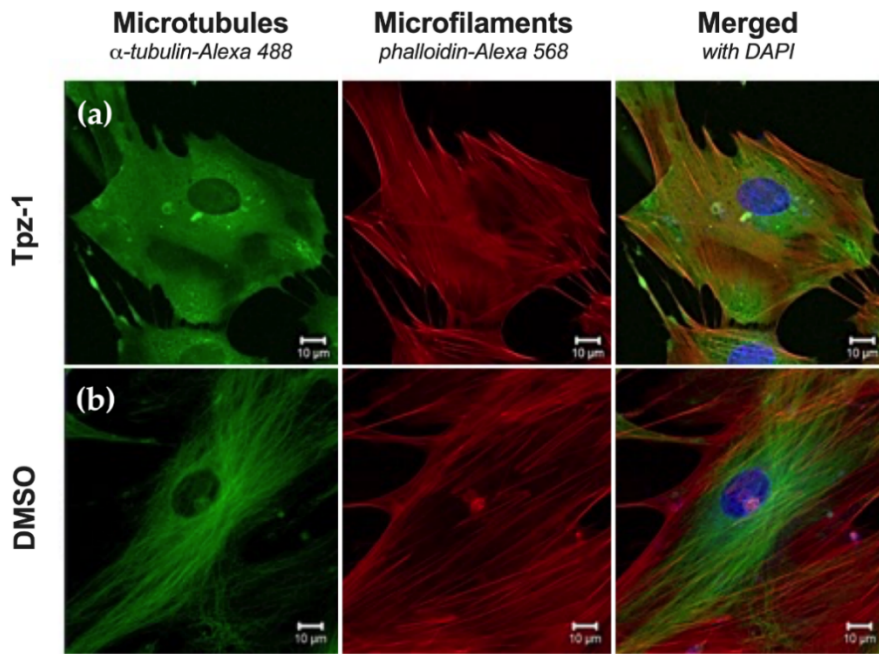
bars represent the standard deviations of the average of two technical replicates. Decreased MFI, implying kinase hypophosphorylation was evident in p38 (0.01 μM $p = 0.034225$; 0.1 μM $p = 0.009669$), CREB (0.01 μM $p = 0.043251$; 0.1 μM $p = 0.004603$), Akt (0.01 μM $p = 0.035648$; 0.1 μM $p = 0.002076$), and STAT3 (0.01 μM $p = 0.037819$; 0.1 μM $p = 0.00785$); whereas increased MFI, implying hyperphosphorylation was observed in Fgr (0.01 μM $p = 0.033102$; 0.1 μM $p = 0.014181$), Hck (0.1 μM $p = 0.0426$), and ERK 1/2 (0.01 μM $p = 0.024866$, 0.1 μM $p = 0.020551$). Statistical analysis was achieved by two-tailed Student's paired *t*-test, and the asterisk annotations in each graph represent statistical significance of the treatments against the vehicle control; (*) $p < 0.05$, (**) $p < 0.01$. Data acquisition and analysis was achieved via xPONENT 3.1 software (Luminex, Austin, TX, USA).

2.6.9. Tpz-1 Treatment Impedes Microtubule Organization

To ascertain the effect of Tpz-1 on the cytoskeleton and cell division, non-cancerous Hs27 and cancerous HeLa cell lines were treated and stained to visualize DNA content (DAPI; blue), actin microfilaments (Alexa 568; red), and microtubules (Alexa 488; green). Hs27 cells are large fibroblasts with an elongated shape, making them ideal for observing alterations in cytoskeletal organization; similarly, HeLa's rapid proliferation and large surface area renders them optimal for observing mitotic spindle changes.

For this experiment, Hs27 cells were treated with 10 μM Tpz-1, 5 $\mu\text{g/mL}$ Cytochalasin-D, 1 μM Paclitaxel, or 1% v/v DMSO for 4 h before fixation and staining. DMSO-treated cells were considered representative of canonical fibroblast morphology, consisting of elongated filaments of both actin and tubulin. Cytochalasin-D and Paclitaxel were used as controls to show microfilament and microtubule organization disruption,

respectively. Our analysis revealed a condensed morphology and interruption to microtubule assembly in Hs27 cells treated with Tpz-1 (**Figure 2.6**). Similarly, HeLa cells were treated for 24 h with 0.19 μM Tpz-1 or DMSO, Cytochalasin-D, or Paclitaxel controls at the concentrations indicated above. Images were captured at the same stage of mitosis for all treatments, with condensed chromosomes (DAPI; blue) convened at the equatorial plate. Treatment of HeLa with Tpz-1 resulted in multipolar spindle formation (**Figure 2.7**). Together these results point to Tpz-1 as a microtubule disrupting agent.



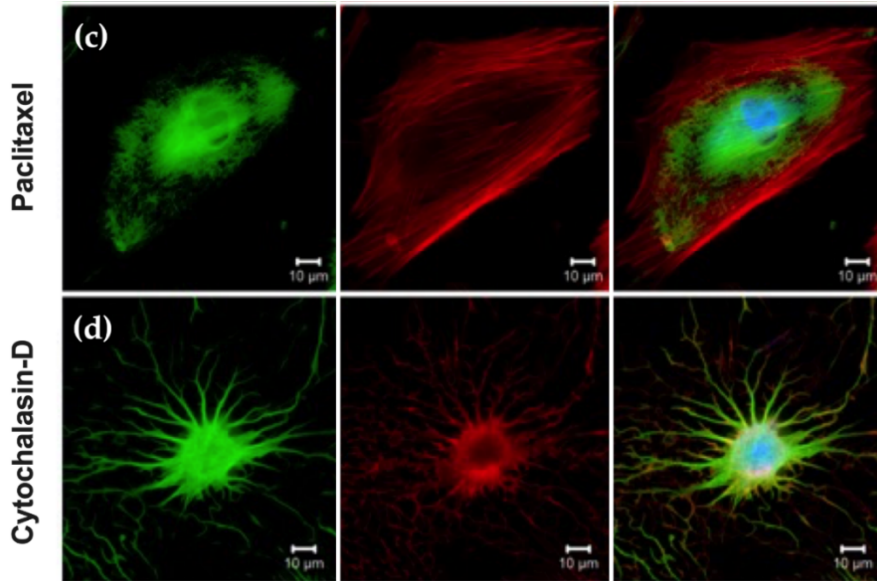


Figure 2.6. Tpz-1 (10 μ M) inhibits tubulin polymerization in Hs27 cells after 4 h of exposure.

(a) Tpz-1, **(b)** 1% v/v DMSO, **(c)** 1 μ M Paclitaxel, and **(d)** 5 μ g/mL Cytochalasin-D treated cells were stained with α -tubulin-Alexa-488 (microtubules), phalloidin-Alexa-568 (microfilaments), and DAPI (nucleus) prior to immunofluorescent analysis by confocal microscopy. DMSO was included as vehicle control, and Paclitaxel and Cytochalasin-D as microtubule and microfilament disruptive agents, respectively.

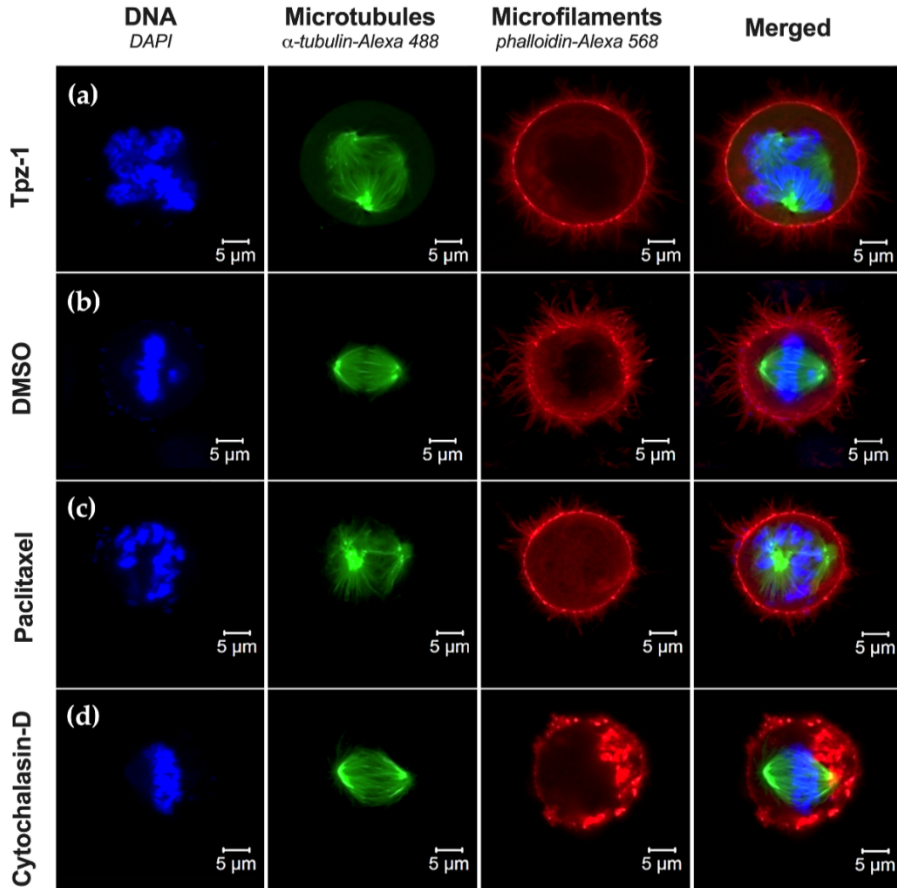


Figure 2.7. Tpz-1 (0.19 μ M) disrupts spindle formation and polarity in HeLa cells undergoing mitosis.

(a) Tpz-1, (b) 1% v/v DMSO, (c) 1 μ M Paclitaxel, and (d) 5 μ g/mL Cytochalasin-D treated cells were stained with α -tubulin-Alexa-488 (microtubules), phalloidin-Alexa-568 (microfilaments), and DAPI (nucleus) prior to examination by confocal microscopy. DMSO was included as vehicle control, and Paclitaxel and Cytochalasin-D as microtubule and microfilament disruptive agents, respectively. Only cells undergoing mitosis were imaged.

2.7. DISCUSSION

There remains an unmet need for targeted treatments to help patients of all ages with refractory and secondary acute leukemias [50,70–72]. This study identified a unique

thieno[2,3-c]pyrazole derivative, Tpz-1, that induced cell death of HL-60 acute myeloid leukemia cells at nanomolar concentrations. Apoptosis was validated as the primary mode of Tpz-1-induced cell death in HL-60 cells by detecting Annexin V-FITC bound to exposed phosphatidylserine at the cell surface (**Figure 2.3a**). In addition, caspase-8 inactivity (**Figure S2.3**) and statistically significant caspase-3/7 activation (**Figure 2.3b**), reactive oxygen species accumulation (**Figure 2.3c**), and loss of mitochondrial integrity (**Figure 2.3d**) were observed by flow cytometry after Tpz-1 exposure and suggest the involvement of the intrinsic apoptotic pathway in compound-induced cell death. Many of these markers for apoptosis were also evident to a comparable degree in the acute lymphocytic leukemia cell line CCRF-CEM (**Figures S2.1 and S2.2**). However, Tpz-1's effect on the cell cycle of CCRF-CEM remains unclear due to excessive DNA fragmentation at the tested concentrations (**Figure S2.4**).

Thienopyrazoles derivatives have well-documented anticancer activity, yet this class of compounds has been mostly ignored. As with their parent moieties, thienopyrazoles have been described in the literature as kinase inhibitors, anti-inflammatories, and receptor modulating agents [38–40]. Many previous studies have focused on the activity of thieno[3,2-c]pyrazole derivatives. However, thieno[2,3-c]pyrazole compounds are also emerging as desirable antitumor, antiviral, antimicrobial, and anti-inflammatory agents [42,45,46,73]. Furthermore, highly specific serine/threonine/tyrosine kinase, enzyme, and ligand-gated ion channel antagonist activity have been associated with thieno[2,3-c]pyrazoles [43,74–76]. As with similar thienopyrazole derivatives, Tpz-1 disrupted the activity of MAP and Src kinase pathways,

resulting in the decreased phosphorylation of p38, CREB, Akt, and STAT3 and hyperphosphorylation of Fgr, Hck, and ERK 1/2.

The MAP kinase (MAPK) pathway plays an essential role in extracellular signal transduction and is often dysregulated in many cancers. Cellular responses associated with MAPK cascades include proliferation, differentiation, and apoptosis [77]. After treatment with Tpz-1, we observed a change in phosphorylation of MAP-associated kinases ERK 1/2, STAT3, CREB, p38, and Akt (**Figure 2.5**). ERK 1/2 was one of three kinases hyperphosphorylated after treatment of cells with Tpz-1. ERK is an extracellular signal-regulated kinase whose activation canonically enhances proliferation by controlling cell cycle progression. However, ERK 1/2 activity has alternatively induced G2/M arrest and apoptosis [25,78,79], which we observed with Tpz-1 (**Figure 2.4**). Active ERK facilitates the transfer of extracellular signals to the nucleus by phosphorylation of transcription factors such as STAT3 and CREB. STAT3 and CREB are proto-oncogenes often persistently active in cancer, thus making them valuable therapeutic targets [80–82]. Despite our observed increase in ERK phosphorylation, STAT3 and CREB phosphorylation was decreased after treatment with Tpz-1. We theorize that this hypophosphorylation of STAT3 and CREB results from Tpz-1's concomitant antagonism of p38 and Akt, as STAT3 and CREB are also known downstream targets of p38 and Akt signaling pathways [83–86].

In addition, ERK plays a role in M-phase progression, chromosome alignment, and microtubule assembly [87,88]. Increased ERK phosphorylation by Tpz-1 could thus potentially disrupt microtubules and lead to mitotic spindle dysfunction. Together, this information suggests that ERK activity contributes to the G2/M phase-dependent

apoptosis (**Figure 2.4**) and microtubule/spindle disruption (**Figures 2.6 and 2.7**) we observed after exposing cells to Tpz-1.

The Src pathway plays an essential role in extracellular signal transduction, and its activation drives tumor progression and metastasis in many cancers. Fgr and Hck are blood cell-specific Src kinases that were hyperphosphorylated in cells exposed to Tpz-1 (**Figure 2.5**). Despite its reputation as a proto-oncogene, elevated Hck activity may act as a tumor suppressor in some leukemias, including AML [89,90], which is relevant to our use of HL-60 cells herein. Likewise, Fgr is constitutively active in many cancers but is also known for its ROS-dependent activation and promotion of healthy mitochondrial complex II function [91,92]. Therefore, our observed increase in Fgr phosphorylation could be attributed to ROS accumulation in cells exposed to Tpz-1 (**Figures 2.3c and S2.1c**).

Interestingly, in a previous search for small molecule mitotic inhibitors that induce apoptosis of multicellular tumor spheroids, Tpz-1 (compound 5248881) was also identified as a lead compound in a screen of over 10,000 molecules from the ChemBridge DIVERset library [47]. The authors revealed that 5248881 induced a similar expression pattern to well-known tubulin inhibitors, inhibited tubulin polymerization in vitro, and caused G2/M cell cycle arrest. Furthermore, this study also determined that 5248881 induced apoptosis by staining the spheroids for caspase-cleaved keratin-18 and active caspase-3 [47].

Our results did not show arrest but have shown that Tpz-1 interferes with the cell cycle (**Figure 2.4**), causes cell death and a concurrent loss of cells in the G2/M phase in the HL-60 cell line (**Figure 2.4a,c**), and damages the mitotic spindle of dividing cells

(**Figure 2.7**). Furthermore, another recently published study revealed that Tpz-1 (compound MTPC) could target tumors in mice by encapsulating the compound in gold nanorod-loaded PLGA-PEG nanoparticles [48]. Together, these previous publications and the current study support the continued development of Tpz-1 as a chemotherapeutic candidate.

In conclusion, Tpz-1 is a potent and cytotoxic thieno[2,3-c]pyrazole derivative with potent and specific anticancer activity in vitro. Despite compelling evidence of the diverse biological activity of thienopyrazoles, these findings have brought to light a scarcity of publications focused on this unique scaffold. While the contribution of the thienopyrazole moiety to Tpz-1's biological activity remains unknown, our data parallels previously studied thieno[2,3-c]pyrazoles. Research to further elucidate Tpz-1's mechanism of action is ongoing. Until then, we hope that this work inspires our colleagues to consider thienopyrazole-based compounds in small molecule anticancer drug formulations.

2.8. OPEN ACCESS

This article is published under an open access Creative Commons Attribution 4.0 International License (CC BY 4.0) which allows any part of the article, including tables and figures, to be shared and adapted for use in any medium provided that the original article is cited, a link to the license is available, and any changes are indicated. A copy of this license can be viewed at: <https://creativecommons.org/licenses/by/4.0/>.

CHAPTER 3: THE USE OF WEB-BASED BIOINFORMATIC PLATFORMS TO DISTINGUISH POTENTIAL TARGETS OF TPZ-1

3.1. OBJECTIVE

Tpz-1 was identified as a remarkably potent and specific in vitro anticancer agent with a unique thieno[2,3-c]pyrazole-derived structure. Tpz-1 induced cell death *via* mitochondrial apoptosis in HL-60 acute myeloid leukemia cells, as confirmed by in vitro phosphatidylserine externalization, caspase-3 activation, ROS accumulation, and mitochondrial depolarization (JC-1) flow cytometry assays. This chapter aims to expand on our knowledge of Tpz-1 by identifying potential targets and molecular mechanisms affected by treatment. To accomplish this, we utilize open access web-based data mining tools to evaluate and compare Tpz-1's chemical structure and the whole transcriptome changes Tpz-1 induced in HL-60 cells. The use of redundant bioinformatic tools was employed to enable more a robust prediction of the potential targets and metabolic effects of Tpz-1. These predictions are intended to inform the most reasonable next steps in the biological evaluation and optimization of this highly potent cancer-specific cytotoxic compound.

3.2. ABSTRACT

This chapter analyzes the potential molecular targets and pathways affected by novel thienopyrazole derivative Tpz-1. To accomplish this, we compared the in vitro performance of Tpz-1 to the predictions of a total of six structure or gene expression-based open access in silico platforms. Our analysis revealed that morphological changes begin to occur within 6 hours of 0.05 μM Tpz-1 exposure in HeLa H2B-GFP cells, and cell behavior is consistent with disrupted cytoskeletal and extracellular matrix

interactions. Our in silico results showed an effect of Tpz-1 on cancer cell survival, metabolism, proliferation, and mitosis primarily through the discoordination of cytoskeletal dynamics and the deprivation of cells from the receipt and transmission of extracellular signals. However, SwissADME pharmacokinetic analysis revealed that the structure of Tpz-1 presents some risk for human toxicity and must therefore be optimized to enhance the biological effects we have predicted. This study pinpoints functional annotation data derived from whole transcriptome and structure-based analyses that can be helpful in the design of Tpz-1 analogs. From an early drug discovery perspective, this study also offers biologists a statistically robust and modern approach to deconvoluting the biological targets of novel compounds that arise from phenotypic screenings.

3.3. INTRODUCTION

Tpz-1 is a cytotoxic thieno[2,3-c]pyrazole derivative that potently induces apoptosis [47], alters MAP/Src kinase phosphorylation, and disrupts microtubule/mitotic spindle dynamics [93] at micromolar concentrations. Our in vitro experiments revealed that Tpz-1 activity was largely consistent with the activity of other thienopyrazole derivatives, thus we utilized web-based bioinformatic tools to analyze the drug-likeness of Tpz-1's structure and the genome-wide transcriptional changes induced by our compound. The goal of this study was to identify potential structure-function relationships and elucidate the most likely molecular mechanism(s) of Tpz-1.

Target prediction is an important milestone in early preclinical drug development and can help guide future drug optimization efforts and discern potential toxicities associated with compound metabolism or the identified target [94,95]. While the target

of Tpz-1 could be distinguished by traditional wet-lab techniques, in silico target prediction (target fishing) methods have gained momentum as reliable computational alternatives [95]. Ligand-based target fishing methods are centered around small molecules' structure and assume similarly structured molecules will have a similar biological effect. Conversely, structure-based methods rely on information about protein structure and assume that similar proteins will have similar ligand affinity [95].

The present target prediction study of Tpz-1 aims to take a well-rounded approach, utilizing open-source computational tools to elucidate potential mode(s) of action based on the canonical SMILES chemical structure and differential gene expression (whole transcriptome) data collected from HL-60 cells exposed to our compound. Additionally, because of its unique and understudied thieno[2,3-c]pyrazole structure, text mining was employed to establish similarities between Tpz-1 and biomedical literature concerning antineoplastic thiophene and pyrazole-based compounds, as together, these groups form the thienopyrazole moiety and appear significant to Tpz-1's biological activity [93]. In a previous study by Fayad et al. [47], Tpz-1 (compound 5248881) was shown to inhibit tubulin polymerization similar to the known mitotic inhibitor drug Colchicine at concentrations above 2.5 μM ; however, this effect was not observed at lower concentrations, suggesting that cytotoxicity could be driven by other mechanisms at lower concentrations. Overall, the morphology of Tpz-1-treated cell mitotic spindles, apparent G2/M phase-selective cytotoxicity of the drug, and widespread gene expression changes observed in our whole transcriptome analysis at concentrations < 1.0 μM revealed that post-translational Aurora kinase inhibition is the purported primary target of the molecule at concentrations below 2.0 μM . Additional in

silico and biochemical assays are thus required to validate the interaction of Tpz-1 with Aurora kinase; these experiments are currently pending completion.

3.4. MATERIALS AND METHODS

3.4.1. Morphology of Tpz-1-treated cancer cells

3.4.1.1. Timelapse Microscopy

To assess the effect of Tpz-1 on the morphology of treated cells, the histone 2B-GFP expressing HeLa (H2B-GFP) cell line was utilized. The cells were cultured from a cell stock acquired from Dr. Anita Quintana's laboratory at The University of Texas at El Paso. Cells were cultured in DMEM medium supplemented with 10% FBS, antibiotics, and in a manner consistent with our other in vitro analyses with Tpz-1 [93].

Upon reaching 80-90% confluence, cells were detached from their vessel and seeded into thin-bottom 96-well microplates at a density of 4,000 cells per well; the plate was then incubated overnight to permit cell attachment. The next day, the ImageXpress Pico automated cell imaging system (Molecular Devices, San Jose, CA, USA) was prepped for the time-lapse experiment by attaching the environmental cassette, setting the ambient conditions to 37 °C and 5% CO₂ using the instrument's web-based IN Carta image analysis software, and allowing the cassette to reach optimal ambient temperature and gas before introducing the plate of cells.

Once ready, the plate was secured into the cassette, and the 40x objective was focused to the bottom of the well in the smallest imaging area permitted by the instrument. The cells were then treated with 0.2 μM, 0.1 μM, or 0.05 μM Tpz-1 or controls (1% v/v DMSO, 1mM H₂O₂, and untreated) and immediately imaged on the bright field and GFP channels to visualize the whole cell and histones, respectively.

Images of each well were acquired every 15 minutes for 30 hours to capture a full round of cell division. The resulting images and timestamps of the corresponding elapsed time were compiled into an mp4 video in IN Carta.

3.4.2. Tpz-1 target identification by transcriptomics

3.4.2.1. RNA Extraction

HL-60 cells were seeded at a density of 2,000,000 cells per mL in a 24-well plate and treated with 2x the 24-hour CC₅₀ of Tpz-1 or vehicle control for 6 h before RNA extraction. Qiagen's RNeasy Mini Kit was used and its enclosed RNA isolation protocol was followed. After extraction, a NanoDrop spectrophotometer (ThermoFisher, ND-ONE-W) was used to verify the quality and quantity of RNA; only samples with A260/A280 ratios above 1.8 were considered for transcriptome analysis.

3.4.2.2. Whole Transcriptome and CuffDiff Analysis

For whole transcriptome analysis, cDNA library preparation, sequencing, RNA-seq data quality control, timing, alignment, reads quantification, and CuffDiff differentially expressed gene (DEG) analysis the published protocols for experimental compound P3C were uniformly followed [35]. Only DEGs with log₂ fold change (log₂FC) > 2.0 or < -2.0 and *p*-value = 5e-05 were considered significant. All sequencing, alignment, and differential gene expression data was collected by the Genomic Analysis Core Facility at UTEP. All biological interpretations of the data were carried out by the author.

3.4.2.3. Database for Annotation, Visualization, and Integrated Discovery (DAVID)

The Database for Annotation, Visualization, and Integrated Discovery (DAVID) web-based platform consists of functional annotation tools that are powered by the

DAVID Knowledgebase (v2022q1) and enable users to investigate the biological meaning of gene lists [96–98]. The DAVID platform was utilized to visualize Tpz-1's differential gene expression profile ($p = 5e05$) on KEGG PATHWAY maps. To perform the analysis, official gene symbols obtained from CuffDiff analysis were uploaded to DAVID, and the 'Functional Annotation Tool' was selected. From the results, a chart of relevant KEGG pathways was generated and terms with Benjamini adjusted p -value < 0.05 were considered significant [99]. For each KEGG pathway, the DAVID Pathway Viewer was used to overlay genes on pathway maps and indicate affected components.

3.4.2.4. KEGG PATHWAY Database

The Kyoto Encyclopedia of Genes and Genomes (KEGG) PATHWAY database contains a collection of molecular interaction/reaction diagrams and can be used to map genes in a network [100]. The KEGG PATHWAY database was accessed *via* the DAVID platform to gain a preliminary understanding of Tpz-1 activity, and to obtain cell death pathways. Red stars (downregulated DEGs) and blue stars (upregulated DEGs) were manually added to the cell cycle, apoptosis, autophagy, and necroptosis maps to indicate affected components of each pathway.

3.4.2.5. ConnectivityMap

CLUE (<https://clue.io>) is a free cloud-based platform developed by the Broad Institute that allows users to analyze complex gene expression datasets [101]. The CLUE ConnectivityMap (CMap) database is loaded with over 1 million gene expression profiles from 80,000+ genetic and small molecule substances that disrupt cellular processes (perturbagens).

The CMap Query application is a resource that enables users to compare gene expression signatures of experimentally-treated human cells with the signatures of perturbagens in the database using the L1000 assay [102]. L1000 is a robust high-throughput gene expression assay developed at the Broad Institute and funded in part by the Library of Integrated Network-Based Cellular Signatures (LINCS) Program. In the L1000 assay, DEGs of experimental samples are compared to the > 1 million signature '1.0' and/or the 'Latest' > 3 million signature versions of the CMap LINCS database. The application permits analysis of a maximum of 150 upregulated genes and 150 downregulated genes; however, the relationships identified in the L1000 assay have shown approximately 80% similarity to direct mRNA measurements [102]. Highly similar gene expression (positive connections) suggest the experimental treatment and perturbagen may exert similar effects on a cell [101].

For this analysis, the significantly upregulated ($> 2.0 \log_2\text{FC}$) and downregulated ($< -2.0 \log_2\text{FC}$) genes ($p = 5e-05$) from CuffDiff were sorted from greatest to least \log_2 fold change, and the top 150 genes from each list were isolated for CMap Query analysis. Genes from the list that were 'invalid' were searched against the HGNC (HUGO Gene Nomenclature Committee; <https://genenames.org>) database and modified to reflect their current HUGO symbol [103]. Additionally, genes deemed 'valid but not used in query' were removed because they fell outside of the Best Inferred Gene (BING) space. The BING space reflects the subset of genes used by the Query application to compute similarities between experimental gene sets and expression signatures in the CMap database [101]. The removed genes were replaced with the next gene in each list with the greatest $\log_2\text{FC}$ value until there were 150 valid genes in

both up- and down-regulated queries. We individually queried the '1.0' version of the CMap database with these modified up- and down-regulated gene lists.

CMap Query results were rank-ordered by positive Connectivity Score (τ), and perturbagens with a summary score ≥ 95.00 were considered significantly connected to our experimental treatment. CMap connectivity scores are a standardized value that indicates the similarity of an experimental gene set to the expression signatures of reference perturbagens. Scores ≥ 95.00 indicate the connectivity between experimental DEGs and a given perturbagen is stronger than 95% of all reference signatures in the CMap database [101,102]. To enhance the robustness of our results, the summary CS across all cell lines was used; red/orange color was used to indicate $\tau \geq 95.00$.

3.4.2.6. Ingenuity Pathway Analysis (IPA)

The web-based IPA software (build version 389077M, Qiagen, Redwood City, CA) was used to separately analyze lists of the top 100 up- and down-regulated DEGs and their corresponding fold-change values that we obtained from whole transcriptome analysis [35,104,105]. The genes for each list were selected by sorting according to most positive or most negative fold-change value. All 200 mRNAs were successfully mapped. In this analysis, the Ingenuity Pathway Analysis (IPA) 'Core Analysis' function was used to compare the molecules in our Tpz-1 experimental datasets to the Qiagen Knowledge Base for the purpose of identifying significant associations with diseases, pathways, upstream regulators, and biological functions (entities).

Built-in IPA features such as Canonical Pathway, Causal Network Analysis, Upstream Regulator Analysis, and Graphical Summary were utilized. The statistical significance of each associated entity is represented by p -value and/or z -score. P -values

were calculated by right-tailed Fisher's exact test, and values < 0.05 indicate significant and non-random overlap between experimental data and the Knowledge Base. In contrast, z-scores indicate a prediction of activation or inhibition of a given disease, function, or upstream regulator; entities with scores ≥ 2 are predictive of activation and ≤ -2 of inhibition. Additionally, a $-\log(p\text{-value})$ of 1.3 was used as the threshold of statistical significance ($p < 0.05$) in canonical pathway bar charts.

Coloration indicates an entity's z-score: orange for activation, blue for inhibition, white for z-score = 0, and gray for no activity pattern available. Ingenuity's Target Explorer [106] was subsequently used to investigate the biological relationships and interaction networks of each entity. Although similar to ConnectivityMap, the primary difference is that IPA predicts biological relationships between our experimental data and published literature in the Qiagen Knowledge Base, whereas ConnectivityMap derives predictions from in vitro (L1000) assays.

This IPA experiment was performed in collaboration with Dr. Sourav Roy's laboratory at The University of Texas at El Paso. The author was responsible for providing the differential gene expression lists and interpreting the IPA data.

3.4.3. Tpz-1 target identification by chemical structure

3.4.3.1. SMILES Chemical Notation

We used the canonical Simplified Molecular Input Line Entry System (SMILES) notation to denote the chemical structure of compound Tpz-1 (IUPAC name: N-[(E)-(2-methoxyphenyl)methylideneamino]-3-methyl-1-phenylthieno[2,3-c]pyrazole-5-carboxamide; PubChem CIDs: 5331400/5443760/1125175; PubChem SID: 331572 [107]; ChemBridge ID: 5248881 [47]; MTPC [48]). The canonical SMILES string for Tpz-

1, CC1=NN(C2=C1C=C(S2)C(=O)NN=CC3=CC=CC=C3OC)C4=CC=CC=C4, was obtained from PubChem.

3.4.3.2. ChEMBL

The ChEMBL database (<http://ebi.ac.uk/chembl/>), curated by the European Molecular Biology Laboratory European Bioinformatic Institute (EMBL-EBI), contains over 2 million distinct bioactive molecules and their corresponding chemical, bioactivity, and genomic information [108,109]. The ChEMBL ‘Compound Report Card’ for Tpz-1 (ChEMBL4441641) and other similar molecules were accessed in an effort to identify potential targets and related publications.

3.4.3.3. SwissDrugDesign

SwissDrugDesign is an in silico drug design project supported by the Swiss National Science Foundation and Swiss Institute of Bioinformatics that provides several free and web-based tools to aid in virtual small molecule screenings. The tools that were used in our analysis of Tpz-1 were SwissTargetPrediction, SwissSimilarity, and SwissADME. The canonical SMILES chemical structure notation for Tpz-1 was used for all three platforms.

SwissTargetPrediction (<http://www.swisstargetprediction.ch>) is an online ligand-based target prediction tool that aims to predict the most probable protein target of a small molecule based on its similarity with known experimentally active compounds [110]. The prediction is based on the combined 2D and 3D similarity of a query molecule to a library of over 327,000 bioactive molecules on more than 2,000 human protein targets [110]. SwissTargetPrediction probability values indicate the probability of a given molecule to have a given protein as its target and are calculated from the

Combined-Scores of the most similar bioactive molecules ('known actives') with activity against each target. A Combined-Score of > 0.5 indicates a high probability of the queried molecule targeting a given protein. Proteins are ranked by their probability of being a true target (shown as green bars); 'known actives (3D/2D)' denotes the number of known bioactive molecules with 3D/2D similarity to the query molecule.

SwissSimilarity (<http://www.swisssimilarity.ch>) is a ligand-based tool that retrieves compounds similar to a queried molecule [111]. The output of SwissSimilarity can be used to study structure-activity relationships, as molecules with high similarity scores are generally expected to target the same proteins as the query molecule. Similarity scores on the platform range from 0 for totally dissimilar to 1 for identical compounds. In this analysis, the molecular structure of Tpz-1 was compared to bioactive compounds in the full ChEMBL bioactivity database (2,059,285 molecules) using a combined 2D and 3D ligand-based screening method.

SwissADME (<http://swissadme.ch>) is another tool which predicts the physicochemical, pharmacokinetic, druglikeness, and medicinal chemistry properties of queried molecules using lipophilicity iLOGP [112] and gastrointestinal absorption/brain penetration BOILED-Egg [113] models. This platform enables the early virtual assessment of absorption, distribution, metabolism, and excretion (ADME) properties of molecules that are in the discovery phase (i.e. Tpz-1) to help identify poor pharmacokinetic properties that could lead to the drug's clinical failure [114].

3.4.3.4. COREMINE Medical Text Mining

To assess for potential connections in the literature between thiophenes, pyrazoles, neoplasms, and Tpz-1's biological activity, the PubGene COREMINE

Medical text mining application was used to present the relationship between these terms as a graphic network (<http://www.coremine.com/medical>). Thienopyrazole was not an available search term, thus its parent thiophene and pyrazole rings were queried in the context of cancer (neoplasms). The COREMINE Medical platform documents connections between terms by mining the biomedical literature of the MEDLINE database [115]. Associations between ‘thiophenes’, ‘pyrazole compound’, and ‘neoplasms’ were extracted from literature that co-mentioned all three terms. In addition, all available years of published articles were mined in our search. Only gene/protein, molecular function, drug, and biological process category results with significance scores < 0.05 were considered in our analysis [115–117].

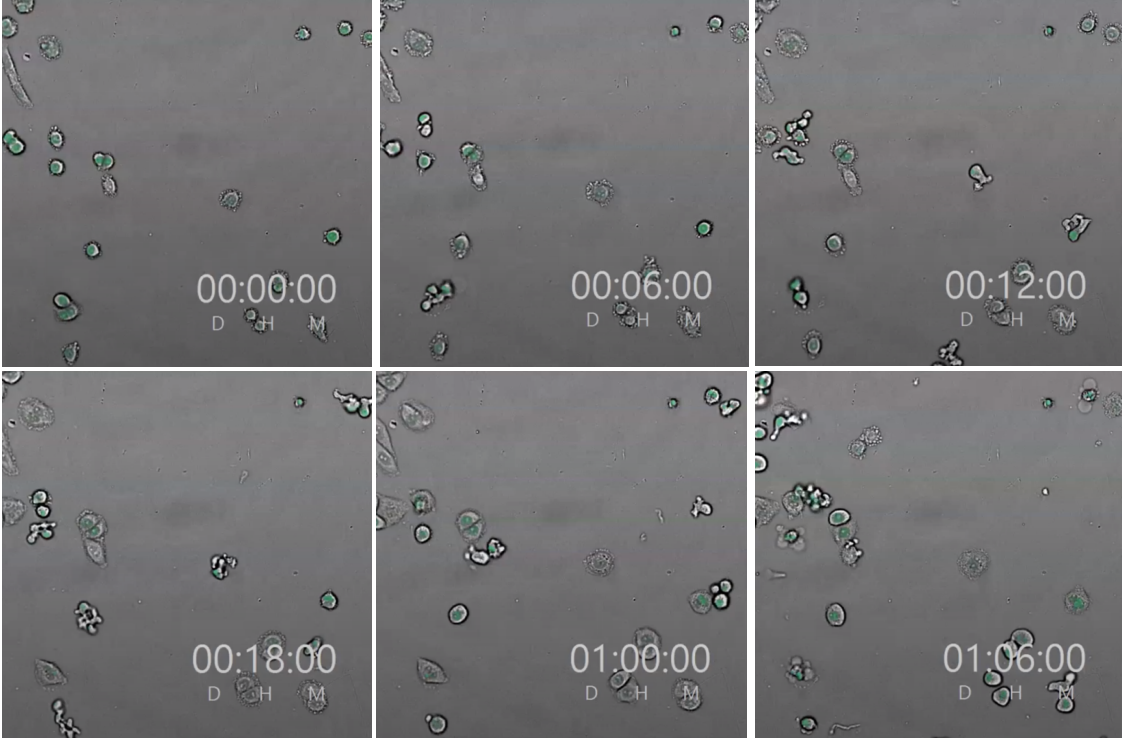
3.5. RESULTS

3.5.1. Timelapse microscopy revealed morphological changes associated with Tpz-1 treatment

In the images shown for this experiment, the green-colored area of each cell depicts the localization of histone H2B to approximate the organization of chromatin. Cells treated with 0.10 μ M and 0.05 μ M doses of Tpz-1 began to display significant changes in morphology between 6 and 12 hours of treatment. Treated cells dissociated from the bottom of the culture vessel and adopted an elongated structure that varied between cells but was evident at both Tpz-1 concentrations (**Figure 3.1a,b**). This elongated cellular shape was associated with aberrant cytokinesis, with cells forming more than two daughters or failing to separate fully. Additionally, mitosis of these odd-shaped cells was severely delayed compared to 1% v/v DMSO and untreated controls

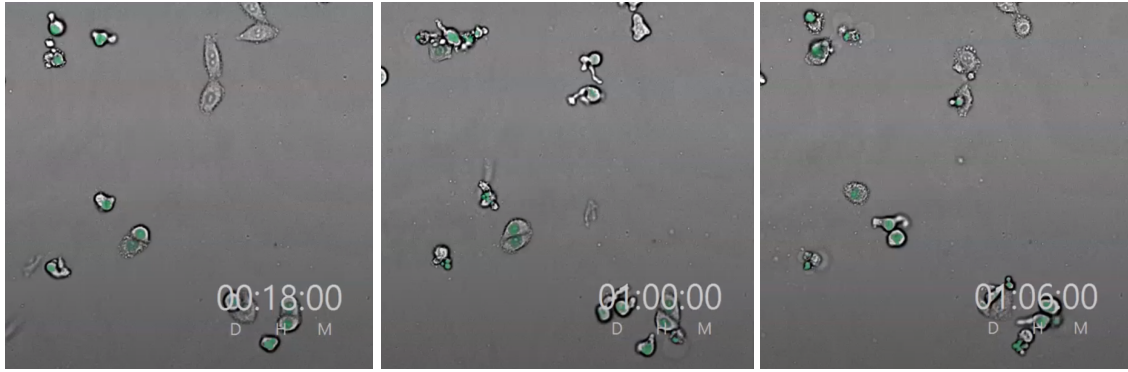
(Figure 3.1a-d). Furthermore, some affected cells appeared to readily fragment and float around to form conglomerates of cellular debris.

(a) **Tpz-1 0.10 μ M**

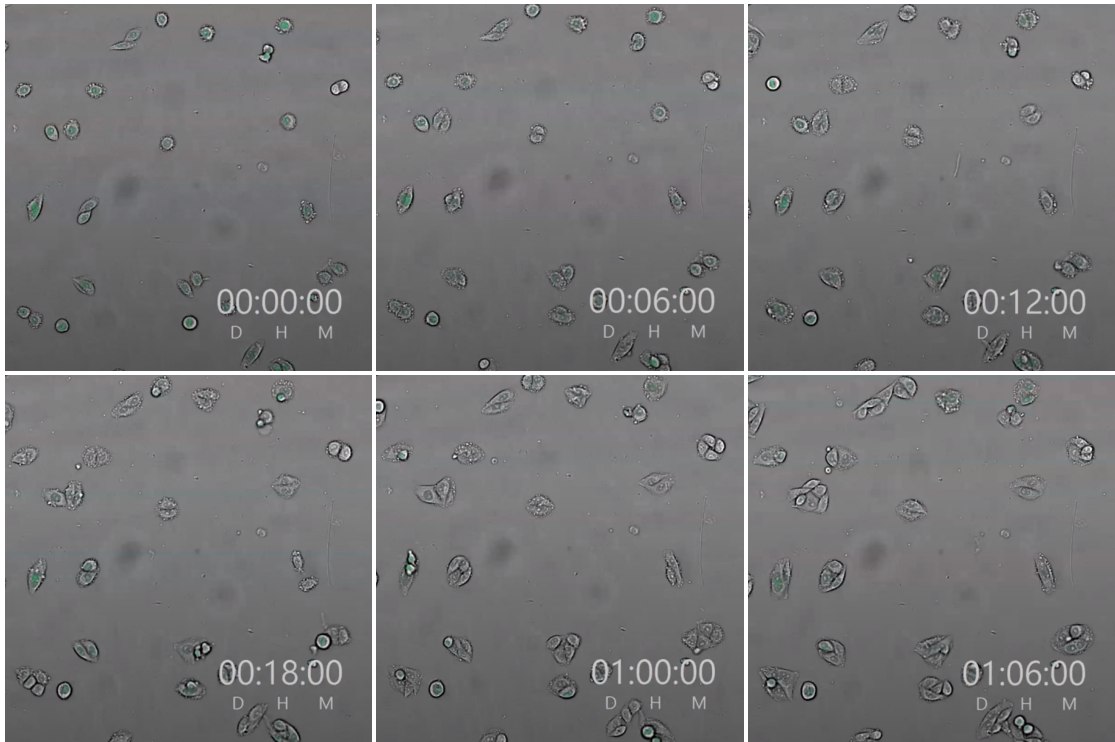


(b) **Tpz-1 0.05 μ M**





(c) Untreated



(d) 1% v/v DMSO

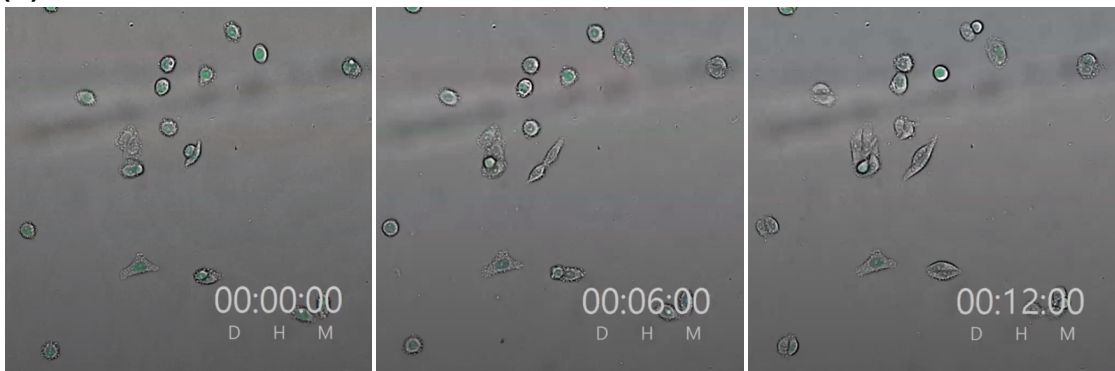




Figure 3.1. Morphological changes in HeLa H2B-GFP cells treated with Tpz-1 for 30 hours. **(a)** 0.1 μM Tpz-1; **(b)** 0.05 μM Tpz-1; **(c)** Untreated; **(d)** Vehicle, 1% v/v DMSO.

3.5.2. Tpz-1 mechanistic analysis *via* transcriptomics revealed extensive alterations to gene expression

3.5.2.1. Differential Gene Expression and KEGG Pathway Analysis

Whole transcriptome and a subsequent CuffDiff analysis identified 667 upregulated and 1121 downregulated genes after Tpz-1 treatment that met our criteria of > 2.0 or < -2.0 $\log_2\text{FC}$ and $p = 5e-05$.

To gain an understanding of the biological pathways most prominently downregulated by Tpz-1, the KEGG PATHWAY database was accessed *via* DAVID analysis of the downregulated gene list. There were 14 pathways significantly downregulated (adjusted $p < 0.05$) after treatment (**Table 3.1**), of these, eight (57.1%) terms have been correlated with cancer: proteoglycans in cancer (31 genes), axon guidance (28 genes), Hippo signaling (24 genes), regulation of actin cytoskeleton (27 genes), focal adhesion (25 genes), small cell lung cancer (15 genes), Rap1 signaling (25 genes), ECM–receptor interaction (14 genes), and bladder cancer (9 genes). Moreover, seven (50%) of the identified KEGG PATHWAY terms suggest that Tpz-1 activity involves the downregulation of cell–cell and extracellular matrix (ECM)

interactions: proteoglycans in cancer, axon guidance, adherens junction (15 genes), regulation of actin cytoskeleton, focal adhesion, Rap1 signaling, and ECM–receptor interaction. With exception of the Hippo signaling pathway, overlap of gene involvement amongst several pathways was evident, particularly Akt serine/threonine kinase 3 (AKT3), oncogene R-Ras (RRAS), proto-oncogene tyrosine-protein kinase Src (SRC), epidermal growth factor receptor (EGFR), tyrosine kinase-type cell surface receptor HER2 (ERBB2), fibroblast growth factor receptor 1 (FGFR1), fibronectin 1 (FN1), integrin subunit alpha 2/6/V (ITGA2/6/V), phosphoinositide-3-kinase regulatory subunit 3 (PIK3R3), and Vav guanine nucleotide exchange factor 2 (VAV2), which were included in at least 4 pathways each. Four (28.6%) of the downregulated pathways were related to herpes simplex virus 1 infection, arrhythmogenic right ventricular cardiomyopathy, AGE-RAGE signaling in diabetic complications, and Yersinia infections and were not relevant to Tpz-1’s anticancer activity, thus they were omitted from further investigation.

Table 3.1. Relevant KEGG pathways downregulated by Tpz-1.

Term	# of Genes	p-value	Benjamini	Genes
Proteoglycans in cancer	31	1.70e-06	5.20e-04	AKT3, CD44, ELK1, RRAS, ARHGEF12, SRC, WNT6, CAMK2D, CCND1, CDNK1A, EGFR, ERBB2, FGFR1, FN1, FZD6, FZD7, HPSE, ITPR3, ITGA2, ITGAV, MAPK11, MAPK13, PXN, PIK3R3, PLCE1, PLCG1, RDX, SDC4, THBS1, TGFB2, VAV2
Axon guidance	28	4.40e-06	6.60e-04	ENAH, EPHB2, EPHB3, RRAS, ARHGEF12, SRGAP1, SRGAP3, SRC, BMPR2, CAMK2D, CFL2, EFNA3, EFNB1, EFNB2,

				NEO1, PAK4, PARD3, PARD6B, PIK3R3, PLCG1, PLXNA3, PLXNB1, PRKCZ, RGS3, SEMA3C, SEMA3F, SSH3, SEMA4F
Hippo signaling pathway	24	2.80e-05	2.80e-03	BBC3, LLGL2, NKD1, SMAD1, TEAD3, WTIP, WWC1, WNT6, AJUBA, BMPR2, CTNNA1, CCND1, DLG5, FZD6, FZD7, ID1, PARD3, PARD6B, PRKCZ, SAV1, STK3, TCF7L2, TGFB2, TP73
Adherens junction	15	4.00e-05	3.00e-03	BAIAP2, FER, LMO7, SRC, SSX2IP, WASL, YES1, CTNNA1, EGFR, ERBB2, FGFR1, PARD3, PTPRF, SORBS1, TCF7L2
Regulation of actin cytoskeleton	27	2.90e-04	1.40e-02	BAIAP2, CRK, ENAH, FGD1, RRAS, ARHGEF12, SRC, WASL, ABI2, CHRM3, CFL2, EGFR, FGFR1, FGFR4, FN1, ITGA2, ITGA6, ITGAV, ITGB4, MYH10, PAK4, PXN, PIP4K2C, PIK3R3, RDX, SSH3, VAV2
Focal adhesion	25	4.90e-04	2.10e-02	AKT3, CRK, ELK1, JUN, RASGRF1, SRC, CAPN2, COL4A2, CCND1, EGFR, ERBB2, FN1, ITGA2, ITGA6, ITGAV, ITGB4, LAMB1, LAMB3, LAMC1, PAK4, PXN, PIK3R3, TLN2, THBS1, VAV2
Small cell lung cancer	15	7.00e-04	2.60e-02	AKT3, TRAF4, TRAF5, COL4A2, CCND1, CCNE2, CDKN1A, FN1, ITGA2, ITGA6, ITGAV, LAMB1, LAMB3, LAMC1, PIK3R3
Rap1 signaling	25	9.10e-	3.00e-02	AKT3, CRK, ENAH,

pathway		04		RAP1GAP, RRAS, RAPGEF2, SRC, EFNA3, EGFR, FGFR1, FGFR4, ID1, MAGI3, MAPK11, MAPK13, PARD3, PARD6B, PIK3R3, PLCE1, PLCG1, PRKCZ, SIPA1L2, TLN2, THBS1, VAV2
ECM–receptor interaction	14	1.40e-03	3.80e-02	CD44, AGRN, COL4A2, DAG1, FN1, ITGA2, ITGA6, ITGAV, ITGB4, LAMB1, LAMB3, LAMC1, SDC4, THBS1
Bladder cancer	9	2.00e-03	4.40e-02	SRC, CCND1, CDKN1A, CDKN2A, DAPK1, DAPK2, EGFR, ERBB2, THBS1

Similarly, the KEGG PATHWAY database was accessed *via* DAVID for the genes upregulated by Tpz-1. There were 4 KEGG pathways significantly upregulated (adjusted $p < 0.05$) after treatment (**Table 3.2**): human cytomegalovirus infection, Yersinia infection, NOD-like receptor signaling, and Lipid and atherosclerosis pathways. There were two genes which all four upregulated pathways shared: C-X-C motif chemokine ligand 8 (CXCL8) and mitogen-activated protein kinase 12 (MAPK12/p38 γ). In addition, there were eight genes shared amongst 75% of the upregulated pathways: C-C motif chemokine ligand 5 (CCL5/RANTES), Rho guanine nucleotide exchange factor 1 (ARHGEF1), inositol 1,4,5-triphosphate receptor 1 (ITPR1/ACV), nuclear factor of activated T cells 1 and 2 (NFATC1/2), phospholipase C beta 2 (PLCB2), apoptosis-associated speck-like protein containing a CARD (PYCARD), and caspase 1 (CASP1).

Table 3.2. KEGG pathways upregulated by Tpz-1.

Term	# of Genes	p -value	Benjamini	Genes
------	------------	------------	-----------	-------

Human cytomegalovirus infection	23	4.3e-05	8.9e-03	CCL5, CXCL8, GNAI2, GNG7, MYC, RB1, RAC2, RAC3, ARHGEF1, ADCY7, B2M, CDK6, ITPR1, IL10RA, IL6R, HLA-B, MAPK12, NFATC1, NFATC2, PLCB2, PTGER2, PRKCA, PTK2B
Yersinia infection	17	5.9e-05	8.9e-03	CXCL8, GIT2, NLRC4, PYCARD, RAC2, RAC3, ARHGEF1, ARPC4, CASP1, ITGAS, MAPK12, NFATC1, NFATC2, PTK2B, RHOG, RPS6KA1, VAV1
NOD-like receptor signaling	19	2.1e-04	2.1e-02	ANTXR2, BCL2, CCL5, CXCL8, NLRC4, NAIP, PYCARD, TRAF3, CASP1, CARD8, CARD9, IKBKE, ITPR1, IFI16, MAPK12, PLCB2, PRKCD, P2RX7, TRPM2
Lipid and atherosclerosis	20	5.3e-04	3.9e-02	BCL2, CCL5, CXCL8, LYN, POU2F2, PYCARD, ARHGEF1, TRAF3, TNFRSF10A, APAF1, CASP1, IKBKE, ITPR1, MAPK12, NFATC1, NFATC2, PLCB2, PRKCA, TLR2, VAV1

3.5.2.2. ConnectivityMap

Our query of CMap database version 1.0 yielded nine perturbations with gene signatures similar to Tpz-1 treatment (**Figure 3.2**), indicated by summary Connectivity Score (τ) (**Table 3.3**): ribonuclease T2 (RNASET2; $\tau = 99.47$); CD99 molecule (CD99, $\tau = 97.78$); ubiquinol-cytochrome c reductase, Rieske iron-sulfur polypeptide 1 (UQCRFS1; $\tau = 97.41$); kinesin family member 5C (KIF5C; $\tau = 97.40$);

dehydrogenase/reductase SDR family member 2 (DHRS2; $\tau = 97.25$); cytotoxic lipid peroxidation product 4-hydroxy-2-nonenal ($\tau = 97.11$); DENN/MADD domain containing 1B (DENND1B; $\tau = 97.00$); thyroid hormone receptor interactor 13 (TRIP13; $\tau = 96.57$); and cytochrome c oxidase subunit Vb (COX5B; $\tau = 95.06$).

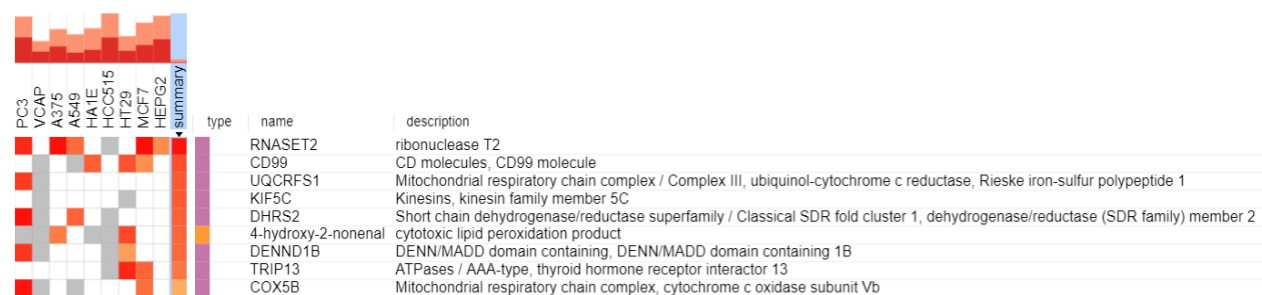


Figure 3.2. ConnectivityMap database ‘1.0’ query with the Top 150 upregulated and Top 150 downregulated genes; all uploaded genes were within the BING space. Only perturbagens with summary connectivity scores ≥ 95.00 are shown.

Except for one compound, 4-hydroxy-2-nonenal, all other results corresponded to gene knockdowns.

Table 3.3. Perturbagens with similar differential gene expression signatures to Tpz-1.

‘Type’ denotes perturbagen classification: KD = gene knockdown, CP = compound.

Symbol	Type	Gene Name	τ	Cancer-Related Function
RNASET2	KD	ribonuclease T2	99.47	Its inhibition opposes the cleavage/degradation of lysosomal and mitochondrial RNA; has conflicting roles in apoptosis; and affects structure of actin cytoskeleton and focal adhesions [118–120].
CD99	KD	CD99 molecule	97.78	Inhibition interferes with cell adhesion, morphology, and survival; activates Src kinases; and has oncojanus effects [121–

				124].
UQCRFS1	KD	ubiquinol-cytochrome c reductase, Rieske iron-sulfur polypeptide 1	97.41	Inhibition interrupts mitochondrial respiratory chain complex III maturation, electron transfer, and reactive oxygen species production [125–127].
KIF5C	KD	kinesin family member 5C	97.40	Unknown; could interfere with intracellular transport and microtubule cytoskeleton [128,129].
DHRS2	KD	dehydrogenase/reductase SDR family member 2	97.25	Oncojanus; has an effect on lipid metabolism, cell cycle, and oxidative damage response [130].
HNE	CP	4-hydroxy-2-nonenal	97.11	Toxic product of lipid peroxidation; oxidative stress marker; induces cell cycle arrest and intrinsic/extrinsic apoptosis; and inhibits NFκB pathway <i>via</i> IκBK [131–136].
DENND1B	KD	DENN/MADD domain containing 1B	97.00	Knockdown will reduce Rab35 GTPase activity, potentially impacting endocytosis, cytokinesis, and other processes [137].
TRIP13	KD	thyroid hormone receptor interactor 13	96.57	Knockdown is associated with dysregulated spindle-assembly checkpoint, proliferation, and mitotic exit; and promotes mitotic slippage [138–140].
COX5B	KD	cytochrome c oxidase subunit 5b	95.06	Knockdown associated with mitochondrial dysfunction, reduced production of ATP, ROS accumulation, growth arrest, and senescence [141,142].

3.5.2.3. Ingenuity Pathway Analysis

The majority of the top 100 Tpz-1-downregulated genes (**Figure 3.3**) were associated with cancer (98/100; p -value range = $9.24E-04$ – $1.62E-13$), organismal injury and abnormalities (98/100; p = $9.76E-04$ – $1.62E-13$), endocrine system disorders (93/100; p = $4.09E-04$ – $2.49E-13$), reproductive system disease (84/100; p = $8.57E-04$ – $6.34E-12$), and gastrointestinal disease (94/100; p = $7.80E-04$ – $8.99E-10$). Whereas the top 100 upregulated genes (**Figure 3.4**) were associated with inflammatory response (66/100; p -value range = $3.76E-04$ – $1.49E-14$), connective tissue disorders (38/100; p -value range = $3.18E-04$ – $4.63E-12$), inflammatory disease (42/100; p -value range = $3.18E-04$ – $4.63E-12$), organismal injury and abnormalities (99/100; p -value range = $3.81E-04$ – $4.63E-12$), and skeletal and muscular disorders (37/100; p -value range = $3.18E-04$ – $4.63E-12$). This indicates the therapeutic potential of Tpz-1 in and beyond cancer, particularly for endocrine, reproductive, or gastrointestinal diseases; as well as the potential for inflammatory side effects.

The molecules from our downregulated gene list with the greatest reduction in expression fold change (FC) were: keratin 19 (KRT19; -11.895 FC), desmoplakin (DSP; -11.500 FC), discoidin domain receptor tyrosine kinase 1 (DDR1; -11.370 FC), epidermal growth factor receptor (EGFR; -11.104 FC), keratin 7 (KRT7; -10.929 FC), plastin 3 (PLS3; -10.721), keratin 8 (KRT8; -10.632 FC), prominin 1 (PROM1; -9.514 FC), cellular communication network 1 (CCN1; -9.264 FC), and keratin 17 (KRT17; -9.321 FC) (**Figure 3.3**). Additionally, lysozyme (LYZ; 13.459 FC), lymphocyte cytosolic protein 1 (LCP1; 10.626 FC), placenta associated 8 (PLAC8; 9.877 FC), zinc finger protein 655 (ZNF655; 9.531 FC), phosphoinositide-3-kinase adaptor protein 1

(PIK3AP1; 9.114 FC), FERM domain containing kindlin 3 (FERMT3; 9.105 FC), linker for activation of T cells family member 2 (LAT2; 8.988 FC), integrin subunit alpha L (ITGAL; 8.878 FC), growth factor independent 1 transcriptional repressor (GFI1; 8.796 FC), and RAS guanyl releasing protein 2 (RASGRP2; 8.765 FC) showed the greatest increase in expression (**Figure 3.4**).

Molecular and cellular functions most associated with Tpz-1 gene downregulation (**Figure 3.3**) were cellular movement (52/100; $p = 9.50E-04 - 4.83E-14$), cell-to-cell signaling and interaction (32/100; $p = 9.67E-04 - 2.36E-10$), cellular assembly and organization (50/100; $p = 9.67E-04 - 2.36E-10$), cellular function and maintenance (43/100; $p = 9.67E-04 - 2.36E-10$), and cell morphology (45/100; $p = 9.50E-04 - 1.37E-09$). Whereas Tpz-1 gene upregulation was associated with cell-to-cell signaling and interaction (48/100; $p = 3.74E-04 - 6.49E-16$), cell death and survival (55/100; $p = 3.74E-04 - 3.32E-15$), cellular compromise (28/100; $p = 2.50E-04 - 3.15E-14$), cellular development (56/100; $p = 3.74E-04 - 4.46E-14$), and cellular growth and proliferation (53/100; $p = 3.74E-04 - 4.46E-14$) (**Figure 3.4**). These findings are consistent with our previously reported cytotoxic evaluation of Tpz-1 [93].

In IPA, an 'upstream regulator' is defined as any drug or molecule that has a downstream effect on molecules in the experimental dataset. Notably, EGFR was the only downregulated gene that was also identified as a top upstream regulator of Tpz-1 activity ($p = 6.96E-11$), though the resultant downstream effects could not be predicted. Other upstream regulators of Tpz-1 downregulated gene bioactivity included beta-estradiol ($p = 5.80E-12$), coagulation factor II thrombin receptor F2R ($p = 2.92E-11$), estrogen receptor ($p = 1.05E-10$), and proto-oncogene H-RAS ($p = 1.17E-10$) (**Figure**

3.3). The expression of beta-estradiol, F2R, estrogen receptor, and HRAS have been individually implicated in cancer progression, and are also known to crosstalk with EGFR [143–151]. Upstream regulators associated with Tpz-1 upregulated genes include: vitamin A derivative tretinoin ($p = 3.78E-10$), interleukin 33 IL33 (activated; $p = 7.08E-09$), phorbol ester compound tetradecanoylphorbol acetate (activated; $p = 1.00E-08$), lipopolysaccharide (activated; $p = 1.03E-08$), and ETV6-RUNX1 fusion protein (inhibited; $p = 1.57E-08$) (**Figure 3.4**). The predicted effect of Tpz-1 on these molecules, with exception of lipopolysaccharide, have proven therapeutic in cancers, particularly leukemias [152–156].

Causal networks derived from the IPA Knowledge Base aim to identify biological relationships between experimental gene expression data and published literature [157]. Networks that were related to our downregulated gene list were SMAD family member 4 SMAD4 ($p = 1.78E-13$), TATA-box binding protein TBP (inhibited; $p = 1.09E-12$), nuclear receptor subfamily 0 group B member 1 NR0B1 (activated; $p = 2.58E-12$), matrix metalloproteinase 10 MMP10 ($p = 3.26E-12$), and protease inhibitor 4-hydroxymercuribenzoate (activated; $p = 5.33E-12$) (**Figure 3.3**). Additionally, H2.0 like homeobox HLX (inhibited; $p = 9.40E-13$), signal transducer and activator of transcription 4 STAT4 (activated; $p = 2.47E-11$), interferon lfn (activated; $p = 4.21E-11$), GATA binding protein 1 (GATA1), and LXR ligand-LXR-Retinoic acid-RXR α complex ($p = 8.41E-11$) were the causal networks associated with our upregulated gene list (**Figure 3.4**). These networks are associated with cellular transcription, signal transduction, metabolism, differentiation, and tissue remodeling processes; all of which are routinely implicated in cancer.

Top Canonical Pathways				
Name		p-value	Overlap	
Epithelial Adherens Junction Signaling		5.74E-05	3.8%	6/158
Germ Cell-Sertoli Cell Junction Signaling		8.89E-05	3.5%	6/171
Semaphorin Signaling in Neurons		1.39E-04	6.5%	4/62
Glucocorticoid Receptor Signaling		8.01E-04	1.5%	9/581
Hepatic Fibrosis / Hepatic Stellate Cell Activation		1.41E-03	2.6%	5/194

© 2000-2021 QIAGEN. All rights reserved.
 Tpz1_transcriptome_Down_100 - 2021-07-05 09:47 AM

Top Upstream Regulators			
Upstream Regulators			
Name		p-value	Predicted Activation
beta-estradiol		5.80E-12	
F2R		2.92E-11	
EGFR		6.96E-11	
estrogen receptor		1.05E-10	
HRAS		1.17E-10	
Causal Network			
Name		p-value	Predicted Activation
SMAD4		1.78E-13	
TBP		1.09E-12	Inhibited
NROB1		2.58E-12	Activated
MMP10		3.26E-12	
4-hydroxymercuribenzoate		5.33E-12	Activated

© 2000-2021 QIAGEN. All rights reserved.
 Tpz1_transcriptome_Down_100 - 2021-07-05 09:47 AM

Top Diseases and Bio Functions			
Diseases and Disorders			
Name		p-value range	# Molecules
Cancer		9.24E-04 - 1.62E-13	98
Organismal Injury and Abnormalities		9.76E-04 - 1.62E-13	98
Endocrine System Disorders		4.09E-04 - 2.49E-13	93
Reproductive System Disease		8.57E-04 - 6.34E-12	84
Gastrointestinal Disease		7.80E-04 - 8.99E-10	94
Molecular and Cellular Functions			
Name		p-value range	# Molecules
Cellular Movement		9.50E-04 - 4.83E-14	52
Cell-To-Cell Signaling and Interaction		9.67E-04 - 2.36E-10	32
Cellular Assembly and Organization		9.67E-04 - 2.36E-10	50
Cellular Function and Maintenance		9.67E-04 - 5.78E-10	43
Cell Morphology		9.50E-04 - 1.37E-09	45
Physiological System Development and Function			
Name		p-value range	# Molecules
Embryonic Development		8.64E-04 - 1.37E-09	49
Hair and Skin Development and Function		8.02E-04 - 1.37E-09	30
Organ Development		8.57E-04 - 1.37E-09	37
Organismal Development		8.79E-04 - 1.37E-09	57
Tissue Development		8.64E-04 - 1.37E-09	55

© 2000-2021 QIAGEN. All rights reserved.

Figure 3.3. IPA results for top 100 genes downregulated by Tpz-1.

Top Canonical Pathways		
Name	p-value	Overlap
Phagosome Formation	2.53E-07	5.4 % 8/149
Rac Signaling	2.85E-05	4.3 % 6/138
Regulation of Cellular Mechanics by Calpain Protease	4.02E-05	5.6 % 5/89
Osteoarthritis Pathway	6.63E-05	3.0 % 7/234
Hepatic Fibrosis Signaling Pathway	7.82E-05	2.1 % 9/419

© 2000-2021 QIAGEN. All rights reserved.
 Tpz1_transcriptome_Up_100 - 2021-07-05 09:59 AM

Top Upstream Regulators		
Upstream Regulators		
Name	p-value	Predicted Activation
tretinoin	3.78E-10	
IL33	7.08E-09	Activated
tetradecanoylphorbol acetate	1.00E-08	Activated
lipopolysaccharide	1.03E-08	Activated
ETV6-RUNX1	1.57E-08	Inhibited

Causal Network		
Name	p-value	Predicted Activation
HLX	9.40E-13	Inhibited
STAT4	2.47E-11	Activated
Ifn	4.21E-11	Activated
GATA1	8.12E-11	
LXR ligand-LXR-Retinoic acid-RXRα	8.41E-11	

© 2000-2021 QIAGEN. All rights reserved.
 Tpz1_transcriptome_Up_100 - 2021-07-05 09:59 AM

Top Diseases and Bio Functions		
Diseases and Disorders		
Name	p-value range	# Molecules
Inflammatory Response	3.76E-04 - 1.49E-14	66
Connective Tissue Disorders	3.18E-04 - 4.63E-12	38
Inflammatory Disease	3.18E-04 - 4.63E-12	42
Organismal Injury and Abnormalities	3.81E-04 - 4.63E-12	99
Skeletal and Muscular Disorders	3.18E-04 - 4.63E-12	37

Molecular and Cellular Functions		
Name	p-value range	# Molecules
Cell-To-Cell Signaling and Interaction	3.74E-04 - 6.49E-16	48
Cell Death and Survival	3.74E-04 - 3.32E-15	55
Cellular Compromise	2.50E-04 - 3.15E-14	28
Cellular Development	3.74E-04 - 4.46E-14	56
Cellular Growth and Proliferation	3.74E-04 - 4.46E-14	53

Physiological System Development and Function		
Name	p-value range	# Molecules
Hematological System Development and Function	3.76E-04 - 6.49E-16	57
Immune Cell Trafficking	3.74E-04 - 6.49E-16	44
Hematopoiesis	3.12E-04 - 4.46E-14	31
Lymphoid Tissue Structure and Development	3.68E-04 - 4.46E-14	41
Tissue Development	3.12E-04 - 4.46E-14	35

© 2000-2021 QIAGEN. All rights reserved.

Figure 3.4. IPA results for top 100 genes upregulated by Tpz-1.

3.5.3. Tpz-1 structural analysis indicated key functional groups with potential to drive anticancer activity and in vivo toxicities

3.5.3.1. SwissTargetPrediction

Our SwissTargetPrediction query of Tpz-1 (**Table 3.4**) did not result in the identification of any probable targets ($P^* = 0.115736675$). Despite this, Tpz-1 displayed strong structural similarity to: thiophene-based JNK1/2/3 inhibitor compound CHEMBL1682010 (Similarity: 0.934) [158]; imidazole-based neuronal and inducible NOS inhibitor CHEMBL1911987 (Similarity: 0.927) [159]; 2-aminoimidazolone-based PIM1, DYRK1A/2, and CLK1 inhibitor CHEMBL1803071 (Similarity: 0.925) [160]; azabenzimidazole-derived AURKB, CDK2, and IKBKE inhibitor CHEMBL2010815 (Similarity: 0.923) [161]; and 1-acyl-2-benzylpyrrolidine-based orexin receptor (HCRTR1/2) antagonist CHEMBL3741194 (Similarity: 0.923) [162]. Notably, none of these structurally similar bioactive molecules contained a thienopyrazole, and may explain the low reliability of Tpz-1's predicted targets by this platform.

Table 3.4. The top 15 potential targets of Tpz-1 identified by SwissTargetPrediction.

Target	Common name	Uniprot ID	ChEMBL ID	Target Class	Prob (P^*)	Known actives (3D/2D)
c-Jun N-terminal kinase 1	MAPK8	P45983	CHEMBL2276	Kinase	0.1157	540/0
c-Jun N-terminal kinase 3	MAPK10	P53779	CHEMBL2637	Kinase	0.1157	323/0
c-Jun N-terminal kinase 2	MAPK9	P45984	CHEMBL4179	Kinase	0.1157	201/0
Nitric-oxide synthase, brain	NOS1	P29475	CHEMBL3568	Enzyme	0.1157	85/0
Nitric oxide synthase, inducible	NOS2	P35228	CHEMBL4481	Enzyme	0.1157	171/0

Cyclin-dependent kinase 5/CDK5 activator 1	CDK5R1 CDK5	Q15078 Q00535	CHEMBL1907600	Kinase	0.1157	353/0
Serine/threonine-protein kinase PIM1	PIM1	P11309	CHEMBL2147	Kinase	0.1157	262/0
Dual-specificity tyrosine-phosphorylation regulated kinase 1A (by homology)	DYRK1A	Q13627	CHEMBL2292	Kinase	0.1157	201/0
Dual specificity protein kinase CLK1 (by homology)	CLK1	P49759	CHEMBL4224	Kinase	0.1157	100/0
Dual-specificity tyrosine-phosphorylation regulated kinase 2	DYRK2	Q92630	CHEMBL4376	Kinase	0.1157	30/0
Serine/threonine-protein kinase Aurora-B	AURKB	Q96GD4	CHEMBL2185	Kinase	0.1157	381/0
Cyclin-dependent kinase 2	CDK2	P24941	CHEMBL301	Kinase	0.1157	453/0
Inhibitor of nuclear factor kappa B kinase epsilon subunit	IKBKE	Q14164	CHEMBL3529	Kinase	0.1157	25/0
Orexin receptor 2	HCRTR2	O43614	CHEMBL4792	Family A GPCR	0.1157	1099/0
Orexin receptor 1	HCRTR1	O43613	CHEMBL5113	Family A GPCR	0.1157	936/0

3.5.3.2. SwissSimilarity

The results of our query revealed 400 bioactive molecules with similarity scores > 0.5; over half of them containing a thienopyrazole group. The top 12 SwissSimilarity hits (**Figure 3.5**) were evaluated further to determine their structural and functional relationship to Tpz-1. Of note, all top hits retained the carboxamide, thienopyrazole, and

phenyl groups of Tpz-1, and may indicate the significance of these components to the molecule's potent cytotoxicity.

The most similar hit was CHEMBL4441641 (Similarity: 0.999), a stereoisomer of Tpz-1. Hitherto, PubChem ID 5331400 was our only known record of Tpz-1, however, the ChEMBL database identified redundant entries for Tpz-1 under PubChem IDs 5443760 and 1125175. Interestingly, CHEMBL4441641 was identified as an effective inhibitor of human ectonucleoside triphosphate diphosphohydrolase 5 (ENTPD5) with antitumor activity in LnCaP prostate adenocarcinoma cells, and is patented by The University of Texas [163]. Aside from the [47] and [48] studies and our own [93] there have been no significant advances in Tpz-1's functional characterization.

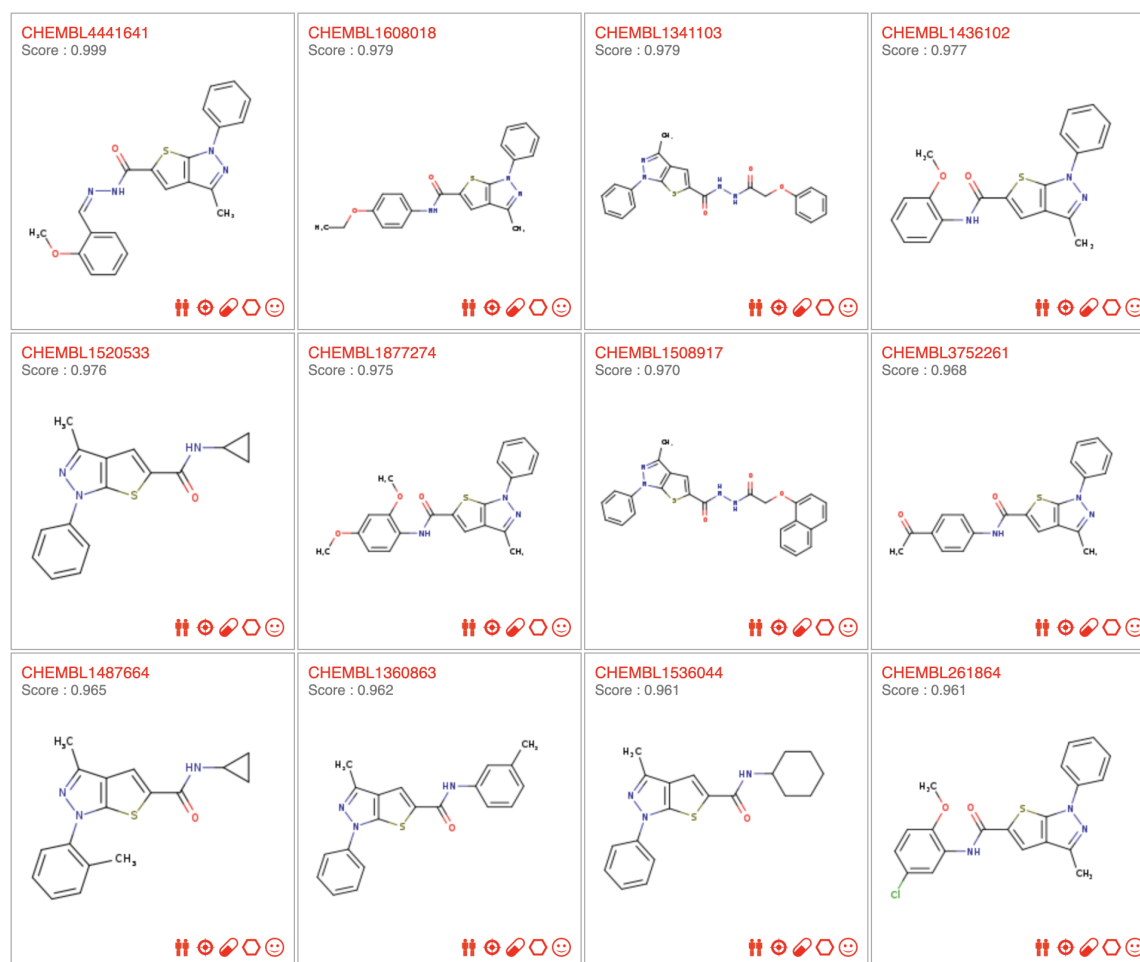


Figure 3.5. Top 12 bioactive molecules in the ChEMBL database with structural similarity to Tpz-1; ranked by SwissSimilarity ‘Similarity Score’.

3.5.3.3 ChEMBL Database

The ChEMBL platform predicted at 90% confidence the potential human targets of CHEMBL441641 (**Table 3.5**) [164].

Table 3.5. ChEMBL target predictions for CHEMBL441641 (Tpz-1) at 90% confidence.

Target ChEMBL ID	Target Name
CHEMBL2617	Tryptase beta-1
CHEMBL278	Integrin alpha-4
CHEMBL3807	T-cell protein-tyrosine phosphatase
CHEMBL1829	Histone deacetylase 3
CHEMBL1907588	Acetylcholine receptor; alpha1/beta1/delta/gamma
CHEMBL3712907	Transmembrane domain-containing protein TMIGD3
CHEMBL5568	Proto-oncogene tyrosine-protein kinase ROS
CHEMBL2789	Estradiol 17-beta- dehydrogenase 2
CHEMBL2095172	GABA-A receptor; alpha-1/beta-2/gamma-2
CHEMBL1868	Vascular endothelial growth factor receptor 1
CHEMBL6120	Solute carrier family 22 member 12
CHEMBL3891	Calpain 1
CHEMBL325	Histone deacetylase 1
CHEMBL1907591	Neuronal acetylcholine receptor; alpha4/beta4
CHEMBL2390810	Microtubule-associated protein 2

As for the other top SwissSimilarity hits (**Figure 3.5**), knowledge of their biological activity was limited to unpublished publicly deposited data in the PubChem (<https://pubchem.ncbi.nlm.nih.gov/>) Bioassay database [165]. Some exceptions were

compound CHEMBL3752261 (Similarity: 0.968), an apoptosis-inducing and non-structural protein 4B (NS4B) targeted anti-hepatitis C drug candidate [166,167]; and CHEMBL261864 (Similarity: 0.961), a non-cytotoxic RNase L and innate immunity activating broad-spectrum antiviral agent [168].

3.5.3.4. SwissADME

To better understand the potential pharmacokinetics, bioavailability, and toxicity of Tpz-1 *in vivo*, the SwissADME platform was utilized. SwissADME evaluates the overall drug-likeness of a queried molecule by predicting its absorption, distribution, metabolism, and excretion (ADME) properties with predictive models that are based on molecular structure. The query results are summarized in two graphics: the BOILED-Egg plot, which demonstrates the compound's potential gastrointestinal (GI) absorption (egg white), blood-brain barrier permeation (egg yolk), and efflux by P-glycoproteins (red/blue circle); and the Bioavailability Radar, which depicts six important parameters of oral bioavailability and their optimal values (pink area) [114].

The predicted pharmacokinetics of Tpz-1 (**Figure 3.6**) were somewhat favorable, displaying suitable size, polarity, flexibility, and strong passive GI absorption. However, Tpz-1 was unfavorably predicted to be hydrophobic (Water Solubility/Lipophilicity scores), highly unsaturated (ratio of single bonds to double bonds/rings), and could metabolize poorly (cytochrome P450 inhibitor); additionally, the presence of a potentially reactive imine (carbon-nitrogen double bond) group elicited a structural alert [169], and its molecular weight and lipophilicity (Leadlikeness) are also in need of optimization [170].

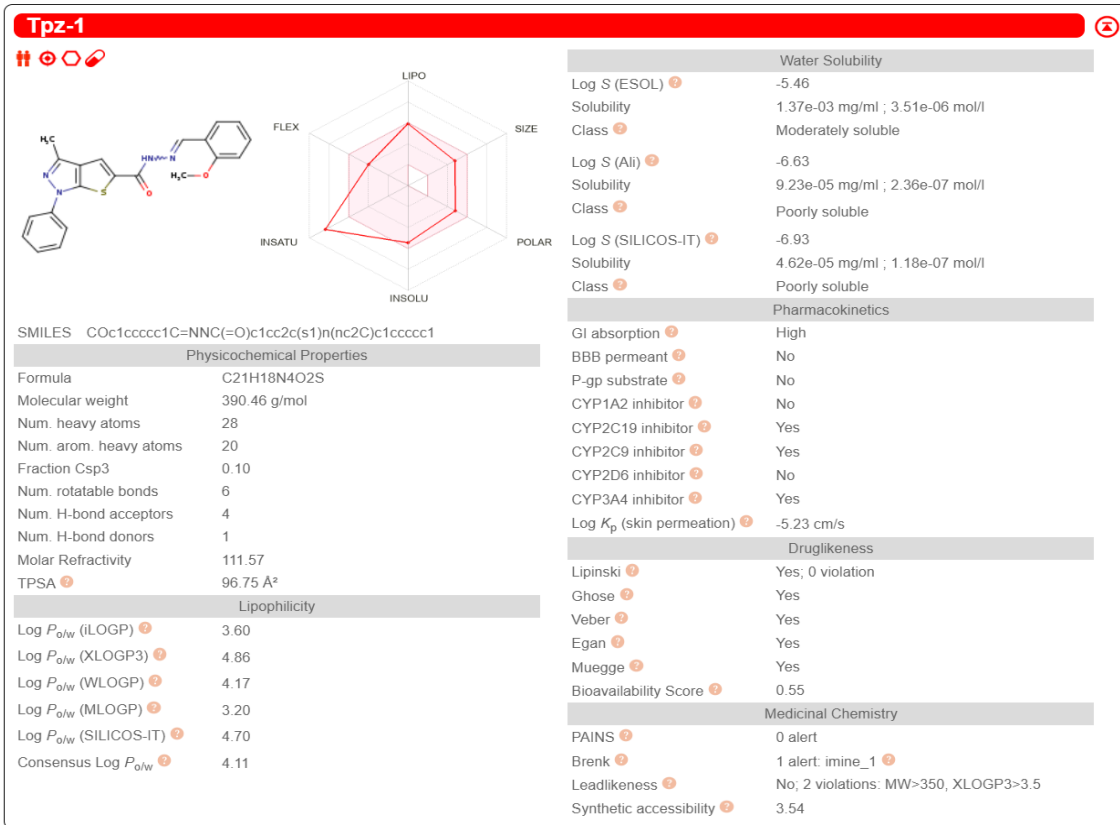
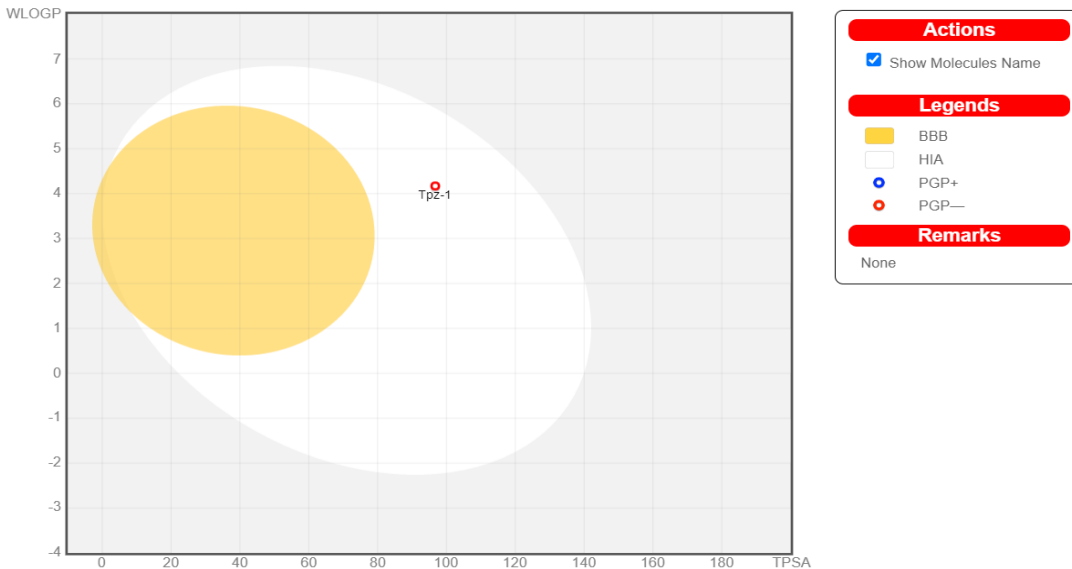


Figure 3.6. SwissADME BOILED-Egg (gastrointestinal absorption/blood brain barrier penetration) and iLOGP (lipophilicity) results for Tpz-1.

3.5.3.5. COREMINE query of pyrazole compounds, thiophenes, and neoplasms

Extracted associations from MEDLINE literature co-mentioning 'Pyrazole Compound', 'Neoplasms', and 'Thiophenes' included 1504 Gene/Proteins, 118 Molecular functions, 592 Biological processes, and 2562 Drugs. Of these associations, 1163 Gene/Proteins, 456 Biological processes, and 75 Molecular functions, and 1924 Drugs had significance values (p) < 0.05.

The top 10 biological process connections identified in our query (**Figure 3.7**) were angiogenesis (61,466 connections; $p = 4.17529E-06$), cell migration (57,323 connections; $p = 8.83591E-06$), epithelial to mesenchymal transition (33,054 connections; $p = 8.07096E-06$), cell proliferation (128,121 connections; $p = 1.41166E-06$), apoptotic process (126,290 connection; $p = 1.68584E-06$), signal transduction (148,472 connections; $p = 6.88977E-06$), cell cycle (97,209 connections; $p = 4.59181E-06$), cell growth (89,566 connections; $p = 5.18161E-06$), cell death (97,645 connections; $p = 9.0063E-06$), and growth (199,363 connections; $p = 2.79673E-06$).

The top 10 gene/protein associations (**Figure 3.8**) were B-Raf proto-oncogene (BRAF; 17,739 connections; $p = 1.1897E-05$), kallikrein-related peptidase 3 (KLK3; 18,657 connections; $p = 5.40296E-06$), tuberous sclerosis 1 (TSC1; 30,828 connections; $p = 3.66019E-06$), tumor protein p53 (TP53; 46,928 connections; $p = 2.34066E-06$), B-cell lymphoma 2 (BCL2; 42,679 connections; $p = 1.09965E-05$), epidermal growth factor receptor (EGFR; 38,640 connections; $p = 6.64911E-06$), erb-b2 receptor tyrosine kinase 2 (ERBB2; 25,576 connections; $p = 4.96213E-06$), E-cadherin (CDH1; 28,827 connections; $p = 1.05595E-05$), CD274 molecule (16,979 connections;

$p = 1.06736E-05$), and Kirsten rat sarcoma viral oncogene homolog (KRAS; 21,906 connections; $p = 1.19765E-05$).

The top 10 associated molecular functions (**Figure 3.9**) were luciferin monooxygenase activity (26,880 connections; $p = 0.000375731$), methylated-DNA-[protein]-cysteine S-methyltransferase activity (12,042 connections; $p = 4.5219E-05$), telomerase activity (16,793 connections; $p = 5.29734E-05$), fibroblast growth factor-activated receptor activity (13,544 connections; $p = 0.000165914$), motor activity (52,404 connections; $p = 0.00018353$), kinase activity (43,755 connections; $p = 0.000159403$), DNA binding (50,477 connections; $p = 0.000708572$), catalytic activity (83,572 connections; $p = 0.001196781$), N-methyl-D-aspartate selective glutamate receptor activity (23,041 connections; $p = 0.00090111$), and ubiquitin-specific protease activity (14,009 connections; $p = 0.000289273$).

The top 10 drug relationships (**Figure 3.10**) were carboplatin (21,301 connections; $p = 1.82064E-05$), fluorodeoxyglucose F18 (22,514 connections; $p = 1.58442E-05$), breast cancer type 1 susceptibility protein measurement (21,885 connections; $p = 1.70471E-05$), fluorouracil (38,610 connections; $p = 5.31468E-06$), cisplatin (56,911 connections; $p = 3.92629E-06$), gemcitabine (22,945 connections; $p = 1.12086E-05$), doxorubicin (51,010 connections; $p = 4.95727E-06$), paclitaxel (39,122 connections; $p = 9.29734E-06$), docetaxel (21,533 connections; $p = 1.25424E-05$), and epidermal growth factor (57,263 connections; $p = 9.46582E-06$).

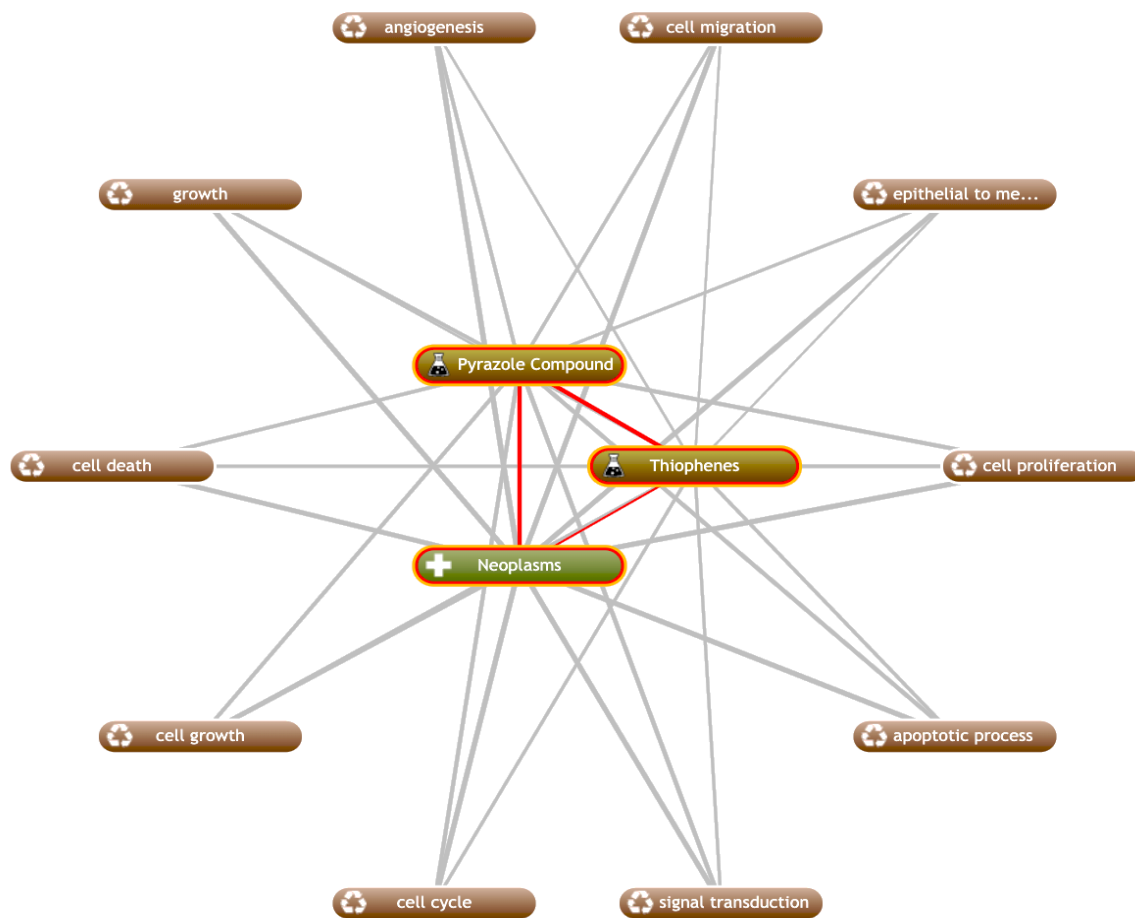


Figure 3.7. Top 10 biological processes co-mentioned in MEDLINE literature containing the terms 'Pyrazole Compound', 'Thiophenes', and 'Neoplasms'.

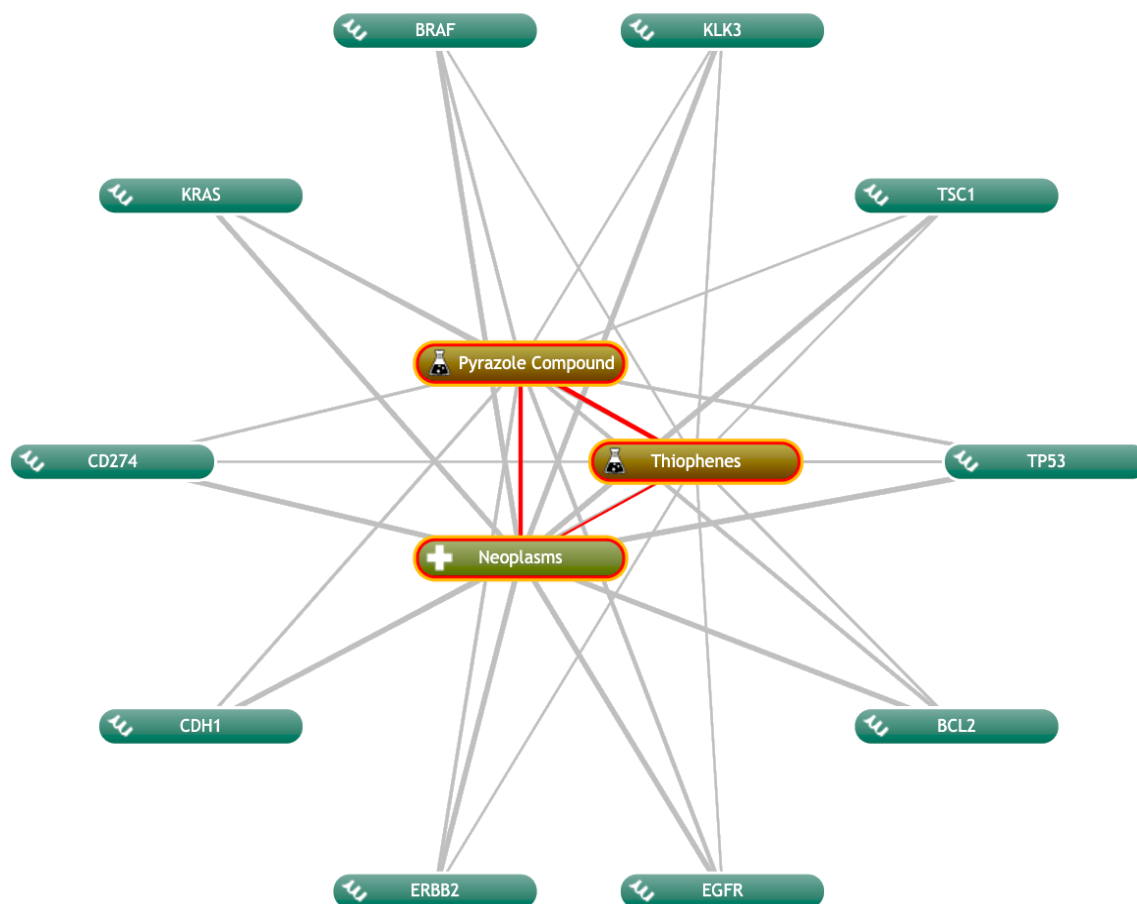


Figure 3.8. Top 10 genes/proteins co-mentioned in MEDLINE literature containing the terms ‘Pyrazole Compound’, ‘Thiophenes’, and ‘Neoplasms’.



Figure 3.9. Top 10 molecular functions co-mentioned in MEDLINE literature containing the terms 'Pyrazole Compound', 'Thiophenes', and 'Neoplasms'.

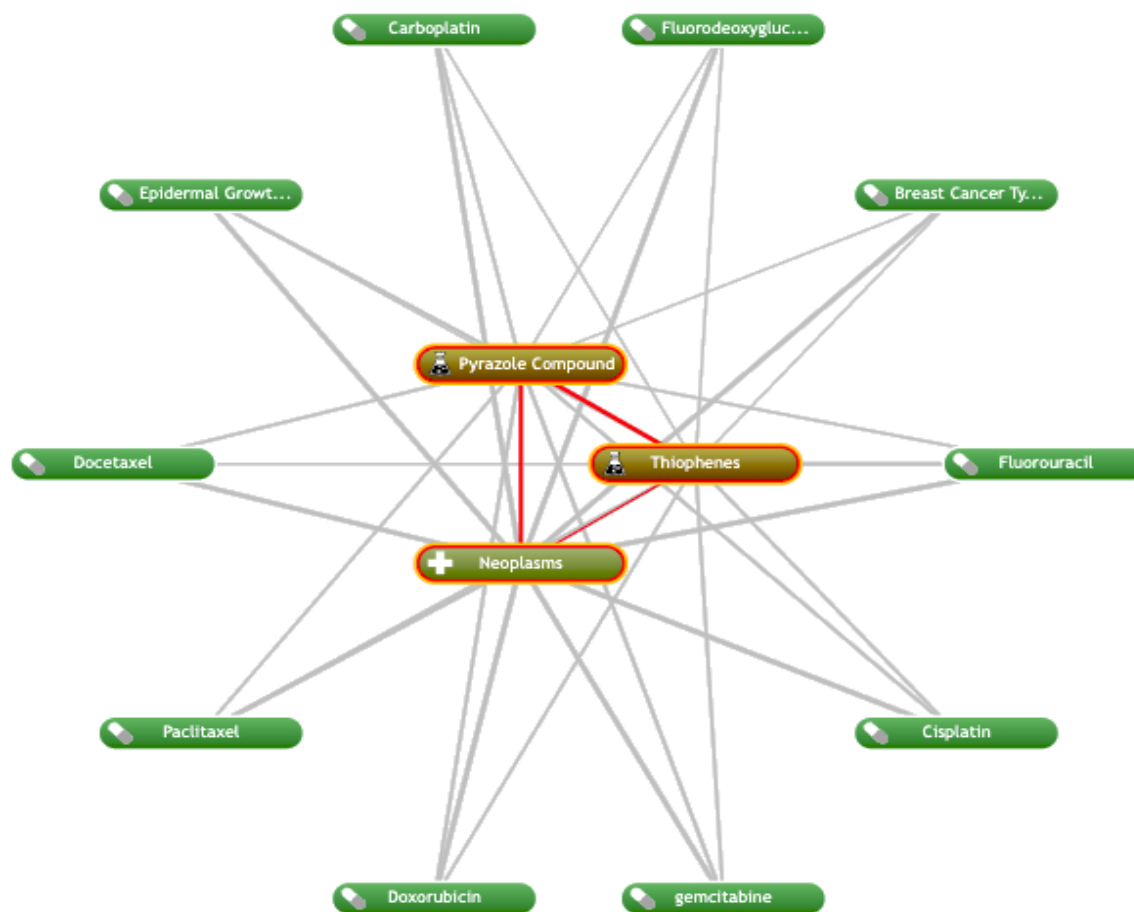


Figure 3.10. Top 10 drugs co-mentioned in MEDLINE literature containing the terms 'Pyrazole Compound', 'Thiophenes', and 'Neoplasms'.

3.6. DISCUSSION

3.6.1. Tpz-1-treated cells lose cytoskeletal integrity within hours of treatment

Tpz-1-treated cells presented with a morphology that is consistent with an impaired cytoskeleton (**Figure 3.1**). Treated cells displayed irregular behavior, amorphism, and flexibility which is likely to disrupt normal intra- and extracellular interactions. Depending on the unique cellular interactions that take place, the fluid morphology of treated cells could theoretically promote different cell fates through assorted mechanisms. Given the importance of the cytoskeleton to faithful cell division,

outcomes of Tpz-1 treatment likely include delayed mitosis, erroneous chromosome segregation, and programmed cell death. Treated cell morphology is consistent with our in vitro study described in the previous chapter [93], the findings of Fayad et al. [47], and the transcriptome and structure-based in silico predictions detailed below. This experiment clearly establishes cytoskeletal disruption as a primary mechanism of Tpz-1's cellular effect, even at very low concentration (0.05 μ M). Future investigations of Tpz-1 and its analogs should consider cytoskeleton and mitotic spindle-associated proteins as possible targets.

3.6.2. Transcriptome analysis revealed a network of cancer-related pathways downregulated by Tpz-1

With exception of the Hippo signaling pathway, overlap of gene involvement amongst several pathways was evident, particularly AKT3, RRAS, SRC, EGFR, ERBB2, FGFR1, FN1, ITGA2/6/V, PIK3R3, and VAV2, which were associated with a minimum of four pathways each.

3.6.2.1. Cell-ECM and Cell-Cell Interaction Mechanisms

3.6.2.1.1. Proteoglycans in cancer

The ECM is primarily comprised of crosslinked fibrous proteins and proteoglycans (PGs) [171,172]. Collagen provides most of the ECM's physical scaffold, while proteoglycans fill the remaining interstitial space to add tensile strength and facilitate signal transduction [172–174]. Proteoglycans are found on cells, in cells, and in the ECM and can be classified by their glycosaminoglycan chains: hyaluronan (HA), heparan sulfate (HSPG), chondroitin sulfate (CSPG), and keratan sulfate (KSPG) [175].

Upstream constituents of the signaling pathways for all four proteoglycan subtypes were downregulated after treatment with Tpz-1, particularly HA and HSPGs

(**Supplementary Figure S3.1**). Importantly, the signals transmitted by these molecules have been associated with cell survival, adhesion, and migration. Notable downregulated elements were the CD44 molecule, Erb-B2 receptor tyrosine kinase 2 (ERBB2/HER2), SRC proto-oncogene, epidermal growth factor receptor (EGFR), integrin subunit alpha 2 (ITGA2), integrin subunit alpha V (ITGAV), fibronectin 1 (FN1), frizzled class receptors 6/7 (FZD6/7), fibroblast growth factor receptor 1 (FGFR1), syndecan 4 (SDC4), and Wnt family member 6 (WNT6). These results show that Tpz-1 cytotoxicity involves a downregulation of proteoglycan pathway elements at the cell surface which are known to crosslink with the cytoskeleton and are essential to cell survival, motility, and transmission of extracellular communications [176–179].

3.6.2.1.2. Rap1 signaling

The Rap1 GTPase has been implicated in processes involving cell–cell and cell–ECM adherence [180]. In Tpz-1-treated cells, inhibition of RRAS and CRK could lead to the downregulation of MAPK (MAPK11/13) and PI3K-Akt (PIK3R3, AKT3) signaling cascades, causing subsequent mitigation of cell proliferation and survival *via* Rap1-related pathways (**Supplementary Figure S3.2**). Tpz-1 may also disrupt cell polarity *via* downregulated par-3 family cell polarity regulator (PARD3), par-6 family cell polarity regulator beta (PARD6B), and protein kinase C zeta (PRKCZ).

3.6.2.1.3. ECM–receptor interaction

The extracellular matrix (ECM) is a three-dimensional network of water, proteins, and other biomolecules that surrounds cells to provide structural support and facilitate chemical and mechanical processes within all organs and tissues [172,174,181]. Composition of the ECM is dynamic and unique to each tissue, and is important for

normal tissue architecture, homeostasis, and communication of signals between cells and their environment [172,181–183]. The ECM controls cell survival, proliferation, and many other cell behaviors, thus dysregulation of its composition can also drive cancer [174,181,183]. Cells communicate with the ECM primarily through transmembrane integrins or proteoglycans, and are reliant on these interactions for their survival [184].

After Tpz-1 treatment, many components of the ECM–receptor interaction pathway was downregulated. Specifically, ECM proteins collagen type IV alpha 2 chain (COL4A2), laminin subunits beta 1/3 (LAMB1/3) and gamma 1 (LAMC1), thrombospondin 1 (THBS1), fibronectin 1 (FN1), and agrin (AGRN) were affected; as were the membrane-embedded integrin subunits alpha 2/6/V (ITGA2/6/V) and beta 4 (ITGB4), proteoglycans CD44 and syndecan 4 (SDC4), and glycoprotein dystroglycan 1 (DAG1) (**Supplementary Figure S3.3**). Together, these results suggest that loss of ECM interactions plays a significant role in Tpz-1's anticancer effect.

3.6.2.1.4. Adherens junctions

Adherens junctions are cell–cell adhesion structures that form strong or weak intercellular connections *via* interaction of transmembrane Cadherin and cytoplasmic Catenin proteins functionally linked to the actin cytoskeleton [185–187]. Similarly, the Nectin-Afadin adhesion complex also facilitates adherens junction coupling to actin [186].

Downstream components of the Nectin-Afadin and Cadherin-Catenin pathways were downregulated after treatment with Tpz-1, most notably: catenin alpha 1 (CTNNA1), WASP like actin nucleation promoting factor (WASL), BAR/IMD domain containing adaptor protein 2 (BAIAP2), and transcription factor 7 like 2 (TCF7L2)

(**Supplementary Figure S3.4**). The inhibition of these pathways shows that Tpz-1 treatment is likely to disrupt important cytoskeletal interactions that contribute to cell polarity and adhesion.

3.6.2.1.5. Focal adhesion

Focal adhesions are points of attachment and communication between the ECM, transmembrane integrins, and the actin cytoskeleton [188]. Signaling through integrins also controls cell motility, proliferation, and survival [189].

Treatment with Tpz-1 caused downregulation of ECM components collagen type IV alpha 2 chain (COL4A2), laminin subunits beta 1/3 (LAMB1/3), and laminin subunit gamma 1 (LAMC1); coupled with downregulation of integrin subunits alpha 2/6/V (ITGA2/6/V) and beta 4 (ITGB4), paxillin (PXN), and phosphoinositide-3-kinase regulatory subunit 3 (PIK3R3) (**Supplementary Figure S3.5**). This might ultimately lead to the downregulation of AKT serine/threonine kinase 3 (AKT3) and cyclin D1 (CCND1) signaling, thereby promoting Tpz-1-induced cell cycle inhibition and death.

3.6.2.2. Axon guidance molecules in cancer

Formation and survival of neural networks is mediated by molecules such as the netrins, ephrins, slits, and semaphorins. In addition to their role in the brain, these 'axon guidance' molecules have been implicated in tumor cell angiogenesis, apoptosis, motility, and invasion processes [190–192].

Tpz-1 treatment primarily downregulated ephrin and semaphorin molecules that are involved in regulation of the actin cytoskeleton. Notable downregulated elements were EPH receptors B2/3 (EPHB2/3), cofilin 2 (CFL2), ephrin A3 (EFNA3), ephrin B1 and B2 (EFNB1/2), semaphorin 3C/F (SEMA3C/F), semaphorin 4F (SEMA4F), plexin

A3 (PLXNA3), plexin B1 (PLXNB1), and p21-activated kinase 4 (PAK4)

(**Supplementary Figure S3.6**). These results provide supporting evidence that Tpz-1 interferes with the cytoskeletal dynamics, and perhaps structural stability, of treated cells.

3.6.2.3. Hippo signaling

The Hippo signaling pathway is a conserved, but only partially characterized, mammalian pathway that controls tissue growth, homeostasis, and organ size by regulating the rates of cell proliferation versus apoptosis [193]. Adherens junctions and cell polarity complexes have been implicated in Hippo pathway regulation, and their knockdown affects cell survival and adhesion [194,195]. Notable elements of the Hippo pathway downregulated by Tpz-1 include serine/threonine kinase 3 (STK3), ajuba LIM protein (AJUBA), SMAD family member 1 (SMAD1), NKD inhibitor of WNT signaling pathway 1 (NKD1), cyclin D1 (CCND1), and catenin alpha 1 (CTNNA1)

(**Supplementary Figure S3.7**). These results indicate that Tpz-1 treatment downregulates proteins involved in cell contact inhibition, proliferation, and polarity.

3.6.2.4. Regulation of actin cytoskeleton

The actin cytoskeleton is a dynamic structure whose remodeling in response to stimuli is essential to cell morphology, movement, and mitosis [196,197]. In addition, the actin cytoskeleton contributes to the stability of cell–cell and cell–ECM adhesions [198]. Three Rho GTPases, Rho, Rac, and Cdc42, regulate actin polymerization in all eukaryotic cells [198].

Based on our results, Tpz-1 treatment caused downregulation of receptor tyrosine kinase (RTK), integrin (ITG), and G-protein coupled receptor (GPCR) signaling

pathways related to focal adhesion, stress fibers, and actin assembly (**Supplementary Figure S3.8**). Implicated genes include: epidermal growth factor receptor (EGFR), fibroblast growth factor receptors 1/4 (FGFR1/4), R-Ras (RRAS), Rho guanine nucleotide exchange factor 12 (ARHGEF12), myosin heavy chain 10 (MYH10), fibronectin 1 (FN1), integrin subunit alpha 2/6/V (ITGA2/6/V), integrin subunit beta 4 (ITGB4), CRK proto-oncogene (CRK/P38), SRC proto-oncogene (SRC), p21-activated kinase 4 (PAK4), cofilin 2 (CFL2), WASP like actin nucleation promoting factor (WASL), and ENAH actin regulator (ENAH). This data further demonstrates how Tpz-1's inhibitory effect on cytoskeleton-related protein expression could contribute to cell death.

3.6.2.5. Small cell lung and bladder cancers

Small cell lung (**Supplementary Figure S3.9**) and bladder cancer pathways (**Supplementary Figure S3.10**) were also significantly downregulated in our whole transcriptome analysis of Tpz-1. Specifically, inhibition of pro-proliferative cyclin dependent kinase inhibitor 1A (CDKN1A), cyclin D1 (CCND1), cyclin E2 (CCNE2), and TNF receptor associated factors 4/5 (TRAF4/5) signaling *via* integrin and EGFR/ERBB2 was observed and demonstrate the potential toxicity of Tpz-1 toward additional cancer types in vitro.

3.6.2.6. Transcriptome analysis also identified the upregulation of several cellular pathways by Tpz-1

Though Tpz-1 induced the upregulation of pathways that were not directly linked to cancer, there are connections between the genes associated with human cytomegalovirus infection, Yersinia infection, NOD-like receptor signaling, lipid and

atherosclerosis and several of the cancer-related pathways we know to be affected, including: the cell cycle, apoptosis, cytoskeleton, MAPK, PI3K-Akt, and JAK-STAT signaling pathways [93].

3.6.2.7. *Tpz-1 induced gene expression changes that influence the cell cycle*

The above pathways significantly affected by Tpz-1 led us to conduct a secondary investigation of Tpz-1's effect on the cell cycle. Notably, the cell cycle regulators cyclin D1 (CCND1) and cyclin E2 (CCNE2) were downregulated by Tpz-1 and indicate the compound's effect on slowing or halting the progression of cells through the G1 phase (**Supplementary Figure S.3.11**). Also, the downregulation of late mitotic regulator CDC14B suggests that Tpz-1 could also affect the successful mitotic exit of cells. Furthermore, the upregulation of tumor suppressor RB1 might also lead to the restriction of Tpz-1-treated cells from G0/G1 phase progression [199,200]. Moreover, the increased expression of mitotic checkpoint and c-myc antagonist MAD1L1 has been implicated in the delay of cell proliferation and growth in the context of chromosomal missegregation [201–203].

Together, these results support the findings of our previous cell cycle and cytoskeleton analyses [93], and support that the activity of Tpz-1 is dependent on the cell cycle and that cells undergoing mitosis may show increased sensitivity to the cytotoxic effects of the compound.

3.6.2.8. *Tpz-1-treated cells appear to be primed for programmed cell death*

An evaluation of all 1,788 differentially regulated genes was additionally conducted to determine Tpz-1's effect on three well-studied modes of programmed cell death: apoptosis (**Supplementary Figure S3.12**), autophagy (**Supplementary Figure**

S3.13), and necroptosis (**Supplementary Figure S3.14**). Several genes were found to be dysregulated in all three cell death pathways. Three upregulated genes (BCL2, TNFRSF10A, ITPR1), and five downregulated genes (PIK3C2A, PIK3R3, CAPN2, AKTIP, AKT3) were shared amongst at least two of the three studied programmed cell death pathways.

This data insinuates that widespread metabolic dysregulation occurs as a result of Tpz-1 treatment, and this dysregulation primes cells for programmed cell death through inflammatory and non-inflammatory pathways. This data also proposes that apoptosis may not be the preferred mode of cell death induced by Tpz-1, and depending on the cell cycle phase, environment, and metabolic condition of an individual cell, autophagy or necroptosis could predominate.

3.6.2.9. ConnectivityMap analysis supports an effect of Tpz-1 on the cytoskeleton

Across the significant ConnectivityMap perturbagens (**Table 3.3**), Tpz-1 activity appeared most similar to the gene expression profiles of queries in the PC3 cell line (**Figure 3.2**). Five of the nine gene knockdown perturbagens had connectivity scores \geq 95.00 in the PC3 cell line, compared to four of nine in HT29 and MCF7 cells. These results provide a strong rationale for the future in vitro evaluation of Tpz-1 against solid tumor cell lines.

Additionally, many of the perturbagens identified in the ConnectivityMap query were associated with oxidative stress, cell cycle disruption, cytoskeletal changes, and failed cytokinesis in the context of cancer (RNAseT2, UQCRFS1, KIF5C, DHRS2, HNE, DENND1B, TRIP13, COX5B). Together, this data reaffirms the notion that Tpz-1 cytotoxicity is related to aberration of mitosis and cytoskeleton-related pathways.

3.6.2.9.1. RNaseT2

RNaseT2 is a conserved and ubiquitously expressed endonuclease with a role in the cleavage and degradation of its RNA substrates. RNaseT2 can be secreted or intracellular; its secreted form is known for its immunomodulatory properties, while localization of the intracellular form suggests its involvement in the lysosomal degradation of RNA and mitochondrial RNA metabolism [118–120]. Altered expression of RNaseT2 has been observed in various cancers, including colorectal cancer, melanoma, and acute lymphoblastic leukemia, and can have pleiotropic effects [118–120]. In addition, RNaseT2 cleavage products have been shown to activate toll-like receptor 8 (TLR8), which is a fundamental activator of innate immunity and inflammation.

The transcriptional changes induced by Tpz-1 were highly connected to the effects of RNaseT2 knockdown in PC3 prostate ($\tau = 98.89$), A375 skin ($\tau = 99.58$), A549 lung ($\tau = 96.93$), MCF7 breast ($\tau = 99.59$), and HepG2 liver ($\tau = 95.98$) cancer cell lines. The summary connectivity score for RNaseT2 knockdown across all cell lines was 99.47. This information suggests that RNaseT2 inhibition could be a potential broad-spectrum outcome of Tpz-1 treatment in tumorigenic cells.

3.6.2.9.2. CD99

The CD99 molecule, also known as MIC2 or E2, is a transmembrane glycoprotein known for its role in several cellular processes, including cell adhesion, morphology, and survival [121,123,204]. CD99 is commonly overexpressed in hematopoietic malignancies are *oncojanus*, meaning they can be oncogenic or suppressive depending on the circumstances [121,122,204]. The expression signature

of Tpz-1 was highly connected to CD99 knockdown in non-cancerous HA1E kidney ($\tau = 97.31$), and cancerous HT29 colorectal ($\tau = 97.66$) and MCF7 breast ($\tau = 95.85$) cell lines. The connectivity of Tpz-1's gene expression signature to CD99 knockdown is highly relevant to Tpz-1's cytotoxic effect because CD99 has been touted as a biomarker for acute myeloid leukemia cells, and we used AML-derived HL60 cells in our whole transcriptome analysis.

In the context of AML (MOLM13 cell line), CD99 knockdown was reported to induce apoptosis *via* oncogenic stress by activating of Src family kinases RAS, c-MYC, BCR-ABL, and SYK [124,205–207]. In addition, silencing CD99 in MOLM13 cells caused cell cycle arrest in S/G₂/M and gene expression changes associated with DNA damage, replication stress, and unfolded protein responses; this effect was attributed to the oncogenic stress caused by rapid Src pathway activation [124]. We have identified a similar phenotype induced by Tpz-1, as several RAS associating genes (RASSF2/5, RASAL1/3, RASA3, RASGRP2), MYC, and SYK were significantly upregulated in the transcriptome, and we have observed the potential bias of Tpz-1 cytotoxicity toward cells in the G₂/M phase *in vitro* [93].

3.6.2.9.3. UQCRFS1

Rieske iron-sulfur polypeptide 1 (UQCRFS1) encodes an integral protein in the mitochondrial respiratory chain complex III that is responsible for its maturation, electron transfer, and reactive oxygen species production [125–127]. UQCRFS1 is known to be amplified in several cancers and may contribute to tumor progression [208–210].

As can be imagined, UQCRFS1 knockdown significantly impairs mitochondrial membrane potential and can thus contribute to cancer cell death. UQCRFS1

knockdown was connected to Tpz-1-induced gene expression changes for the PC3 cell line ($\tau = 98.32$), suggesting there may exist some cell-type specificity of this mitochondrial mode of action.

3.6.2.9.4. KIF5C

Kinesins are microtubule motor proteins [128,211]. KIF5C is a kinesin heavy chain protein of the classical kinesin complex that is most known for its role in motor neuron maintenance [128]. Although the connectivity scores between kinesin family member 5C (KIF5C) knockdown and the Tpz-1 transcriptome were less than 95.00 in individual cell lines, the summary score across all available cell lines was 97.40.

There is little known about KIF5C's role in cancer, however, because of its functional redundancy with KIF5 isoforms KIF5A/B, it can be postulated that knockdown of this gene could effectively reorganize the microtubule cytoskeleton and impede intracellular transport [129,212].

3.6.2.9.5. DHRS2

Dehydrogenase/reductase member 2 (DHRS2; Hep27) is a short-chain dehydrogenase/reductase family member whose activity in cancer has been conflictingly reported. While some studies suggest an oncosuppressive effect of DHRS2, others have correlated its expression with cancer development [130]. Tpz-1 gene expression was connected to DHRS2 knockdown in two reference cell lines, PC3 ($\tau = 99.52$) and A549 ($\tau = 97.15$). Of note, DHRS2 has known roles in lipid metabolism, oxidative damage prevention, and the cell cycle, which could be relevant to the anticancer activity of Tpz-1 [130].

3.6.2.9.6. HNE

HNE is a toxic product of lipid peroxidation/oxidative stress whose expression has been associated with cell cycle arrest, Fas- and p53-mediated apoptosis, NFκB inhibition, and pleiotropic activity in the context of cancer [131–136]. In its inactive form, NFκB exists in the cytosol and is bound to its inhibitory protein IκB [131]. Only when IκB is phosphorylated by IκB kinase (IκBK) will it dissociate so NFκB can translocate to the nucleus, where it is free to bind DNA and activate transcription [131]. HNE indirectly inhibits NFκB signaling through its interaction with IκBK, which prevents the IκB phosphorylation that is essential for NFκB dissociation [131,135].

The expression signature of Tpz-1 was comparable to HNE in the A375 melanoma ($\tau = 96.40$) and HT29 colorectal cancer ($\tau = 97.93$) cell lines, suggesting the biological activity of these two compounds may be similar in these cell types. However, more research would need to be conducted to clarify the molecular mechanism of HNE in these specific cell lines. Tpz-1 has not yet been evaluated against A375, but we have previously shown that its activity is pro-apoptotic in HT29 cells ($CC_{50} = 0.91 \mu\text{M}$) [93].

3.6.2.9.7. DENND1B

DENN/MADD domain containing 1B (DENND1B; connecden2) is a guanine exchange nucleotide factor that activates endosomal Rab35 [213]. Rab35 is a GTPase whose activity is associated with endosomal trafficking of cell surface proteins, cytokinesis, cytoskeleton organization, and cancer [137,213].

Accordingly, knockdown of DENND1B will reduce the activation of Rab35, and could theoretically promote cell death by disrupting cell surface signaling, cell–cell attachment (through disrupted trafficking of cadherins to the cell surface), cytoskeletal organization, and cytokinesis — each of these very relevant to our investigation of Tpz-

1 [137]. Tpz-1 gene expression was connected to DENND1B knockdown in two reference cell lines, PC3 ($\tau = 98.45$) and HT29 ($\tau = 95.47$).

3.6.2.9.8. TRIP13

Thyroid hormone receptor protein 13 (TRIP13) is known to be upregulated in various cancers and is associated with spindle assembly checkpoint, chromosomal instability, and DNA repair pathways [214–218]. TRIP13 knockdown was connected to the expression profile of Tpz-1 in HT29 ($\tau = 98.91$) and MCF7 ($\tau = 97.14$) cell lines, both of which we have confirmed the compound's cytotoxicity against [93].

Paradoxically, the physiological effects of TRIP13 overexpression mirrors the aneuploidy and chromosomal disorganization we observed in microscopic analysis of Tpz-1-treated HeLa cells [93], and TRIP13 was not differentially regulated in our transcriptome. Regardless, it appears plausible that TRIP13-related pathways overlap with those affected by Tpz-1, specifically those involving the mitotic spindle assembly checkpoint and chromosomal instability.

3.6.2.9.9. COX5B

Cytochrome c oxidase subunit 5b (COX5B) is a subunit of complex IV of the mitochondrial respiratory chain and is known to be differentially regulated in various cancers *via* c-Myc and Bcl2-mediated pathways [219–221]. Additionally, COX5B has been proposed as a prognostic biomarker in Myc-expressing breast cancers, considering its overexpression has been correlated to tissues with high metabolic demands [141,222]. Knockdown of COX5B has been associated with disrupted mitochondrial function, reduced ATP production, ROS accumulation, growth arrest, and senescence [141,142].

COX5B knockdown was significantly correlated to Tpz-1 transcriptional activity in the PC3 ($r = 99.45$) and MCF7 ($r = 96.83$) reference cell lines. The physiology of COX5B knockdown is similar to Tpz-1 activity in that we have previously observed loss of mitochondrial membrane potential, ROS accumulation, and growth arrest in HL60 and CCRF-CEM cells [93].

3.6.2.10. Ingenuity Pathway Analysis further connects Tpz-1 cytotoxicity to cytoskeleton-associated signaling pathways

To gain a better understanding of the cancer-related major biological themes associated with gene downregulation by Tpz-1, we assessed the IPA-provided graphical summary of our data (**Figures 3.3 and S3.15**) with the Qiagen Ingenuity Target Explorer. The 'Graphical Summary' feature illustrates potential connections between the significant canonical pathways, upstream regulators, diseases, and biological functions identified by IPA; chemicals are excluded. In the image, color indicates the directional relationship of each entity to Tpz-1 data based on the z-score. Positive z-scores are denoted in orange, and imply activation, whereas negative scores are shown in blue and represent inhibition.

Inhibition of upstream regulators transforming growth factor beta 3 (TGFB3), interferon gamma (IFNG), vascular endothelial growth factor A (VEGFA), angiotensinogen (AGT), and tumor necrosis factor (TNF) were at the center of the summary network, and they are thus heavily connected to the surrounding entities; each arrow indicates a predicted connection. Also central to the network were several inhibited biological pathways and functions: chemotaxis, invasion of tumor cell lines, cell movement, and high mobility group box 1/amphoterin (HMGB1) signaling.

Other inhibited genes such as interleukin 1A (IL1A), interleukin 4 (IL4), interleukin 5 (IL5), catenin beta 1 (CTNNB1), hypoxia inducible factor 1 subunit alpha (HIF1A), myocardin related transcription factors A/B (MRTFA/B), endothelin 1 (EDN1), and thrombin (F2) were peripherally located in the network and connected to one or more surrounding entity. The inhibition of biological processes such as the homing of cells, migration of embryonic cell lines, invasion of cells, cell movement of tumor cell lines, neoplasia of tumor cells, and reorganization of actin cytoskeleton were similarly found at the edges of the network. Interestingly, activation of ephrin family receptors A1-5 (EFNA1/2/3/4/5) was also predicted.

The results of IPA for the top 100 genes downregulated by Tpz-1 revealed similarities to our previous DAVID/KEGG Pathway analysis. Specifically, the inhibition of cell–ECM, ECM–receptor, and cell–cell interactions, and regulation of the cytoskeleton. However, an inhibitory effect of Tpz-1 on inflammatory cytokines was predicted in IPA and contradicts the predictions of DAVID/KEGG. No overlap was observed with our CMap analysis. Overall, despite the differences, these results provide additional evidence that supports Tpz-1 as a cytoskeleton-disrupting agent.

We assessed the cancer-related major biological themes associated with genes upregulated by Tpz-1 in a consistent manner (**Figures 3.4 and S3.16**). No gene, function, or pathway was predicted to be inhibited by our top 100 upregulated gene list. At the center of the IPA graphical summary for upregulation was the activation of upstream regulators nuclear factor kappa B subunit 1 (NFKB1), tumor necrosis factor (TNF), interleukin 33 (IL33), interleukin 5 (IL5), interleukin 1 beta (IL1B), myeloid differentiation primary response 88 (MYD88), interferon gamma (IFNG), toll like receptor

adaptor molecule 1 (TICAM1), endothelin 1 (EDN1), interleukin 1 alpha (IL1A), and interleukin 2 (IL2). Also at the center of the network was the activation of biological pathways and functions: adhesion of blood cells, adhesion of immune cells, binding of leukocytes, lymphopoiesis, and cell movement.

The activation of signal transducer and activator of transcription 3 (STAT3), toll like receptor 4 (TLR4), proto-oncogene ETS1, and catenin beta 1 (CTNNB1) were located at the edges of the network and were connected to at least one other upstream regulator, function, or pathway. Similarly predicted were the activation of pathways and functions involving the hematopoiesis, differentiation, interaction, binding, and adhesion of mononuclear leukocytes; adhesion of phagocytes; activation of neutrophils; adhesion of myeloid cells; binding of monocytes; and adhesion and binding of granulocytes. Tpz-1 gene upregulation was predicted to induce the activation of several pathways and upstream regulators that have been implicated in cancer, most notably, NFkB signaling (NFkB1, IL33), cytokine signaling (IL5, TNF, IL1A/B), and JAK-STAT signaling (IFNG, STAT3, IL2).

These results are somewhat comparable to our KEGG Pathway analysis, in that both experiments predicted connections between NFkB, JAK-STAT, and TNF signaling pathways and our upregulated gene list. However, the predicted activation of STAT3 contradicts the findings of our Multiplex Luminex kinase array [93], and is a stark reminder that this IPA data offers just a partial picture of Tpz-1 biological activity. Like the ConnectivityMap, our IPA was constructed from a truncated list of differentially expressed genes. Nevertheless, this analysis provides several potential pathways and targets of Tpz-1 that might be worthy of exploring in vitro.

3.6.3. Structural analysis revealed hypothetical molecular targets of Tpz-1

3.6.3.1. Evaluation of Tpz-1's drug-likeness via SwissDrugDesign tools and ChEMBL

Our multifaceted approach to evaluating Tpz-1's potential targets, drug-likeness, and pharmacokinetic profile was made possible with the user-friendly web-based SwissTargetPrediction (**Table 3.4**), SwissSimilarity (**Figure 3.5**), ChEMBL (**Table 3.5**) and SwissADME (**Figure 3.6**) tools. In many ways, these analyses reiterated what we had previously established about Tpz-1 activity: MAPK, cell cycle, and cytoskeleton dynamics are various effects that can result from cancer cell exposure to Tpz-1. However, there may also exist some potential problems with the solubility, reactivity, metabolism, and excretion of the compound in humans.

Despite its shortcomings, Tpz-1 has documented in vitro anticancer activity that is strongly supported by our SwissTargetPrediction results [47,48,93,163]. Moreover, SwissSimilarity revealed the structural likeness of Tpz-1 to at least two thienopyrazole-based antiviral drug candidates [166–168]; which not just implies a potential use for Tpz-1 in treating other diseases, but also implicates the thienopyrazole moiety in driving the compound's therapeutic activity. It is of note that Tpz-1's phenyl-thienopyrazole-carboxamide core structure was retained amongst many of the top SwissSimilarity hits, and it was the nitrogen immediately bound to the carboxamide group that was flagged for its potential toxicity.

Optimization of the Tpz-1 structure by decreasing the number of reactive double bonds or rings could potentially solve some of the solubility and structural issues, and

therefore offers a viable way to improve the potency and specificity of Tpz-1 to enable its advancement to the next phase of the anticancer drug discovery pipeline.

3.6.3.2. COREMINE medical text mining exposed the probable contribution of the thienopyrazole moiety to Tpz-1 function

Due to the unique and underexplored nature of Tpz-1's thienopyrazole scaffold, text mining of biomedical literature was performed to identify peer-reviewed publications that co-mentioned the terms 'thiophenes', 'pyrazoles', and 'neoplasms'. The resulting graphic networks were restricted to the top 10 gene/protein, molecular function, drug, and biological processes with $p < 0.05$ (**Figures 3.7-3.10**) to predict the possible anticancer effects of thienopyrazole-derived compounds like Tpz-1.

3.6.3.2.1. Gene/protein associations

The top 10 gene/protein associations from COREMINE each contained between 16,979 and 46,928 literature connections to the search terms. All associations were highly significant, with p -values $< 1.19765E-05$. Detailed below are each of the individual gene/protein associations and their relationships to cancer.

The B-Raf proto-oncogene (BRAF; Entrez Gene ID: 673) (**Figure 3.8**) encodes a protein that regulates MAP/ERK signaling to affect cell division [223]. Mutations of BRAF are common to numerous types of cancer [223]. Moreover, Kallikrein-family proteins are a group of serine proteases that have been implicated in cancer and have potential as cancer biomarkers [224]. The protein coding kallikrein related peptidase 3 (KLK3; Entrez Gene ID: 354) (**Figure 3.8**) is restricted in expression toward the prostate and is also known as 'PSA' in the clinical setting, where it is used in the diagnosis and monitoring of prostate cancer [224]. Additionally, TSC complex subunit 1, also known as

the tuberous sclerosis 1 (TSC1; Entrez Gene ID: 7248) (**Figure 3.8**) is a tumor suppressor gene that encodes the protein hamartin. This protein inhibits cell growth by negative regulating mammalian target of rapamycin complex 1 (mTORC1) signaling. Hamartin is also known for its role in facilitating heat shock protein 90 (Hsp90)-mediated folding of proteins to prevent their proteasomal degradation [225,226].

The tumor suppressor p53 gene (TP53; Entrez Gene ID: 7157) (**Figure 3.8**) encodes the protein P53, which is frequently mutated in cancer [227]. The P53 protein responds to cellular stresses to regulate gene expression and induce cell cycle arrest, apoptosis, senescence, and other metabolic changes [227]. Also, the BCL2 apoptosis regulator gene (BCL2; Entrez Gene ID: 596) (**Figure 2**) encodes an anti-apoptotic mitochondrial protein [22,228]. Constitutive expression of the BCL2 protein has been implicated in tumorigenesis [228]. Furthermore, the epidermal growth factor receptor (EGFR; Entrez Gene ID: 1956) gene (**Figure 3.8**) encodes a transmembrane receptor that binds to epidermal growth factor (EGF) to drive cell proliferation [229]. Erb-b2 receptor tyrosine kinase 2 (ERBB2; Entrez Gene ID: 2064) (**Figure 3.8**) is a protein encoding gene that is a member of the EGF receptor family and known to be overexpressed in various cancers [230]. In addition, Cadherin 1 (E-cadherin/CDH1; Entrez Gene ID: 999) (**Figure 3.8**) is a gene that encodes a calcium-dependent cell-cell adhesion protein whose mutations have been linked to cancer progression and metastasis [231]. Moreover, The CD274 gene (Entrez Gene ID: 29126) (**Figure 3.8**) encodes an immune inhibitory receptor ligand, PDL1, that is commonly expressed in tumor cells and considered a prognostic marker in many cancer types [232]. Interaction of membrane-bound PDL1 with its receptor inhibits immune activation, thus providing an

immune escape for cancerous cells [232]. Finally, the K-Ras proto-oncogene (KRAS; Entrez Gene ID: 3845) (**Figure 3.8**) encodes a GTPase that has been implicated in numerous cancers [233].

3.6.3.2.2. Drug associations

The top 10 drug associations from COREMINE each contained between 21,301 and 57,263 literature connections to the search terms. Docetaxel was co-mentioned the least, whereas EGF was co-mentioned the most. All relationships were significant, with p -values $< 1.182064E-05$. Each of the drugs are specified below.

The drugs most closely associated with these search terms were anticancer therapeutic agents carboplatin, fluorouracil, cisplatin, gemcitabine, doxorubicin, paclitaxel, and docetaxel (**Figure 3.10**). As well as the cancer diagnostic agent fluorodeoxyglucose F18, the breast cancer type 1 susceptibility protein (BRCA1) measurement assay, and the cell growth and differentiation stimulator epidermal growth factor (EGF) (**Figure 3.10**).

The results of this COREMINE medical text mining analysis reveal the vast amount of MEDLINE database literature evidence that has documented the anticancer activity of pyrazoles and thiophenes, and further supports the likelihood of Tpz-1 being a bona fide mitotic inhibitor. Furthermore, this analysis offers justification for the design and investigation of small molecule thienopyrazole derivatives as novel anticancer drugs.

3.6.3.2.3. Biological process and molecular function associations

The top 10 biological process and molecular function associations from COREMINE each contained between 12,042 and 199,363 literature connections to the

search terms. Methylated-DNA-[protein]-cysteine S-methyltransferase activity and epithelial to mesenchymal transition were the least connected molecular function and biological process, respectively. Whereas catalytic activity was the most connected molecular function, and cell growth was the most connected biological process. All processes and functions were highly significant, with p -values < 0.001196781 .

Like our other in silico analyses involving Tpz-1 transcriptome data, COREMINE illustrated significant connection between the search terms and cell migration, proliferation, and death processes. Apoptosis, signal transduction, and cell cycle biological effects were also identified in the query and corroborate the in vitro effects we observed with Tpz-1. Furthermore, the search terms were found robustly connected to kinase, enzymatic, and DNA binding functions and may explain the widespread gene dysregulation we observed after cancer cell exposure to Tpz-1.

From this analysis it can be postulated that small molecule formulations containing both thiophene and pyrazole rings are capable of interaction with cellular enzymes in and outside of the nucleus (**Figures 3.7 and 3.9**). Altogether, these findings strongly support the thienopyrazole moiety as a critical component of Tpz-1 that should be retained in future analogs designed to treat cancer.

3.6.4. Similarities exist between experimental and predicted targets of Tpz-1

To evaluate the viability of anticancer targets predicted for Tpz-1, we compared the results of each in silico experiment to previously published in vitro data from our group [93] and Fayad et al. [47]. We found a total of 14 cellular targets or functions that were identified by at least four bioinformatic tools or cell-based methods. For each of the 14 predicted associations, a score was calculated to reflect the number of

experiments in which they were identified (**'Total' column, Table 3.6**). The highest overlap between the predictions was found amongst pathways related to cancer (6 bioinformatic/cell-based experiments), cell proliferation (5), signal transduction (5), cell cycle (5), cell growth (5), cell death (5), catalytic activity (5), cell morphology (5), cytoskeletal protein (5), apoptotic process (5), EGFR (5), kinase activity (4), focal adhesion (4), and regulation of actin cytoskeleton (4). Notably, many of these terms also paralleled our COREMINE analysis of biomedical literature that co-mentioned the thienopyrazole parent groups (thiophene and pyrazole) in the context of cancer, further supporting our hypothesis that Tpz-1's thieno[2,3-c]pyrazole moiety drives its anticancer effect.

Table 3.6. A comparison of potential targets and cellular pathways affected by Tpz-1.

Experiment Association	COREMINE	ChEMBL	KEGG	Connectivity Map	IPA	In Vitro [47,93]	Total
Cancer	●	●	●	●	●	●	6
Cell proliferation	●	●	●	●	●	●	6
Cell death	●	●	●	●	●	●	6
Signal transduction	●	●	●	●	●		5
Cell cycle	●	●	●	●		●	5
Cell growth	●	●	●	●	●		5
Catalytic activity	●	●	●	●	●		5
Cell morphology		●	●	●	●	●	5
Cytoskeletal protein		●	●	●	●	●	5
Apoptotic process	●	●	●	●		●	5
EGFR	●	●	●		●		4
Kinase activity	●	●	●	●			4
Focal adhesion		●	●	●	●		4
Regulation of actin cytoskeleton		●	●	●	●		4

Despite EGFR being the only protein from our analyses that displayed overlap between experimental methods, previous studies have established the close association of EGFR with the cytoskeleton [179,234], thus, in theory, its downregulation could be a consequence of Tpz-1's interference with microtubule dynamics.

Similar thieno[2,3-c]pyrazole derivatives have been previously reported to have Aurora kinase inhibiting activity [45]. Thus, based on the biomedical literature and our collective analysis of the in vitro and in silico data presented herein, we believe that Aurora kinases, which are known to regulate microtubule dynamics during mitosis [235,236], are likely a primary molecular target of Tpz-1 at the low micromolar concentrations we have tested. Given our in vitro observations, which include the development of multipolar cell spindles, G2/M-specific cytotoxicity, delay of cell division, early loss of cell shape, and widespread transcriptome changes after Tpz-1 exposure, we hypothesize that Tpz-1 induces cancer cell apoptosis through post-translational inhibition of Aurora kinases when administered at concentrations $< 2.0 \mu\text{M}$. Aurora kinase inhibition may also explain the reduced capacity of Tpz-1 to inhibit tubulin polymerization at concentrations below $2.5 \mu\text{M}$ that was reported by Fayad et al. [47]. However, additional biochemical and molecular docking experiments are necessary to confirm the interaction of Tpz-1 with Aurora family kinases and validate this theory.

CHAPTER 4: CONCLUSIONS

4.1. FINAL DISCUSSION

Cell survival ultimately depends on a cell's ability to receive and interpret signals from its environment; without these external cues, it cannot properly anchor itself or respond to stressful stimuli. In drug discovery, “magic bullet” compounds, which potently and selectively act on a specific target, are traditionally sought after with the goal of reversing a particular disease phenotype while simultaneously minimizing the risk of off-target effects [237]. However, polypharmacology is an alternative approach that suggests the specific modulation of multiple targets could be analogous to “death by a thousand cuts”, whereby the drug hits several sensitive components of a cell to inflict death; it is distinct from drug promiscuity or combined treatment with multiple agents [237–239]. Considering the complex and dynamic nature of cancer, polypharmacology has increasingly become the preferred strategy of small molecule drug discovery initiatives [237–241].

Our high-throughput screening of 2000 molecules from the ChemBridge DIVERSet library revealed a uniquely structured compound, Tpz-1, which induced potent and cancer-specific apoptotic cell death at concentrations $< 2.0 \mu\text{M}$ consistently across a panel of 17 cancer cell lines. In 14 of the cell lines, Tpz-1 was effective at concentrations $< 1.0 \mu\text{M}$. A previous study of the compound in multicellular tumor spheroids revealed that $10 \mu\text{M}$ Tpz-1 inhibited tubulin polymerization similar to the mitotic inhibitor drug colchicine, however, this effect was not observed at concentrations below $2.5 \mu\text{M}$ [47]. We were able to confirm these differences in tubulin polymerization through visualization

of microtubule architecture after 10 μ M Tpz-1 treatment in non-cancerous Hs27 (**Figure 2.6**) and 0.19 μ M Tpz-1 in cervical adenocarcinoma HeLa (**Figure 2.7**) cell lines.

In an attempt to explain this discordance in Tpz-1's anticancer effect, our study utilized in vitro molecular assays in combination with structure- and transcriptome-based in silico predictions to reveal possible alternative protein targets of Tpz-1 at concentrations < 2.0 μ M. Based on a survey of the biomedical literature (**Figures 3.7-3.10**) and evidence we have collected, we hypothesize that at concentrations below 2.0 μ M, Tpz-1 kills cancer cells through the post-translational inhibition of Aurora kinase. We predict that this inhibition of Aurora kinases ultimately stimulates apoptotic cell death by disrupting microtubule dynamics, delaying mitosis, and perturbing cytoskeleton- and cell cycle-linked signaling processes (**Figures 2.3-2.5, Supplementary Figures S3.1-S3.16, and Tables 3.1-3.6**). This destabilization of microtubules leads to morphological effects that can be observed in our timelapse of HeLa H2B-GFP cells over a 30-hour treatment period (**Figure 3.1**). In addition to stress-induced programmed cell death (**Supplementary Figures S3.12-S3.14**), it is possible that some populations of cells may survive or senesce due to errors in chromosome separation that occur after exposure to Tpz-1 (**Figure 2.7**).

Lastly, Tpz-1 is structurally similar to thienopyrazole-based antiviral [166–168] (**Figure 3.5**) and anticancer drug candidates [45], and has also been patented by The University of Texas System for its ectonucleoside triphosphate diphosphohydrolase 5 (ENTPD5) inhibition [163], thus this small molecule compound may indeed be multitargeted and potentially useful in treating several cancer types and other complex conditions. However, potential in vivo toxicities of Tpz-1 could exist due to its relatively

poor solubility and the presence of reactive double bonds. Opportunities for structural optimization of Tpz-1 have been highlighted thanks to the SwissADME platform and are detailed in **Figure 3.6**.

4.2. LIMITATIONS

There are several limitations to this study to address, such as our use of tools that required us to evaluate only the top 100 or 150 differentially expressed genes (i.e., ConnectivityMap and IPA). Moreover, low concentrations of DMSO have been shown to induce HL-60 cell differentiation [242,243], and its use as a solvent could have had some influence on the transcriptome of Tpz-1-treated cells. However, our transcriptome analysis compared the gene expression signatures of Tpz-1-treated and DMSO-treated cells to generate significance and fold change values, thus mitigating the effect of the vehicle on our data.

Also, it is important to note that like many early drug candidates, there exist structural features of Tpz-1 that could introduce problems with compound solubility and/or toxicity in vivo. Thus, structural optimization of Tpz-1 would realistically be needed to meaningfully advance this compound's development as an anticancer drug. Despite these limitations, we believe that the unique approach to target deconvolution described in this dissertation has offered considerable and robust in silico and in vitro evidence that supports Tpz-1's potential as a cytoskeleton disruptor and mitotic inhibitor agent.

4.3. FUTURE DIRECTIONS

We hope that the evidence contained in this dissertation provides our colleagues with a fruitful foundation for future thienopyrazole-based drug design projects, especially those willing to take on the structural optimization of Tpz-1. In addition to compound

optimization, future directions this project could take include the exploration of discrete molecular targets identified in this dissertation (i.e., Aurora kinase) using in silico molecular docking and in vitro biochemical, microscopy, or cell painting assays. Additionally, the application of homogenous and heterogeneous 3D culture techniques could be used to gain a better understanding of Tpz-1's tumor-penetrance in vivo.

4.4. FINAL CONCLUSIONS

Although perhaps more questions about Tpz-1's molecular activity has been raised than answered in this dissertation, ample justification for continuing development of this uniquely structured molecule has been provided. There is a growing body of evidence that illustrates the biological effect of thienopyrazole-based compounds; thus, it is important that the molecular mechanism of Tpz-1 continues to be explored and optimized for testing in animals. As our knowledge of the genetic and epigenetic differences that contribute to cancer expands, so must our range of innovative anticancer drugs to meet the personalized treatment needs of cancer patients; exploring novel chemical groups in small molecule screening projects is just one way we can accomplish this in the drug discovery and development field.

REFERENCES

1. Miller KD, Ortiz AP, Pinheiro PS, Bandi P, Minihan A, Fuchs HE, et al. Cancer statistics for the US Hispanic/Latino population, 2021. *CA Cancer J Clin.* 2021. doi:10.3322/caac.21695
2. Philipovskiy A, Dwivedi AK, Gamez R, McCallum R, Mukherjee D, Nahleh Z, et al. Association between tumor mutation profile and clinical outcomes among Hispanic Latina women with triple-negative breast cancer. *PLoS One.* 2020;15: e0238262. doi:10.1371/journal.pone.0238262
3. Zamora SM, Pinheiro PS, Gomez SL, Hastings KG, Palaniappan LP, Hu J, et al. Disaggregating Hispanic American Cancer Mortality Burden by Detailed Ethnicity. *Cancer Epidemiol Biomarkers Prev.* 2019;28: 1353–1363. doi:10.1158/1055-9965.EPI-18-0872
4. Paulozzi LJ, McDonald JA, Sroka CJ. A Disparity beneath a Paradox: Cancer Mortality among Young Hispanic Americans in the US-Mexico Border Region. *J Racial Ethn Health Disparities.* 2021;8: 1556–1562. doi:10.1007/s40615-020-00920-6
5. Siegel RL, Miller KD, Fuchs HE, Jemal A. Cancer statistics, 2022. *CA Cancer J Clin.* 2022;72: 7–33. doi:10.3322/caac.21708
6. Marusyk A, Polyak K. Tumor heterogeneity: causes and consequences. *Biochim Biophys Acta.* 2010;1805: 105–117. doi:10.1016/j.bbcan.2009.11.002
7. Zhu X, Li S, Xu B, Luo H. Cancer evolution: A means by which tumors evade treatment. *Biomed Pharmacother.* 2021;133: 111016. doi:10.1016/j.biopha.2020.111016
8. Sparreboom A, Verweij J. Advances in cancer therapeutics. *Clin Pharmacol Ther.* 2009;85: 113–117. doi:10.1038/clpt.2008.259
9. National Cancer Institute. Types of Cancer Treatment. 31 Jul 2017 [cited 14 Oct 2021]. Available: <https://www.cancer.gov/about-cancer/treatment/types>
10. Baudino TA. Targeted Cancer Therapy: The Next Generation of Cancer Treatment. *Curr Drug Discov Technol.* 2015;12: 3–20. doi:10.2174/1570163812666150602144310
11. Sinha S, Vohora D. Drug discovery and development. *Pharmaceutical Medicine and Translational Clinical Research.* Elsevier; 2018. pp. 19–32. doi:10.1016/b978-0-12-802103-3.00002-x
12. Kotz J. Phenotypic screening, take two. *Sci-Bus eXch.* 2012;5: 380–380. doi:10.1038/scibx.2012.380

13. Sams-Dodd F. Drug discovery: selecting the optimal approach. *Drug Discov Today*. 2006;11: 465–472. doi:10.1016/j.drudis.2006.03.015
14. Kerr JF, Wyllie AH, Currie AR. Apoptosis: a basic biological phenomenon with wide-ranging implications in tissue kinetics. *Br J Cancer*. 1972;26: 239–257. doi:10.1038/bjc.1972.33
15. Taylor RC, Cullen SP, Martin SJ. Apoptosis: controlled demolition at the cellular level. *Nat Rev Mol Cell Biol*. 2008;9: 231–241. doi:10.1038/nrm2312
16. Kerr JF, Winterford CM, Harmon BV. Apoptosis. Its significance in cancer and cancer therapy. *Cancer*. 1994;73: 2013–2026. doi:10.1002/1097-0142(19940415)73:8<2013::aid-cnrcr2820730802>3.0.co;2-j
17. Saraste A, Pulkki K. Morphologic and biochemical hallmarks of apoptosis. *Cardiovasc Res*. 2000;45: 528–537. doi:10.1016/S0008-6363(99)00384-3
18. Fulda S. Tumor resistance to apoptosis. *Int J Cancer*. 2009;124: 511–515. doi:10.1002/ijc.24064
19. Wong RSY. Apoptosis in cancer: from pathogenesis to treatment. *J Exp Clin Cancer Res*. 2011;30: 87. doi:10.1186/1756-9966-30-87
20. Koff JL, Ramachandiran S, Bernal-Mizrachi L. A time to kill: targeting apoptosis in cancer. *Int J Mol Sci*. 2015;16: 2942–2955. doi:10.3390/ijms16022942
21. Elmore S. Apoptosis: a review of programmed cell death. *Toxicol Pathol*. 2007;35: 495–516. doi:10.1080/01926230701320337
22. Youle RJ, Strasser A. The BCL-2 protein family: opposing activities that mediate cell death. *Nat Rev Mol Cell Biol*. 2008;9: 47–59. doi:10.1038/nrm2308
23. Mortenson MM, Galante JG, Gilad O, Schlieman MG, Virudachalam S, Kung H-J, et al. BCL-2 functions as an activator of the AKT signaling pathway in pancreatic cancer. *J Cell Biochem*. 2007;102: 1171–1179. doi:10.1002/jcb.21343
24. Carneiro BA, El-Deiry WS. Targeting apoptosis in cancer therapy. *Nat Rev Clin Oncol*. 2020;17: 395–417. doi:10.1038/s41571-020-0341-y
25. Wang X, Martindale JL, Holbrook NJ. Requirement for ERK Activation in Cisplatin-induced Apoptosis *. *J Biol Chem*. 2000;275: 39435–39443. doi:10.1074/jbc.M004583200
26. Boice A, Bouchier-Hayes L. Targeting apoptotic caspases in cancer. *Biochim Biophys Acta Mol Cell Res*. 2020;1867: 118688. doi:10.1016/j.bbamcr.2020.118688

27. Kim S-H, Park E-J, Lee CR, Chun JN, Cho N-H, Kim I-G, et al. Geraniol induces cooperative interaction of apoptosis and autophagy to elicit cell death in PC-3 prostate cancer cells. *Int J Oncol*. 2012;40: 1683–1690. doi:10.3892/ijo.2011.1318
28. Zheng W, Thorne N, McKew JC. Phenotypic screens as a renewed approach for drug discovery. *Drug Discov Today*. 2013;18: 1067–1073. doi:10.1016/j.drudis.2013.07.001
29. Bedard PL, Hyman DM, Davids MS, Siu LL. Small molecules, big impact: 20 years of targeted therapy in oncology. *Lancet*. 2020;395: 1078–1088. doi:10.1016/S0140-6736(20)30164-1
30. Lee YT, Tan YJ, Oon CE. Molecular targeted therapy: Treating cancer with specificity. *Eur J Pharmacol*. 2018;834: 188–196. doi:10.1016/j.ejphar.2018.07.034
31. Zhong L, Li Y, Xiong L, Wang W, Wu M, Yuan T, et al. Small molecules in targeted cancer therapy: advances, challenges, and future perspectives. *Signal Transduct Target Ther*. 2021;6: 201. doi:10.1038/s41392-021-00572-w
32. Karrouchi K, Radi S, Ramli Y, Taoufik J, Mabkhot YN, Al-Aizari FA, et al. Synthesis and Pharmacological Activities of Pyrazole Derivatives: A Review. *Molecules*. 2018;23. doi:10.3390/molecules23010134
33. Shah R, Verma PK. Therapeutic importance of synthetic thiophene. *Chem Cent J*. 2018;12: 137. doi:10.1186/s13065-018-0511-5
34. El-Gamal MI, Zaraei S-O, Madkour MM, Anbar HS. Evaluation of Substituted Pyrazole-Based Kinase Inhibitors in One Decade (2011-2020): Current Status and Future Prospects. *Molecules*. 2022;27. doi:10.3390/molecules27010330
35. Gutierrez DA, Contreras L, Villanueva PJ, Borrego EA, Morán-Santibañez K, Hess JD, et al. Identification of a Potent Cytotoxic Pyrazole with Anti-Breast Cancer Activity That Alters Multiple Pathways. *Cells*. 2022;11. doi:10.3390/cells11020254
36. Ashourpour M, Mostafavi Hosseini F, Amini M, Saeedian Moghadam E, Kazerouni F, Arman SY, et al. Pyrazole Derivatives Induce Apoptosis via ROS Generation in the Triple Negative Breast Cancer Cells, MDA-MB-468. *Asian Pac J Cancer Prev*. 2021;22: 2079–2087. doi:10.31557/APJCP.2021.22.7.2079
37. Archana, Pathania S, Chawla PA. Thiophene-based derivatives as anticancer agents: An overview on decade's work. *Bioorg Chem*. 2020;101: 104026. doi:10.1016/j.bioorg.2020.104026
38. El-Borai MA, Rizk HF, Ibrahim SA, Fares AK, El-Tahawy MMT, Beltagy DM. Assessment of anti-hemolytic, cytotoxicity, antioxidant activities and molecular docking study based on thienopyrazole scaffold as pharmacophore. *J Mol Struct*. 2021;1240: 130602. doi:10.1016/j.molstruc.2021.130602

39. Raffa D, Maggio B, Raimondi MV, Cascioferro S, Plescia F, Cancemi G, et al. Recent advanced in bioactive systems containing pyrazole fused with a five membered heterocycle. *Eur J Med Chem*. 2015;97: 732–746. doi:10.1016/j.ejmech.2014.12.023
40. Zaki RM, Saber AF, El-Dean AMK, Radwan SM. A concise review on synthesis, reactions and biological importance of thienopyrazoles. *ARKIVOC*. 2020;2020: 20–60. doi:10.24820/ark.5550190.p011.108
41. Goto M, Murakawa M, Kadoshima-Yamaoka K, Tanaka Y, Inoue H, Murafuji H, et al. Phosphodiesterase 7A inhibitor ASB16165 suppresses proliferation and cytokine production of NKT cells. *Cell Immunol*. 2009;258: 147–151. doi:10.1016/j.cellimm.2009.04.005
42. Goto M, Kadoshima-Yamaoka K, Murakawa M, Yoshioka R, Tanaka Y, Inoue H, et al. Phosphodiesterase 7A inhibitor ASB16165 impairs proliferation of keratinocytes in vitro and in vivo. *Eur J Pharmacol*. 2010;633: 93–97. doi:10.1016/j.ejphar.2010.01.024
43. Brotherton-Pleiss CE, Dillon MP, Ford APDW, Gever JR, Carter DS, Gleason SK, et al. Discovery and optimization of RO-85, a novel drug-like, potent, and selective P2X3 receptor antagonist. *Bioorg Med Chem Lett*. 2010;20: 1031–1036. doi:10.1016/j.bmcl.2009.12.044
44. Fancelli D, Isacchi A, Modugno M, Moll J, Rusconi L, Soncini C, et al. Use of a kinase inhibitor for the treatment of particular resistant tumors. US Patent. 7803829, 2010. Available: <https://patentimages.storage.googleapis.com/ef/4d/bc/1688dad69548a2/US7803829.pdf>
45. Fancelli D, Moll J, Pulici M, Quartieri F, Bandiera T. 1H-thieno[2,3-c]pyrazole compounds useful as kinase inhibitors. US Patent. 7943654, 2011. Available: <https://patentimages.storage.googleapis.com/8f/b4/77/76605de86ac89c/US7943654.pdf>
46. Barberis C, Carry J-C, Doerflinger G, Barbalat-Damour D, Clerc F, Minoux H. Hydrazinocarbonyl-thieno[2,3-C]pyrazoles, process for preparing them, compositions containing them and use thereof. US Patent. 7595320, 2009. Available: <https://patentimages.storage.googleapis.com/69/1c/6f/2129c0744d9be7/US7595320.pdf>
47. Fayad W, Rickardson L, Haglund C, Olofsson MH, D'Arcy P, Larsson R, et al. Identification of agents that induce apoptosis of multicellular tumour spheroids: enrichment for mitotic inhibitors with hydrophobic properties. *Chem Biol Drug Des*. 2011;78: 547–557. doi:10.1111/j.1747-0285.2011.01170.x
48. Darwish WMA, Bayoumi NA. Gold nanorod-loaded (PLGA-PEG) nanocapsules as near-infrared controlled release model of anticancer therapeutics. *Lasers Med Sci*. 2020;35: 1729–1740. doi:10.1007/s10103-020-02964-w

49. Miller KD, Fidler-Benaoudia M, Keegan TH, Hipp HS, Jemal A, Siegel RL. Cancer statistics for adolescents and young adults, 2020. *CA Cancer J Clin.* 2020;70: 443–459. doi:10.3322/caac.21637
50. Hijiya N, Ness KK, Ribeiro RC, Hudson MM. Acute leukemia as a secondary malignancy in children and adolescents: current findings and issues. *Cancer.* 2009;115: 23–35. doi:10.1002/cncr.23988
51. Leone G, Mele L, Pulsoni A, Equitani F, Pagano L. The incidence of secondary leukemias. *Haematologica.* 1999;84: 937–945. Available: <https://www.ncbi.nlm.nih.gov/pubmed/10509043>
52. Bispo JAB, Pinheiro PS, Kobetz EK. Epidemiology and Etiology of Leukemia and Lymphoma. *Cold Spring Harb Perspect Med.* 2020;10. doi:10.1101/cshperspect.a034819
53. Shallis RM, Wang R, Davidoff A, Ma X, Zeidan AM. Epidemiology of acute myeloid leukemia: Recent progress and enduring challenges. *Blood Rev.* 2019;36: 70–87. doi:10.1016/j.blre.2019.04.005
54. Miller KD, Nogueira L, Mariotto AB, Rowland JH, Yabroff KR, Alfano CM, et al. Cancer treatment and survivorship statistics, 2019. *CA Cancer J Clin.* 2019;69: 363–385. doi:10.3322/caac.21565
55. Ruiz-Medina BE, Lerma D, Hwang M, Ross JA, Skouta R, Aguilera RJ, et al. Green barley mitigates cytotoxicity in human lymphocytes undergoing aggressive oxidative stress, via activation of both the Lyn/PI3K/Akt and MAPK/ERK pathways. *Sci Rep.* 2019;9: 6005. doi:10.1038/s41598-019-42228-4
56. Lema C, Varela-Ramirez A, Aguilera RJ. Differential nuclear staining assay for high-throughput screening to identify cytotoxic compounds. *Curr Cell Biochem.* 2011;1: 1–14. Available: <https://www.ncbi.nlm.nih.gov/pubmed/27042697>
57. Cook JD. Linear interpolation calculator. [cited 26 Jan 2022]. Available: <https://www.johndcook.com/interpolator.html>
58. Nakamura-Bencomo S, Gutierrez DA, Robles-Escajeda E, Iglesias-Figueroa B, Siqueiros-Cendón TS, Espinoza-Sánchez EA, et al. Recombinant human lactoferrin carrying humanized glycosylation exhibits antileukemia selective cytotoxicity, microfilament disruption, cell cycle arrest, and apoptosis activities. *Invest New Drugs.* 2021;39: 400–415. doi:10.1007/s10637-020-01020-2
59. Robles-Escajeda E, Das U, Ortega NM, Parra K, Francia G, Dimmock JR, et al. A novel curcumin-like dienone induces apoptosis in triple-negative breast cancer cells. *Cell Oncol.* 2016;39: 265–277. doi:10.1007/s13402-016-0272-x

60. Pistritto G, Trisciuglio D, Ceci C, Garufi A, D'Orazi G. Apoptosis as anticancer mechanism: function and dysfunction of its modulators and targeted therapeutic strategies. *Aging* . 2016;8: 603–619. doi:10.18632/aging.100934
61. Robles-Escajeda E, Lerma D, Nyakeriga AM, Ross JA, Kirken RA, Aguilera RJ, et al. Searching in mother nature for anti-cancer activity: anti-proliferative and pro-apoptotic effect elicited by green barley on leukemia/lymphoma cells. *PLoS One*. 2013;8: e73508. doi:10.1371/journal.pone.0073508
62. Tummers B, Green DR. Caspase-8: regulating life and death. *Immunol Rev*. 2017;277: 76–89. doi:10.1111/imr.12541
63. Sinha K, Das J, Pal PB, Sil PC. Oxidative stress: the mitochondria-dependent and mitochondria-independent pathways of apoptosis. *Arch Toxicol*. 2013;87: 1157–1180. doi:10.1007/s00204-013-1034-4
64. Gutierrez DA, DeJesus RE, Contreras L, Rodriguez-Palomares IA, Villanueva PJ, Balderrama KS, et al. A new pyridazinone exhibits potent cytotoxicity on human cancer cells via apoptosis and poly-ubiquitinated protein accumulation. *Cell Biol Toxicol*. 2019;35: 503–519. doi:10.1007/s10565-019-09466-8
65. Kaiser MA, Sivandzade F, Bhalerao A, Cucullo L. Conventional and electronic cigarettes dysregulate the expression of iron transporters and detoxifying enzymes at the brain vascular endothelium: In vivo evidence of a gender-specific cellular response to chronic cigarette smoke exposure. *Neurosci Lett*. 2018;682: 1–9. doi:10.1016/j.neulet.2018.05.045
66. Sivandzade F, Bhalerao A, Cucullo L. Analysis of the Mitochondrial Membrane Potential Using the Cationic JC-1 Dye as a Sensitive Fluorescent Probe. *Bio Protoc*. 2019;9. doi:10.21769/BioProtoc.3128
67. Martin SJ, Reutelingsperger CP, McGahon AJ, Rader JA, van Schie RC, LaFace DM, et al. Early redistribution of plasma membrane phosphatidylserine is a general feature of apoptosis regardless of the initiating stimulus: inhibition by overexpression of Bcl-2 and Abl. *J Exp Med*. 1995;182: 1545–1556. doi:10.1084/jem.182.5.1545
68. Redza-Dutordoir M, Averill-Bates DA. Activation of apoptosis signalling pathways by reactive oxygen species. *Biochim Biophys Acta*. 2016;1863: 2977–2992. doi:10.1016/j.bbamcr.2016.09.012
69. Tait SWG, Green DR. Mitochondria and cell death: outer membrane permeabilization and beyond. *Nat Rev Mol Cell Biol*. 2010;11: 621–632. doi:10.1038/nrm2952
70. Liu H. Emerging agents and regimens for AML. *J Hematol Oncol*. 2021;14: 49. doi:10.1186/s13045-021-01062-w

71. Al-Hussaini M, DiPersio JF. Small molecule inhibitors in acute myeloid leukemia: from the bench to the clinic. *Expert Rev Hematol.* 2014;7: 439–464. doi:10.1586/17474086.2014.932687
72. Malard F, Mohty M. Acute lymphoblastic leukaemia. *Lancet.* 2020;395: 1146–1162. doi:10.1016/S0140-6736(19)33018-1
73. El-Dean AMK, Zaki RM, Abdulrazzaq AY. A convenient synthesis and biological activity of novel thieno[2,3-c]pyrazole compounds as antimicrobial and anti-inflammatory agents. *Russ J Bioorganic Chem.* 2015;41: 97–104. doi:10.1134/s1068162015010057
74. McLean LR, Zhang Y, Zaidi N, Bi X, Wang R, Dharanipragada R, et al. X-ray crystallographic structure-based design of selective thienopyrazole inhibitors for interleukin-2-inducible tyrosine kinase. *Bioorg Med Chem Lett.* 2012;22: 3296–3300. doi:10.1016/j.bmcl.2012.03.016
75. Akritopoulou-Zanze I, Hajduk PJ. Kinase-targeted libraries: the design and synthesis of novel, potent, and selective kinase inhibitors. *Drug Discov Today.* 2009;14: 291–297. doi:10.1016/j.drudis.2008.12.002
76. Akritopoulou-Zanze I, Darczak D, Sarris K, Phelan KM, Huth JR, Song D, et al. Scaffold oriented synthesis. Part 1: Design, preparation, and biological evaluation of thienopyrazoles as kinase inhibitors. *Bioorg Med Chem Lett.* 2006;16: 96–99. doi:10.1016/j.bmcl.2005.09.042
77. Dhillon AS, Hagan S, Rath O, Kolch W. MAP kinase signalling pathways in cancer. *Oncogene.* 2007;26: 3279–3290. doi:10.1038/sj.onc.1210421
78. Yan Y, Black CP, Cowan KH. Irradiation-induced G2/M checkpoint response requires ERK1/2 activation. *Oncogene.* 2007;26: 4689–4698. doi:10.1038/sj.onc.1210268
79. Lv C, Hong Y, Miao L, Li C, Xu G, Wei S, et al. Wentilactone A as a novel potential antitumor agent induces apoptosis and G2/M arrest of human lung carcinoma cells, and is mediated by HRas-GTP accumulation to excessively activate the Ras/Raf/ERK/p53-p21 pathway. *Cell Death Dis.* 2013;4: e952. doi:10.1038/cddis.2013.484
80. Kamran MZ, Patil P, Gude RP. Role of STAT3 in cancer metastasis and translational advances. *Biomed Res Int.* 2013;2013: 421821. doi:10.1155/2013/421821
81. Xiao X, Li BX, Mitton B, Ikeda A, Sakamoto KM. Targeting CREB for cancer therapy: friend or foe. *Curr Cancer Drug Targets.* 2010;10: 384–391. doi:10.2174/156800910791208535
82. Huynh J, Chand A, Gough D, Ernst M. Therapeutically exploiting STAT3 activity in cancer - using tissue repair as a road map. *Nat Rev Cancer.* 2019;19: 82–96. doi:10.1038/s41568-018-0090-8

83. Riebe C, Pries R, Schroeder KN, Wollenberg B. Phosphorylation of STAT3 in head and neck cancer requires p38 MAPKinase, whereas phosphorylation of STAT1 occurs via a different signaling pathway. *Anticancer Res.* 2011;31: 3819–3825. Available: <https://www.ncbi.nlm.nih.gov/pubmed/22110204>
84. Du K, Montminy M. CREB Is a Regulatory Target for the Protein Kinase Akt/PKB *. *J Biol Chem.* 1998;273: 32377–32379. doi:10.1074/jbc.273.49.32377
85. Liu J, Chen B, Lu Y, Guan Y, Chen F. JNK-dependent Stat3 phosphorylation contributes to Akt activation in response to arsenic exposure. *Toxicol Sci.* 2012;129: 363–371. doi:10.1093/toxsci/kfs199
86. Delghandi MP, Johannessen M, Moens U. The cAMP signalling pathway activates CREB through PKA, p38 and MSK1 in NIH 3T3 cells. *Cell Signal.* 2005;17: 1343–1351. doi:10.1016/j.cellsig.2005.02.003
87. Iwamoto E, Ueta N, Matsui Y, Kamijo K, Kuga T, Saito Y, et al. ERK Plays a Role in Chromosome Alignment and Participates in M-Phase Progression. *J Cell Biochem.* 2016;117: 1340–1351. doi:10.1002/jcb.25424
88. Verlhac MH, de Pennart H, Maro B, Cobb MH, Clarke HJ. MAP kinase becomes stably activated at metaphase and is associated with microtubule-organizing centers during meiotic maturation of mouse oocytes. *Dev Biol.* 1993;158: 330–340. doi:10.1006/dbio.1993.1192
89. Zou D, Yang X, Tan Y, Wang P, Zhu X, Yang W, et al. Regulation of the hematopoietic cell kinase (HCK) by PML/RAR α and PU.1 in acute promyelocytic leukemia. *Leuk Res.* 2012;36: 219–223. doi:10.1016/j.leukres.2011.09.012
90. Shivakrupa R, Radha V, Sudhakar C, Swarup G. Physical and functional interaction between Hck tyrosine kinase and guanine nucleotide exchange factor C3G results in apoptosis, which is independent of C3G catalytic domain. *J Biol Chem.* 2003;278: 52188–52194. doi:10.1074/jbc.M310656200
91. Tibaldi E, Brunati AM, Massimino ML, Stringaro A, Colone M, Agostinelli E, et al. Src-Tyrosine kinases are major agents in mitochondrial tyrosine phosphorylation. *J Cell Biochem.* 2008;104: 840–849. doi:10.1002/jcb.21670
92. Acín-Pérez R, Carrascoso I, Baixauli F, Roche-Molina M, Latorre-Pellicer A, Fernández-Silva P, et al. ROS-triggered phosphorylation of complex II by Fgr kinase regulates cellular adaptation to fuel use. *Cell Metab.* 2014;19: 1020–1033. doi:10.1016/j.cmet.2014.04.015
93. Hess JD, Macias LH, Gutierrez DA. Identification of a Unique Cytotoxic Thieno [2, 3-c] Pyrazole Derivative with Potent and Selective Anticancer Effects In Vitro. *Biology* . 2022. Available: <https://www.mdpi.com/article/10.3390/biology11060930>

94. Hart CP. Finding the target after screening the phenotype. *Drug Discov Today*. 2005;10: 513–519. doi:10.1016/S1359-6446(05)03415-X
95. Sydow D, Burggraaff L, Szengel A, van Vlijmen HWT, IJzerman AP, van Westen GJP, et al. Advances and Challenges in Computational Target Prediction. *J Chem Inf Model*. 2019;59: 1728–1742. doi:10.1021/acs.jcim.8b00832
96. DAVID Functional Annotation Bioinformatics Microarray Analysis. [cited 12 Jun 2022]. Available: <https://david.ncifcrf.gov/home.jsp>
97. Huang DW, Sherman BT, Lempicki RA. Systematic and integrative analysis of large gene lists using DAVID bioinformatics resources. *Nat Protoc*. 2009;4: 44–57. doi:10.1038/nprot.2008.211
98. Huang DW, Sherman BT, Lempicki RA. Bioinformatics enrichment tools: paths toward the comprehensive functional analysis of large gene lists. *Nucleic Acids Res*. 2009;37: 1–13. doi:10.1093/nar/gkn923
99. Benjamini Y, Hochberg Y. Controlling the false discovery rate: A practical and powerful approach to multiple testing. *J R Stat Soc*. 1995;57: 289–300. doi:10.1111/j.2517-6161.1995.tb02031.x
100. KEGG: Kyoto Encyclopedia of Genes and Genomes. [cited 30 Jun 2022]. Available: <https://www.kegg.jp/>
101. CLUE Platform. In: ConnectivityMap [Internet]. 2017 [cited 16 Mar 2022]. Available: <https://clue.io/>
102. Subramanian A, Narayan R, Corsello SM, Peck DD, Natoli TE, Lu X, et al. A Next Generation Connectivity Map: L1000 Platform and the First 1,000,000 Profiles. *Cell*. 2017;171: 1437–1452.e17. doi:10.1016/j.cell.2017.10.049
103. HGNC. In: Hugo Gene Nomenclature Committee [Internet]. 2021 [cited 29 Jun 2022]. Available: <https://www.genenames.org/>
104. Farani PSG, Begum K, Vilar-Pereira G, Pereira IR, Almeida IC, Roy S, et al. Treatment With Suboptimal Dose of Benznidazole Mitigates Immune Response Molecular Pathways in Mice With Chronic Chagas Cardiomyopathy. *Front Cell Infect Microbiol*. 2021;11: 692655. doi:10.3389/fcimb.2021.692655
105. Helleman J, Smid M, Jansen MPH, van der Burg MEL, Berns EMJJ. Pathway analysis of gene lists associated with platinum-based chemotherapy resistance in ovarian cancer: the big picture. *Gynecol Oncol*. 2010;117: 170–176. doi:10.1016/j.ygyno.2010.01.010
106. Target Explorer Search - Ingenuity Systems. [cited 12 Jul 2022]. Available: <https://targetexplorer.ingenuity.com/index.htm>

107. National Center for Biotechnology Information. PubChem Compound Summary for CID 5331400. 2022 [cited 19 Jul 2022]. Available: <https://pubchem.ncbi.nlm.nih.gov/compound/5331400>
108. Davies M, Nowotka M, Papadatos G, Dedman N, Gaulton A, Atkinson F, et al. ChEMBL web services: streamlining access to drug discovery data and utilities. *Nucleic Acids Res.* 2015;43: W612-20. doi:10.1093/nar/gkv352
109. Mendez D, Gaulton A, Bento AP, Chambers J, De Veij M, Félix E, et al. ChEMBL: towards direct deposition of bioassay data. *Nucleic Acids Res.* 2019;47: D930–D940. doi:10.1093/nar/gky1075
110. Daina A, Michielin O, Zoete V. SwissTargetPrediction: updated data and new features for efficient prediction of protein targets of small molecules. *Nucleic Acids Res.* 2019;47: W357–W364. doi:10.1093/nar/gkz382
111. Zoete V, Daina A, Bovigny C, Michielin O. SwissSimilarity: A Web Tool for Low to Ultra High Throughput Ligand-Based Virtual Screening. *J Chem Inf Model.* 2016;56: 1399–1404. doi:10.1021/acs.jcim.6b00174
112. Daina A, Michielin O, Zoete V. iLOGP: a simple, robust, and efficient description of n-octanol/water partition coefficient for drug design using the GB/SA approach. *J Chem Inf Model.* 2014;54: 3284–3301. doi:10.1021/ci500467k
113. Daina A, Zoete V. A BOILED-Egg To Predict Gastrointestinal Absorption and Brain Penetration of Small Molecules. *ChemMedChem.* 2016;11: 1117–1121. doi:10.1002/cmdc.201600182
114. Daina A, Michielin O, Zoete V. SwissADME: a free web tool to evaluate pharmacokinetics, drug-likeness and medicinal chemistry friendliness of small molecules. *Sci Rep.* 2017;7: 42717. doi:10.1038/srep42717
115. Melissari E, Di Russo M, Mariotti V, Righi M, Iofrida C, Pellegrini S. Interpreting the gene expression microarray results: a user-based experience. *Arch Ital Biol.* 2013;151: 76–98. doi:10.4449/aib.v151i2.1484
116. Chavalarias D, Wallach JD, Li AHT, Ioannidis JPA. Evolution of Reporting P Values in the Biomedical Literature, 1990-2015. *JAMA.* 2016;315: 1141–1148. doi:10.1001/jama.2016.1952
117. Furnary T, Garcia-Milian R, Liew Z, Whirledge S, Vasiliou V. In Silico Exploration of the Potential Role of Acetaminophen and Pesticides in the Etiology of Autism Spectrum Disorder. *Toxics.* 2021;9. doi:10.3390/toxics9050097
118. Wu L, Xu Y, Zhao H, Li Y. RNase T2 in Inflammation and Cancer: Immunological and Biological Views. *Front Immunol.* 2020;11: 1554. doi:10.3389/fimmu.2020.01554

119. Acquati F, Bertilaccio S, Grimaldi A, Monti L, Cinquetti R, Bonetti P, et al. Microenvironmental control of malignancy exerted by RNASET2, a widely conserved extracellular RNase. *Proc Natl Acad Sci U S A*. 2011;108: 1104–1109. doi:10.1073/pnas.1013746108
120. Lualdi M, Pedrini E, Rea K, Monti L, Scaldaferrì D, Gariboldi M, et al. Pleiotropic modes of action in tumor cells of RNASET2, an evolutionary highly conserved extracellular RNase. *Oncotarget*. 2015;6: 7851–7865. doi:10.18632/oncotarget.3490
121. Pasello M, Manara MC, Scotlandi K. CD99 at the crossroads of physiology and pathology. *J Cell Commun Signal*. 2018;12: 55–68. doi:10.1007/s12079-017-0445-z
122. Manara MC, Pasello M, Scotlandi K. CD99: A Cell Surface Protein with an Oncojanus Role in Tumors. *Genes* . 2018;9. doi:10.3390/genes9030159
123. Kim SH, Choi EY, Shin YK, Kim TJ, Chung DH, Chang SI, et al. Generation of Cells With Hodgkin's and Reed-Sternberg Phenotype Through Downregulation of CD99 (Mic2). *Blood*. 1998;92: 4287–4295. doi:10.1182/blood.V92.11.4287
124. Chung SS, Eng WS, Hu W, Khalaj M, Garrett-Bakelman FE, Tavakkoli M, et al. CD99 is a therapeutic target on disease stem cells in myeloid malignancies. *Sci Transl Med*. 2017;9. doi:10.1126/scitranslmed.aaj2025
125. Fernandez-Vizarra E, Zeviani M. Mitochondrial complex III Rieske Fe-S protein processing and assembly. *Cell Cycle*. 2018;17: 681–687. doi:10.1080/15384101.2017.1417707
126. Klimova T, Chandel NS. Mitochondrial complex III regulates hypoxic activation of HIF. *Cell Death Differ*. 2008;15: 660–666. doi:10.1038/sj.cdd.4402307
127. Jain M, Rivera S, Monclus EA, Synenki L, Zirk A, Eisenbart J, et al. Mitochondrial reactive oxygen species regulate transforming growth factor- β signaling. *J Biol Chem*. 2013;288: 770–777. doi:10.1074/jbc.M112.431973
128. Terada S, Hirokawa N. Moving on to the cargo problem of microtubule-dependent motors in neurons. *Curr Opin Neurobiol*. 2000;10: 566–573. doi:10.1016/s0959-4388(00)00129-x
129. Dunn S, Morrison EE, Liverpool TB, Molina-París C, Cross RA, Alonso MC, et al. Differential trafficking of Kif5c on tyrosinated and detyrosinated microtubules in live cells. *J Cell Sci*. 2008;121: 1085–1095. doi:10.1242/jcs.026492
130. Li Z, Liu H, Bode A, Luo X. Emerging roles of dehydrogenase/reductase member 2 (DHRS2) in the pathology of disease. *Eur J Pharmacol*. 2021;898: 173972. doi:10.1016/j.ejphar.2021.173972

131. Ji C, Kozak KR, Marnett LJ. IkappaB kinase, a molecular target for inhibition by 4-hydroxy-2-nonenal. *J Biol Chem.* 2001;276: 18223–18228. doi:10.1074/jbc.M101266200
132. Bilska-Wilkosz A, Iciek M, Górny M. Chemistry and Biochemistry Aspects of the 4-Hydroxy-2,3-trans-nonenal. *Biomolecules.* 2022;12. doi:10.3390/biom12010145
133. Chaudhary P, Sharma R, Sharma A, Vatsyayan R, Yadav S, Singhal SS, et al. Mechanisms of 4-hydroxy-2-nonenal induced pro- and anti-apoptotic signaling. *Biochemistry.* 2010;49: 6263–6275. doi:10.1021/bi100517x
134. Dalleau S, Baradat M, Guéraud F, Huc L. Cell death and diseases related to oxidative stress: 4-hydroxynonenal (HNE) in the balance. *Cell Death Differ.* 2013;20: 1615–1630. doi:10.1038/cdd.2013.138
135. Timucin AC, Basaga H. Pro-apoptotic effects of lipid oxidation products: HNE at the crossroads of NF- κ B pathway and anti-apoptotic Bcl-2. *Free Radic Biol Med.* 2017;111: 209–218. doi:10.1016/j.freeradbiomed.2016.11.010
136. Gasparovic AC, Milkovic L, Sunjic SB, Zarkovic N. Cancer growth regulation by 4-hydroxynonenal. *Free Radic Biol Med.* 2017;111: 226–234. doi:10.1016/j.freeradbiomed.2017.01.030
137. Chaineau M, Ioannou MS, McPherson PS. Rab35: GEFs, GAPs and effectors. *Traffic.* 2013;14: 1109–1117. doi:10.1111/tra.12096
138. Ma HT, Poon RYC. TRIP13 Regulates Both the Activation and Inactivation of the Spindle-Assembly Checkpoint. *Cell Rep.* 2016;14: 1086–1099. doi:10.1016/j.celrep.2016.01.001
139. Marks DH, Thomas R, Chin Y, Shah R, Khoo C, Benezra R. Mad2 Overexpression Uncovers a Critical Role for TRIP13 in Mitotic Exit. *Cell Rep.* 2017;19: 1832–1845. doi:10.1016/j.celrep.2017.05.021
140. Zeng X, Xu WK, Lok TM, Ma HT, Poon RYC. Imbalance of the spindle-assembly checkpoint promotes spindle poison-mediated cytotoxicity with distinct kinetics. *Cell Death Dis.* 2019;10: 314. doi:10.1038/s41419-019-1539-8
141. Galati D, Srinivasan S, Raza H, Prabu SK, Hardy M, Chandran K, et al. Role of nuclear-encoded subunit Vb in the assembly and stability of cytochrome c oxidase complex: implications in mitochondrial dysfunction and ROS production. *Biochem J.* 2009;420: 439–449. doi:10.1042/BJ20090214
142. Gao S-P, Sun H-F, Jiang H-L, Li L-D, Hu X, Xu X-E, et al. Loss of COX5B inhibits proliferation and promotes senescence via mitochondrial dysfunction in breast cancer. *Oncotarget.* 2015;6: 43363–43374. doi:10.18632/oncotarget.6222

143. Tellez C, Bar-Eli M. Role and regulation of the thrombin receptor (PAR-1) in human melanoma. *Oncogene*. 2003;22: 3130–3137. doi:10.1038/sj.onc.1206453
144. Liu J, Schuff-Werner P, Steiner M. Thrombin/thrombin receptor (PAR-1)-mediated induction of IL-8 and VEGF expression in prostate cancer cells. *Biochem Biophys Res Commun*. 2006;343: 183–189. doi:10.1016/j.bbrc.2006.02.136
145. Gao G, Yang M, Wang F, Dang G, Zhang X, Zhao J, et al. Coagulation factor 2 thrombin receptor promotes malignancy in glioma under SOX2 regulation. *Aging* . 2020;12: 10594–10613. doi:10.18632/aging.103281
146. Arora P, Cuevas BD, Russo A, Johnson GL, Trejo J. Persistent transactivation of EGFR and ErbB2/HER2 by protease-activated receptor-1 promotes breast carcinoma cell invasion. *Oncogene*. 2008;27: 4434–4445. doi:10.1038/onc.2008.84
147. Egloff AM, Rothstein ME, Seethala R, Siegfried JM, Grandis JR, Stabile LP. Cross-talk between estrogen receptor and epidermal growth factor receptor in head and neck squamous cell carcinoma. *Clin Cancer Res*. 2009;15: 6529–6540. doi:10.1158/1078-0432.CCR-09-0862
148. Filardo EJ. Epidermal growth factor receptor (EGFR) transactivation by estrogen via the G-protein-coupled receptor, GPR30: a novel signaling pathway with potential significance for breast cancer. *J Steroid Biochem Mol Biol*. 2002;80: 231–238. doi:10.1016/s0960-0760(01)00190-x
149. Skandalis SS, Afratis N, Smirlaki G, Nikitovic D, Theocharis AD, Tzanakakis GN, et al. Cross-talk between estradiol receptor and EGFR/IGF-IR signaling pathways in estrogen-responsive breast cancers: focus on the role and impact of proteoglycans. *Matrix Biol*. 2014;35: 182–193. doi:10.1016/j.matbio.2013.09.002
150. Cengel KA, Voong KR, Chandrasekaran S, Maggiorella L, Brunner TB, Stanbridge E, et al. Oncogenic K-Ras signals through epidermal growth factor receptor and wild-type H-Ras to promote radiation survival in pancreatic and colorectal carcinoma cells. *Neoplasia*. 2007;9: 341–348. doi:10.1593/neo.06823
151. Feng J, Hua F, Shuo R, Chongfeng G, Huimian X, Nakajima T, et al. Upregulation of non-mutated H-ras and its upstream and downstream signaling proteins in colorectal cancer. *Oncol Rep*. 2001;8: 1409–1413. doi:10.3892/or.8.6.1409
152. Fuka G, Kantner H-P, Grausenburger R, Inthal A, Bauer E, Krapf G, et al. Silencing of ETV6/RUNX1 abrogates PI3K/AKT/mTOR signaling and impairs reconstitution of leukemia in xenografts. *Leukemia*. 2012;26: 927–933. doi:10.1038/leu.2011.322
153. Han ZT, Zhu XX, Yang RY, Sun JZ, Tian GF, Liu XJ, et al. Effect of intravenous infusions of 12-O-tetradecanoylphorbol-13-acetate (TPA) in patients with myelocytic leukemia: preliminary studies on therapeutic efficacy and toxicity. *Proc Natl Acad Sci U S A*. 1998;95: 5357–5361. doi:10.1073/pnas.95.9.5357

154. Warrell RP Jr, Frankel SR, Miller WH Jr, Scheinberg DA, Itri LM, Hittelman WN, et al. Differentiation therapy of acute promyelocytic leukemia with tretinoin (all-trans-retinoic acid). *N Engl J Med.* 1991;324: 1385–1393. doi:10.1056/NEJM199105163242002
155. Hass R. Retrodifferentiation--an alternative biological pathway in human leukemia cells. *Eur J Cell Biol.* 1992;58: 1–11. Available: <https://europepmc.org/article/med/1644056>
156. Qin L, Dominguez D, Chen S, Fan J, Long A, Zhang M, et al. Exogenous IL-33 overcomes T cell tolerance in murine acute myeloid leukemia. *Oncotarget.* 2016;7: 61069–61080. doi:10.18632/oncotarget.11179
157. Krämer A, Green J, Pollard J Jr, Tugendreich S. Causal analysis approaches in Ingenuity Pathway Analysis. *Bioinformatics.* 2014;30: 523–530. doi:10.1093/bioinformatics/btt703
158. Bowers S, Truong AP, Neitz RJ, Neitzel M, Probst GD, Hom RK, et al. Design and synthesis of a novel, orally active, brain penetrant, tri-substituted thiophene based JNK inhibitor. *Bioorg Med Chem Lett.* 2011;21: 1838–1843. doi:10.1016/j.bmcl.2011.01.046
159. Gahman TC, Herbert MR, Lang H, Thayer A, Symons KT, Nguyen PM, et al. Identification and SAR of selective inducible nitric oxide synthase (iNOS) dimerization inhibitors. *Bioorg Med Chem Lett.* 2011;21: 6888–6894. doi:10.1016/j.bmcl.2011.08.112
160. Debdab M, Carreaux F, Renault S, Soundararajan M, Fedorov O, Filippakopoulos P, et al. Leucettines, a class of potent inhibitors of cdc2-like kinases and dual specificity, tyrosine phosphorylation regulated kinases derived from the marine sponge leucettamine B: modulation of alternative pre-RNA splicing. *J Med Chem.* 2011;54: 4172–4186. doi:10.1021/jm200274d
161. Wang T, Block MA, Cowen S, Davies AM, Devereaux E, Gingipalli L, et al. Discovery of azabenzimidazole derivatives as potent, selective inhibitors of TBK1/IKK ϵ kinases. *Bioorg Med Chem Lett.* 2012;22: 2063–2069. doi:10.1016/j.bmcl.2012.01.018
162. Williams JT, Gatfield J, Roch C, Treiber A, Jenck F, Bolli MH, et al. Discovery and optimisation of 1-acyl-2-benzylpyrrolidines as potent dual orexin receptor antagonists. *Med Chem Commun.* 2015;6: 1054–1064. doi:10.1039/C5MD00074B
163. Wang X, Macmillan JB, Huang S, Fang M. ENTPD5 INHIBITORS. World Patent. 2012065139, 2012. Available: <https://patentscope.wipo.int/search/en/detail.jsf?docId=WO2012065139>

164. Bosc N, Atkinson F, Felix E, Gaulton A, Hersey A, Leach AR. Large scale comparison of QSAR and conformal prediction methods and their applications in drug discovery. *J Cheminform.* 2019;11: 4. doi:10.1186/s13321-018-0325-4
165. Wang Y, Xiao J, Suzek TO, Zhang J, Wang J, Zhou Z, et al. PubChem's BioAssay Database. *Nucleic Acids Res.* 2012;40: D400-12. doi:10.1093/nar/gkr1132
166. Cannalire R, Barreca ML, Manfroni G, Cecchetti V. A Journey around the Medicinal Chemistry of Hepatitis C Virus Inhibitors Targeting NS4B: From Target to Preclinical Drug Candidates. *J Med Chem.* 2016;59: 16–41. doi:10.1021/acs.jmedchem.5b00825
167. Chunduru SK, Benetatos CA, Nitz TJ, Bailey TR. COMPOUNDS, COMPOSITIONS AND METHODS FOR TREATMENT AND PROPHYLAXIS OF HEPATITIS C VIRAL INFECTIONS AND ASSOCIATED DISEASES. World Patent. 2005051318, 2005. Available: <https://patentscope.wipo.int/search/en/detail.jsf?docId=WO2005051318>
168. Thakur CS, Jha BK, Dong B, Das Gupta J, Silverman KM, Mao H, et al. Small-molecule activators of RNase L with broad-spectrum antiviral activity. *Proc Natl Acad Sci U S A.* 2007;104: 9585–9590. doi:10.1073/pnas.0700590104
169. Brenk R, Schipani A, James D, Krasowski A, Gilbert IH, Frearson J, et al. Lessons learnt from assembling screening libraries for drug discovery for neglected diseases. *ChemMedChem.* 2008;3: 435–444. doi:10.1002/cmdc.200700139
170. Teague SJ, Davis AM, Leeson PD, Oprea T. The Design of Leadlike Combinatorial Libraries. *Angew Chem Int Ed Engl.* 1999;38: 3743–3748. doi:10.1002/(SICI)1521-3773(19991216)38:24<3743::AID-ANIE3743>3.0.CO;2-U
171. Huang J, Zhang L, Wan D, Zhou L, Zheng S, Lin S, et al. Extracellular matrix and its therapeutic potential for cancer treatment. *Signal Transduct Target Ther.* 2021;6: 153. doi:10.1038/s41392-021-00544-0
172. Frantz C, Stewart KM, Weaver VM. The extracellular matrix at a glance. *J Cell Sci.* 2010;123: 4195–4200. doi:10.1242/jcs.023820
173. Schaefer L, Tredup C, Gubbiotti MA, Iozzo RV. Proteoglycan neofunctions: regulation of inflammation and autophagy in cancer biology. *FEBS J.* 2017;284: 10–26. doi:10.1111/febs.13963
174. Walker C, Mojares E, Del Río Hernández A. Role of Extracellular Matrix in Development and Cancer Progression. *Int J Mol Sci.* 2018;19. doi:10.3390/ijms19103028
175. Sanderson R, Yang Y, Purushothaman A, Khotskaya YB, Ritchie JP, Ramani VC. Proteoglycans and Cancer. In: Zent R, Pozzi A, editors. *Cell-Extracellular Matrix*

- Interactions in Cancer. New York, NY: Springer New York; 2010. pp. 191–215. doi:10.1007/978-1-4419-0814-8_9
176. Delon I, Brown NH. Integrins and the actin cytoskeleton. *Curr Opin Cell Biol.* 2007;19: 43–50. doi:10.1016/j.ceb.2006.12.013
 177. Okina E, Manon-Jensen T, Whiteford JR, Couchman JR. Syndecan proteoglycan contributions to cytoskeletal organization and contractility. *Scand J Med Sci Sports.* 2009;19: 479–489. doi:10.1111/j.1600-0838.2009.00941.x
 178. Dahmke IN, Trampert P, Weinberg F, Mostajeran Z, Lautenschläger F, de Jonge N. Correlative Fluorescence- and Electron Microscopy of Whole Breast Cancer Cells Reveals Different Distribution of ErbB2 Dependent on Underlying Actin. *Front Cell Dev Biol.* 2020;8: 521. doi:10.3389/fcell.2020.00521
 179. Rijken PJ, Hage WJ, van Bergen en Henegouwen PM, Verkleij AJ, Boonstra J. Epidermal growth factor induces rapid reorganization of the actin microfilament system in human A431 cells. *J Cell Sci.* 1991;100 (Pt 3): 491–499. doi:10.1242/jcs.100.3.491
 180. Boettner B, Van Aelst L. Control of cell adhesion dynamics by Rap1 signaling. *Curr Opin Cell Biol.* 2009;21: 684–693. doi:10.1016/j.ceb.2009.06.004
 181. Pickup MW, Mouw JK, Weaver VM. The extracellular matrix modulates the hallmarks of cancer. *EMBO Rep.* 2014;15: 1243–1253. doi:10.15252/embr.201439246
 182. Lu P, Takai K, Weaver VM, Werb Z. Extracellular matrix degradation and remodeling in development and disease. *Cold Spring Harb Perspect Biol.* 2011;3. doi:10.1101/cshperspect.a005058
 183. Hynes RO. The extracellular matrix: not just pretty fibrils. *Science.* 2009;326: 1216–1219. doi:10.1126/science.1176009
 184. Meredith JE Jr, Fazeli B, Schwartz MA. The extracellular matrix as a cell survival factor. *Mol Biol Cell.* 1993;4: 953–961. doi:10.1091/mbc.4.9.953
 185. Vasioukhin V. Adherens Junctions and Cancer. In: Harris T, editor. *Adherens Junctions: from Molecular Mechanisms to Tissue Development and Disease.* Dordrecht: Springer Netherlands; 2012. pp. 379–414. doi:10.1007/978-94-007-4186-7_16
 186. Niessen CM, Gottardi CJ. Molecular components of the adherens junction. *Biochim Biophys Acta.* 2008;1778: 562–571. doi:10.1016/j.bbamem.2007.12.015
 187. Meng W, Takeichi M. Adherens junction: molecular architecture and regulation. *Cold Spring Harb Perspect Biol.* 2009;1: a002899. doi:10.1101/cshperspect.a002899

188. Wozniak MA, Modzelewska K, Kwong L, Keely PJ. Focal adhesion regulation of cell behavior. *Biochim Biophys Acta*. 2004;1692: 103–119. doi:10.1016/j.bbamcr.2004.04.007
189. Eke I, Cordes N. Focal adhesion signaling and therapy resistance in cancer. *Semin Cancer Biol*. 2015;31: 65–75. doi:10.1016/j.semcancer.2014.07.009
190. Chédotal A, Kerjan G, Moreau-Fauvarque C. The brain within the tumor: new roles for axon guidance molecules in cancers. *Cell Death Differ*. 2005;12: 1044–1056. doi:10.1038/sj.cdd.4401707
191. Surawska H, Ma PC, Salgia R. The role of ephrins and Eph receptors in cancer. *Cytokine Growth Factor Rev*. 2004;15: 419–433. doi:10.1016/j.cytogfr.2004.09.002
192. Harburg GC, Hinck L. Navigating breast cancer: axon guidance molecules as breast cancer tumor suppressors and oncogenes. *J Mammary Gland Biol Neoplasia*. 2011;16: 257–270. doi:10.1007/s10911-011-9225-1
193. Badouel C, McNeill H. SnapShot: The hippo signaling pathway. *Cell*. 2011;145: 484-484.e1. doi:10.1016/j.cell.2011.04.009
194. Yang C-C, Graves HK, Moya IM, Tao C, Hamaratoglu F, Gladden AB, et al. Differential regulation of the Hippo pathway by adherens junctions and apical-basal cell polarity modules. *Proc Natl Acad Sci U S A*. 2015;112: 1785–1790. doi:10.1073/pnas.1420850112
195. Snigdha K, Gangwani KS, Lapalikar GV, Singh A, Kango-Singh M. Hippo Signaling in Cancer: Lessons From Drosophila Models. *Front Cell Dev Biol*. 2019;7: 85. doi:10.3389/fcell.2019.00085
196. Heng Y-W, Koh C-G. Actin cytoskeleton dynamics and the cell division cycle. *Int J Biochem Cell Biol*. 2010;42: 1622–1633. doi:10.1016/j.biocel.2010.04.007
197. Lee SH, Dominguez R. Regulation of actin cytoskeleton dynamics in cells. *Mol Cells*. 2010;29: 311–325. doi:10.1007/s10059-010-0053-8
198. Hall A. The cytoskeleton and cancer. *Cancer Metastasis Rev*. 2009;28: 5–14. doi:10.1007/s10555-008-9166-3
199. Dick FA, Dyson NJ. Retinoblastoma Tumor Suppressor Gene. In: Bertino JR, editor. *Encyclopedia of Cancer (Second Edition)*. New York: Academic Press; 2002. pp. 143–152. doi:10.1016/B0-12-227555-1/00214-8
200. Knudsen ES, Pruitt SC, Hershberger PA, Witkiewicz AK, Goodrich DW. Cell Cycle and Beyond: Exploiting New RB1 Controlled Mechanisms for Cancer Therapy. *Trends Cancer Res*. 2019;5: 308–324. doi:10.1016/j.trecan.2019.03.005

201. Jansen RA, Liu JC, Liyanarachchi S, Crijns AP, Yan PS, Huang TH, et al. Prognostic impact of MAD1L1 promoter hypermethylation in advanced ovarian cancer. *J Clin Orthod*. 2006;24: 5021–5021. doi:10.1200/jco.2006.24.18_suppl.5021
202. Lontos M, Koutsami M, Sideridou M, Evangelou K, Kletsas D, Levy B, et al. Deregulated overexpression of hCdt1 and hCdc6 promotes malignant behavior. *Cancer Res*. 2007;67: 10899–10909. doi:10.1158/0008-5472.CAN-07-2837
203. Malmanche N, Maia A, Sunkel CE. The spindle assembly checkpoint: preventing chromosome mis-segregation during mitosis and meiosis. *FEBS Lett*. 2006;580: 2888–2895. doi:10.1016/j.febslet.2006.03.081
204. Mannion AJ, Odell AF, Taylor A, Jones PF, Cook GP. Tumour cell CD99 regulates transendothelial migration via CDC42 and actin remodelling. *J Cell Sci*. 2021;134. doi:10.1242/jcs.240135
205. Evan GI, Wyllie AH, Gilbert CS, Littlewood TD, Land H, Brooks M, et al. Induction of apoptosis in fibroblasts by c-myc protein. *Cell*. 1992;69: 119–128. doi:10.1016/0092-8674(92)90123-t
206. Chen Z, Shojaee S, Buchner M, Geng H, Lee JW, Klemm L, et al. Signalling thresholds and negative B-cell selection in acute lymphoblastic leukaemia. *Nature*. 2015;521: 357–361. doi:10.1038/nature14231
207. Vos MD, Ellis CA, Bell A, Birrer MJ, Clark GJ. Ras Uses the Novel Tumor Suppressor RASSF1 as an Effector to Mediate Apoptosis *. *J Biol Chem*. 2000;275: 35669–35672. doi:10.1074/jbc.C000463200
208. Ohashi Y, Kaneko SJ, Cupples TE, Young SR. Ubiquinol cytochrome c reductase (UQCRFS1) gene amplification in primary breast cancer core biopsy samples. *Gynecol Oncol*. 2004;93: 54–58. doi:10.1016/j.ygyno.2004.01.019
209. Jun KH, Kim SY, Yoon JH, Song JH, Park WS. Amplification of the UQCRFS1 Gene in Gastric Cancers. *J Gastric Cancer*. 2012;12: 73–80. doi:10.5230/jgc.2012.12.2.73
210. Owens KM, Kulawiec M, Desouki MM, Vanniarajan A, Singh KK. Impaired OXPHOS complex III in breast cancer. *PLoS One*. 2011;6: e23846. doi:10.1371/journal.pone.0023846
211. Vale RD, Reese TS, Sheetz MP. Identification of a novel force-generating protein, kinesin, involved in microtubule-based motility. *Cell*. 1985;42: 39–50. doi:10.1016/s0092-8674(85)80099-4
212. Miki H, Okada Y, Hirokawa N. Analysis of the kinesin superfamily: insights into structure and function. *Trends Cell Biol*. 2005;15: 467–476. doi:10.1016/j.tcb.2005.07.006

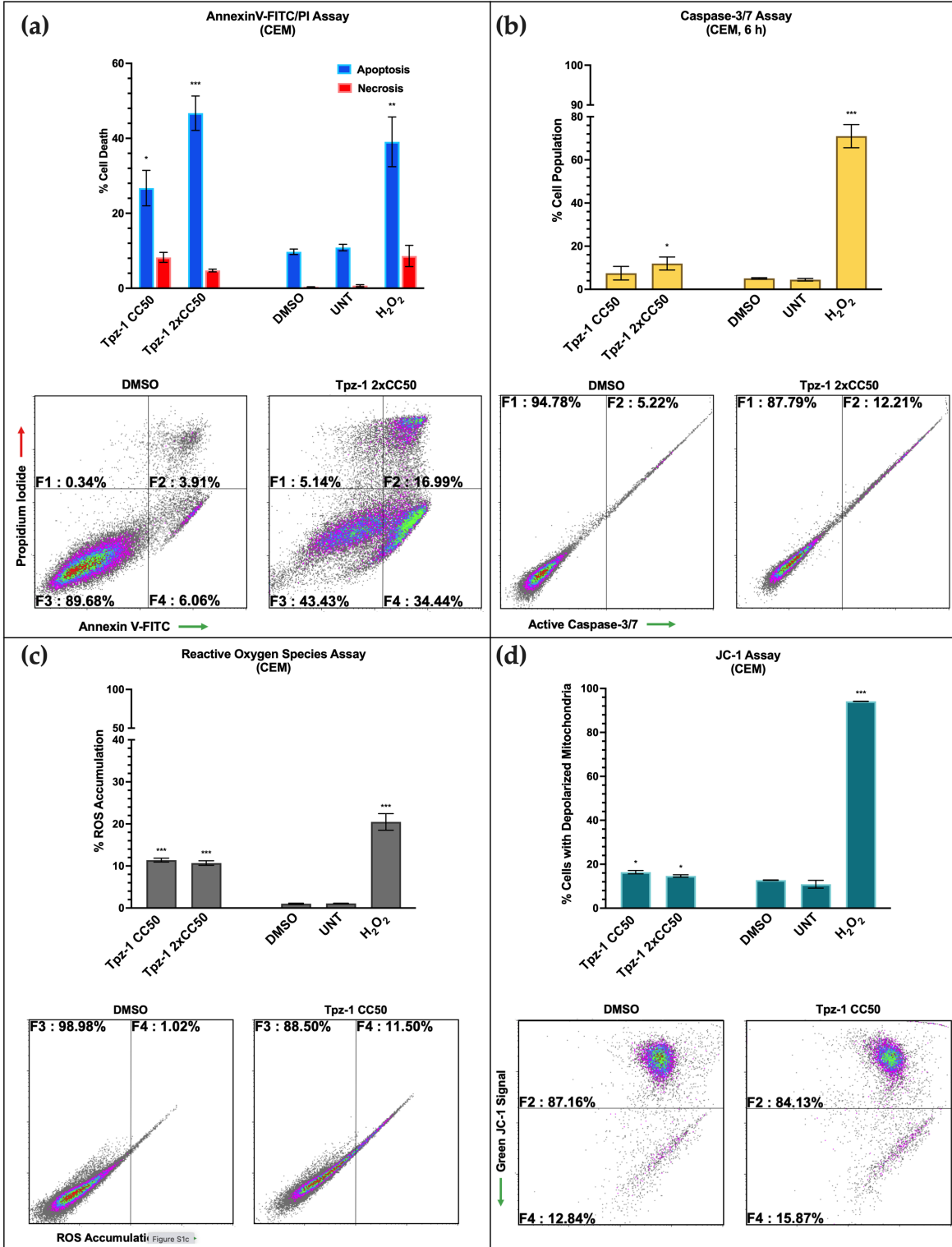
213. Klinkert K, Echard A. Rab35 GTPase: A Central Regulator of Phosphoinositides and F-actin in Endocytic Recycling and Beyond. *Traffic*. 2016;17: 1063–1077. doi:10.1111/tra.12422
214. Lu S, Qian J, Guo M, Gu C, Yang Y. Insights into a Crucial Role of TRIP13 in Human Cancer. *Comput Struct Biotechnol J*. 2019;17: 854–861. doi:10.1016/j.csbj.2019.06.005
215. Tao Y, Yang G, Yang H, Song D, Hu L, Xie B, et al. TRIP13 impairs mitotic checkpoint surveillance and is associated with poor prognosis in multiple myeloma. *Oncotarget*. 2017;8: 26718–26731. doi:10.18632/oncotarget.14957
216. Zhang G, Zhu Q, Fu G, Hou J, Hu X, Cao J, et al. TRIP13 promotes the cell proliferation, migration and invasion of glioblastoma through the FBXW7/c-MYC axis. *Br J Cancer*. 2019;121: 1069–1078. doi:10.1038/s41416-019-0633-0
217. Banerjee R, Russo N, Liu M, Basrur V, Bellile E, Palanisamy N, et al. TRIP13 promotes error-prone nonhomologous end joining and induces chemoresistance in head and neck cancer. *Nat Commun*. 2014;5: 4527. doi:10.1038/ncomms5527
218. Carter SL, Eklund AC, Kohane IS, Harris LN, Szallasi Z. A signature of chromosomal instability inferred from gene expression profiles predicts clinical outcome in multiple human cancers. *Nat Genet*. 2006;38: 1043–1048. doi:10.1038/ng1861
219. Bedi M, Ray M, Ghosh A. Active mitochondrial respiration in cancer: a target for the drug. *Mol Cell Biochem*. 2022;477: 345–361. doi:10.1007/s11010-021-04281-4
220. Morrish F, Giedt C, Hockenbery D. c-MYC apoptotic function is mediated by NRF-1 target genes. *Genes Dev*. 2003;17: 240–255. doi:10.1101/gad.1032503
221. Chen ZX, Pervaiz S. Involvement of cytochrome c oxidase subunits Va and Vb in the regulation of cancer cell metabolism by Bcl-2. *Cell Death Differ*. 2010;17: 408–420. doi:10.1038/cdd.2009.132
222. Ozsvari B, Sotgia F, Lisanti MP. A new mutation-independent approach to cancer therapy: Inhibiting oncogenic RAS and MYC, by targeting mitochondrial biogenesis. *Aging*. 2017;9: 2098–2116. doi:10.18632/aging.101304
223. BRAF B-Raf proto-oncogene, serine/threonine kinase [Homo sapiens (human)] - Gene - NCBI. [cited 7 Jun 2022]. Available: <https://www.ncbi.nlm.nih.gov/gene?Db=gene&Cmd=ShowDetailView&TermToSearch=673>
224. KLK3 kallikrein related peptidase 3 [Homo sapiens (human)] - Gene - NCBI. [cited 7 Jun 2022]. Available: <https://www.ncbi.nlm.nih.gov/gene?Db=gene&Cmd=ShowDetailView&TermToSearch=354>

225. TSC1 TSC complex subunit 1 [Homo sapiens (human)] - Gene - NCBI. [cited 7 Jun 2022]. Available: <https://www.ncbi.nlm.nih.gov/gene?Db=gene&Cmd=ShowDetailView&TermToSearch=7248>
226. Woodford MR, Sager RA, Marris E, Dunn DM, Blanden AR, Murphy RL, et al. Tumor suppressor Tsc1 is a new Hsp90 co-chaperone that facilitates folding of kinase and non-kinase clients. *EMBO J.* 2017;36: 3650–3665. doi:10.15252/embj.201796700
227. TP53 tumor protein p53 [Homo sapiens (human)] - Gene - NCBI. Available: <https://www.ncbi.nlm.nih.gov/gene?Db=gene&Cmd=ShowDetailView&TermToSearch=7157>
228. BCL2 BCL2 apoptosis regulator [Homo sapiens (human)] - Gene - NCBI. [cited 8 Jun 2022]. Available: <https://www.ncbi.nlm.nih.gov/gene?Db=gene&Cmd=ShowDetailView&TermToSearch=596>
229. EGFR epidermal growth factor receptor [Homo sapiens (human)] - Gene - NCBI. [cited 8 Jun 2022]. Available: <https://www.ncbi.nlm.nih.gov/gene?Db=gene&Cmd=ShowDetailView&TermToSearch=1956>
230. ERBB2 erb-b2 receptor tyrosine kinase 2 [Homo sapiens (human)] - Gene - NCBI. [cited 8 Jun 2022]. Available: <https://www.ncbi.nlm.nih.gov/gene?Db=gene&Cmd=ShowDetailView&TermToSearch=2064>
231. CDH1 cadherin 1 [Homo sapiens (human)] - Gene - NCBI. [cited 8 Jun 2022]. Available: <https://www.ncbi.nlm.nih.gov/gene?Db=gene&Cmd=ShowDetailView&TermToSearch=999>
232. CD274 CD274 molecule [Homo sapiens (human)] - Gene - NCBI. [cited 8 Jun 2022]. Available: <https://www.ncbi.nlm.nih.gov/gene?Db=gene&Cmd=ShowDetailView&TermToSearch=29126>
233. KRAS KRAS proto-oncogene, GTPase [Homo sapiens (human)] - Gene - NCBI. [cited 8 Jun 2022]. Available: <https://www.ncbi.nlm.nih.gov/gene?Db=gene&Cmd=ShowDetailView&TermToSearch=3845>
234. Chiasson-MacKenzie C, McClatchey AI. EGFR-induced cytoskeletal changes drive complex cell behaviors: The tip of the iceberg. *Sci Signal.* 2018;11: eaas9473. doi:10.1126/scisignal.aas9473

235. Tsuda Y, Iimori M, Nakashima Y, Nakanishi R, Ando K, Ohgaki K, et al. Mitotic slippage and the subsequent cell fates after inhibition of Aurora B during tubulin-binding agent-induced mitotic arrest. *Sci Rep.* 2017;7: 16762. doi:10.1038/s41598-017-17002-z
236. Bavetsias V, Linardopoulos S. Aurora Kinase Inhibitors: Current Status and Outlook. *Front Oncol.* 2015;5: 278. doi:10.3389/fonc.2015.00278
237. Anighoro A, Bajorath J, Rastelli G. Polypharmacology: challenges and opportunities in drug discovery. *J Med Chem.* 2014;57: 7874–7887. doi:10.1021/jm5006463
238. Morphy R, Kay C, Rankovic Z. From magic bullets to designed multiple ligands. *Drug Discov Today.* 2004;9: 641–651. doi:10.1016/S1359-6446(04)03163-0
239. Csermely P, Agoston V, Pongor S. The efficiency of multi-target drugs: the network approach might help drug design. *Trends Pharmacol Sci.* 2005;26: 178–182. doi:10.1016/j.tips.2005.02.007
240. Chaudhari R, Tan Z, Huang B, Zhang S. Computational polypharmacology: a new paradigm for drug discovery. *Expert Opin Drug Discov.* 2017;12: 279–291. doi:10.1080/17460441.2017.1280024
241. Reddy AS, Zhang S. Polypharmacology: drug discovery for the future. *Expert Rev Clin Pharmacol.* 2013;6: 41–47. doi:10.1586/ecp.12.74
242. Newburger PE, Chovaniec ME, Greenberger JS, Cohen HJ. Functional changes in human leukemic cell line HL-60. A model for myeloid differentiation. *J Cell Biol.* 1979;82: 315–322. doi:10.1083/jcb.82.2.315
243. Tsai MA, Waugh RE, Keng PC. Changes in HL-60 cell deformability during differentiation induced by DMSO. *Biorheology.* 1996;33: 1–15. doi:10.1016/0006-355x(96)00002-9

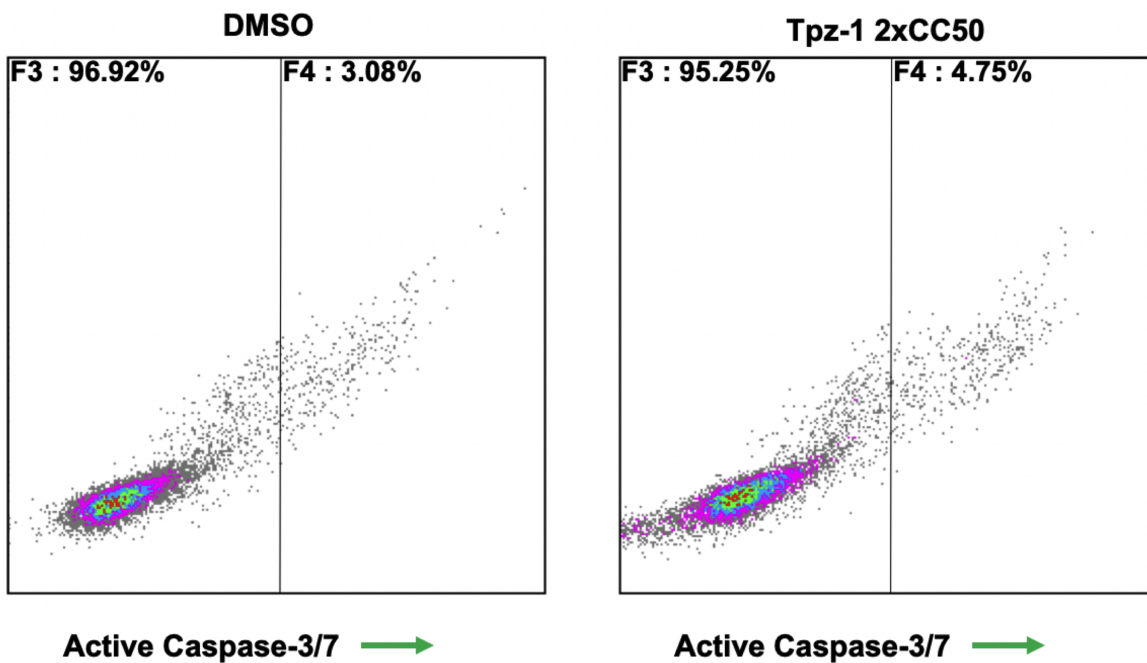
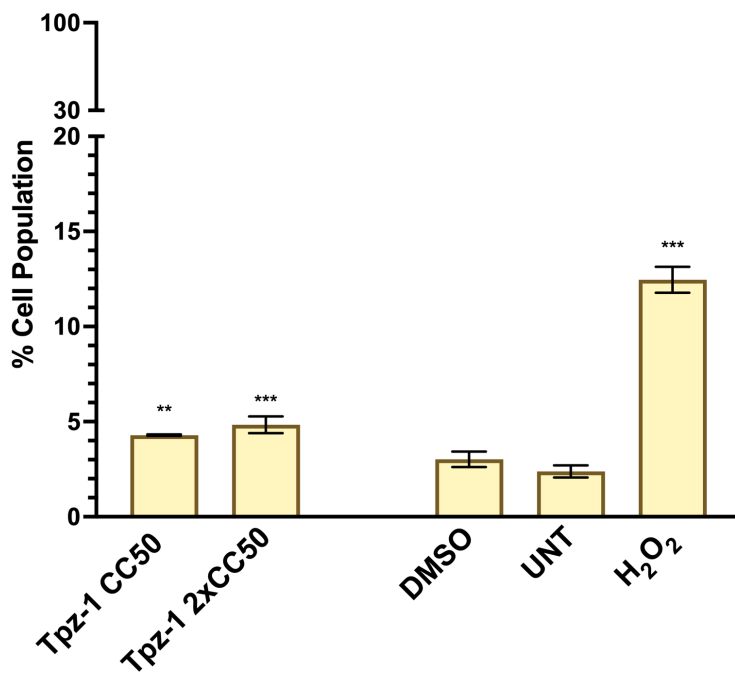
APPENDIX

A.1. SUPPLEMENTARY FIGURES



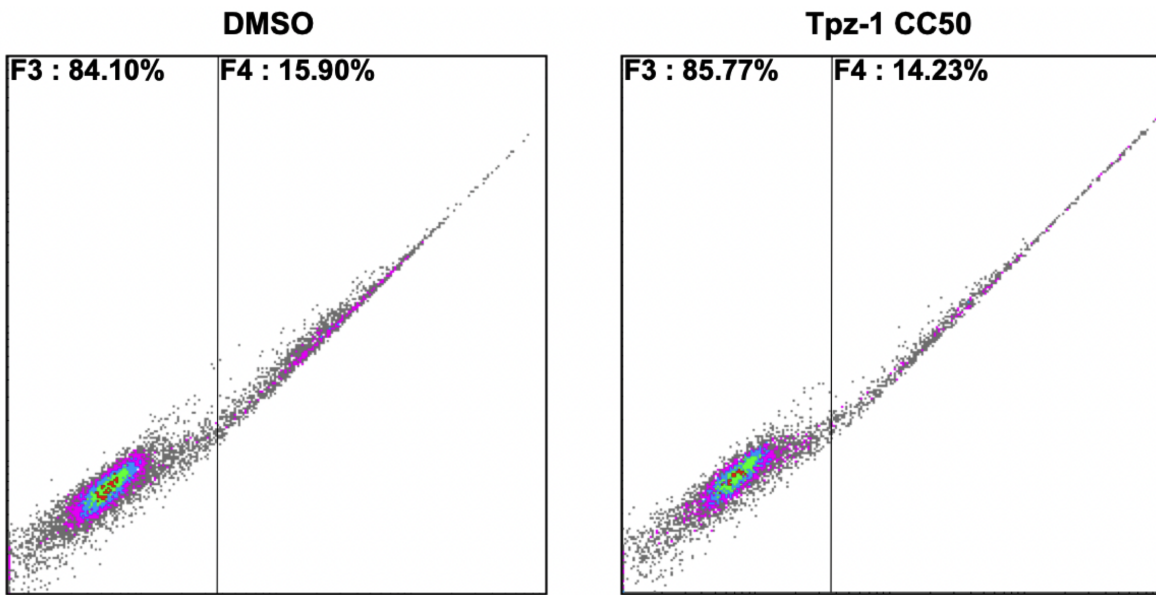
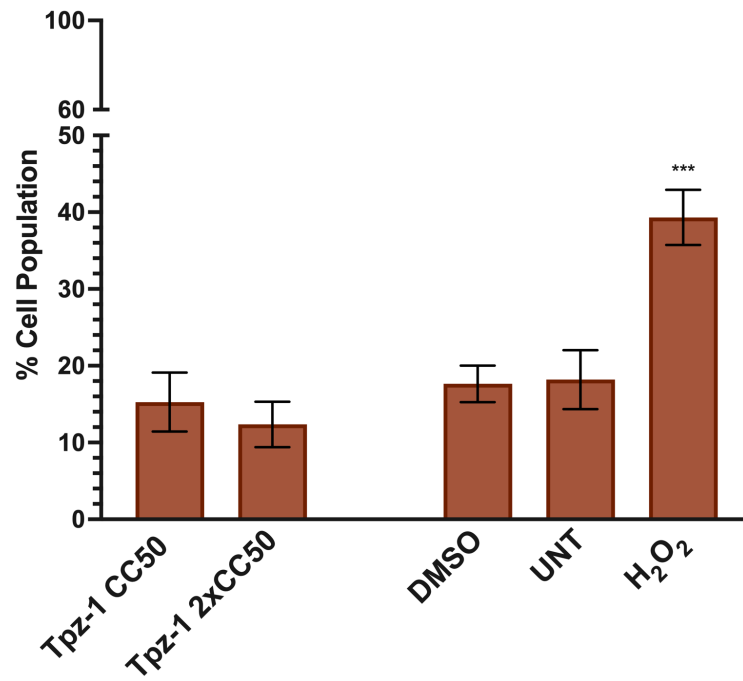
Supplementary Figure S2.1. Tpz-1-induced cell death is mediated by apoptosis in CCRF-CEM cells. **(a)** Analysis of phosphatidylserine externalization by flow cytometry showed apoptosis induction in CCRF-CEM cells after 24 h of exposure to CC₅₀ (0.74 μM; $p = 0.037591$) and 2xCC₅₀ (1.48 μM; $p = 0.000162$) concentrations of Tpz-1. The percentages displayed represent total (early and late) apoptosis values. **(b)** Flow cytometry analysis indicated that Tpz-1 2xCC₅₀ (1.48 μM; $p = 0.017328$) induced significant caspase-3/7 activation after 6 h incubation in CCRF-CEM cells. Positive fluorescence for NucView 488 Caspase-3/7 substrate indicated caspase-3/7 activation. **(c)** Tpz-1 causes reactive oxygen species accumulation in CCRF-CEM cells at CC₅₀ (0.74 μM; $p < 0.00001$) and 2xCC₅₀ (1.48 μM; $p < 0.00001$) concentrations. ROS was quantified using the car-boxy-H₂DCFDA reagent. **(d)** Tpz-1 disrupted mitochondrial membrane potential in CCRF-CEM cells after 5 h of incubation. A modest but significant increase in depolarized mitochondria was seen in cells treated with Tpz-1 CC₅₀ (0.74 μM; $p = 0.021645$) or 2xCC₅₀ (1.48 μM; $p = 0.018111$). Mitochondrial depolarization was quantified using the JC-1 dye; an increase in green fluorescent signal denoted loss of membrane potential. **(a–d)** In a manner consistent with our experiments in HL-60 cells, CCRF-CEM were treated with the 24 h CC₅₀ (0.74 μM) or 2xCC₅₀ (1.48 μM), or 0.1% v/v DMSO or 100 μM H₂O₂ as vehicle and positive controls for cytotoxicity. Untreated (UNT) controls were also included. Representative density plots for each experiment are shown. For statistical analysis, Student's paired *t*-test was utilized; the asterisk annotations represent the statistical significance of the treatments against the vehicle control; (*) $p < 0.05$, (**) $p < 0.01$, (***) $p < 0.001$.

Caspase-3/7 Assay
(CEM, 8 h)



Supplementary Figure S2.2. Caspase-3/7 activity is reduced after 8 h exposure to Tpz-1 in CCRF-CEM cells. Flow cytometry analysis revealed a decreasing trend in caspase-3/7 activity after 8 h incubation with Tpz-1 CC_{50} (0.74 μ M; $p = 0.003435$) and $2xCC_{50}$ (1.48 μ M; $p = 0.000936$) compared to 6 h of treatment. Positive fluorescence for NucView 488 Caspase-3/7 substrate indicated caspase-3/7 activation. 0.1% v/v DMSO and 100 μ M H_2O_2 were used as vehicle and positive controls for cytotoxicity; untreated (UNT) controls were also included. For statistical analysis, Student's paired t -test was utilized; the asterisk annotations represent the statistical significance of the treatments against the vehicle control; (**) $p < 0.01$, (***) $p < 0.001$.

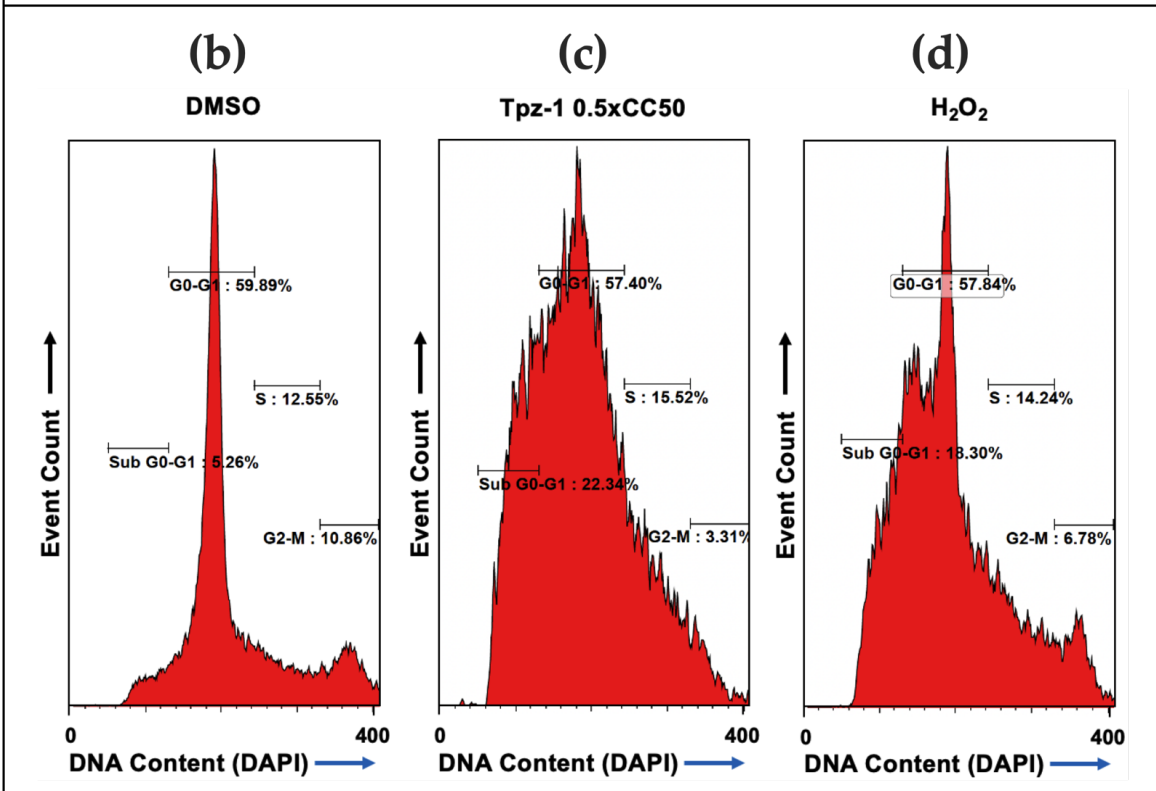
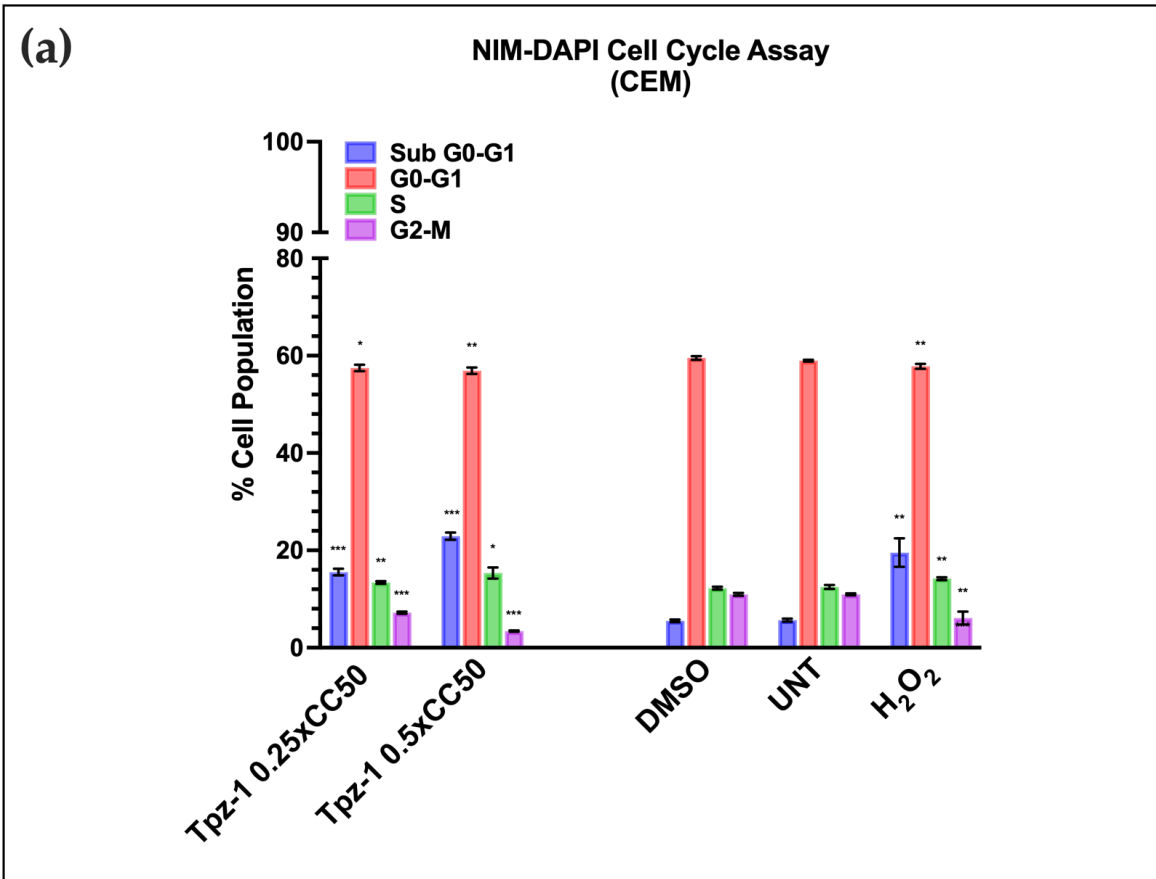
Caspase-8 Assay
(HL-60)



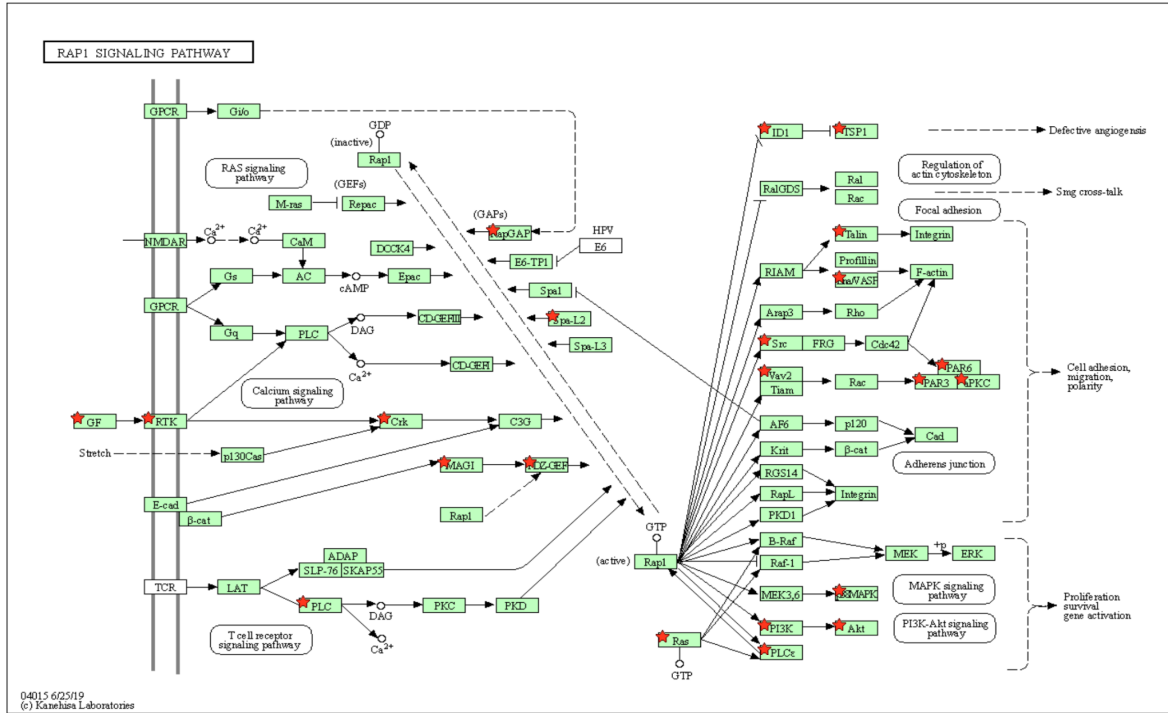
Active Caspase-8 →

Active Caspase-8 →

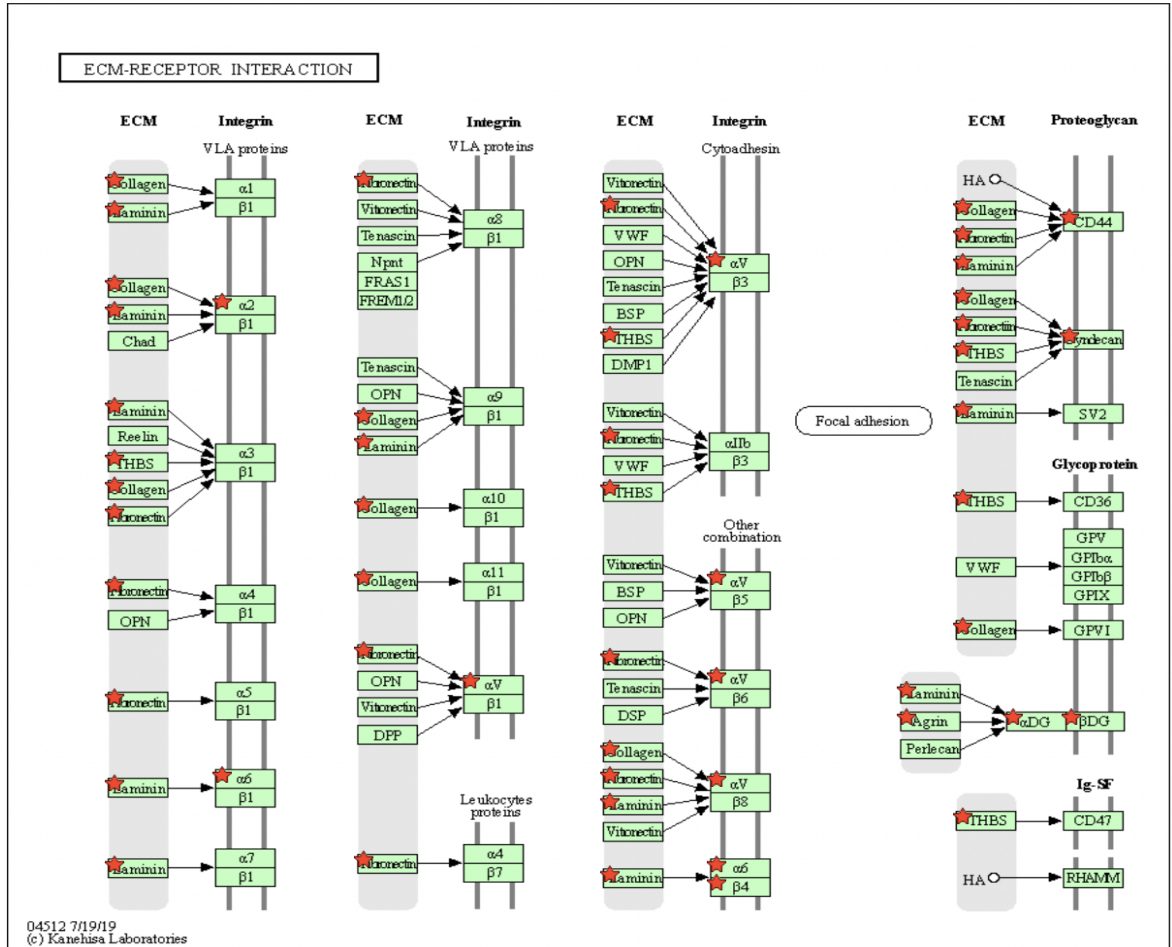
Supplementary Figure S2.3. Caspase-8 is inactive after 4 h in Tpz-1-treated HL-60 cells. Fluorescence of the FITC-conjugated caspase-8-specific inhibitor IETD-FMK was not detected after 4 h treatment with Tpz-1 24 h CC_{50} (0.95 μ M; $p = 0.415291$) or $2xCC_{50}$ (1.9 μ M; $p = 0.073081$). The IETD-FMK-FITC substrate emits a green fluorescent signal when bound to active caspase-8. 0.1% v/v DMSO and 100 μ M H_2O_2 were used as vehicle and positive controls for cytotoxicity; un-treated (UNT) controls were also included. Statistical analysis was achieved by two-tailed Student's paired t-test, and the asterisk annotations in each graph represent the statistical significance of the treatments against the vehicle control; (***) $p < 0.001$.



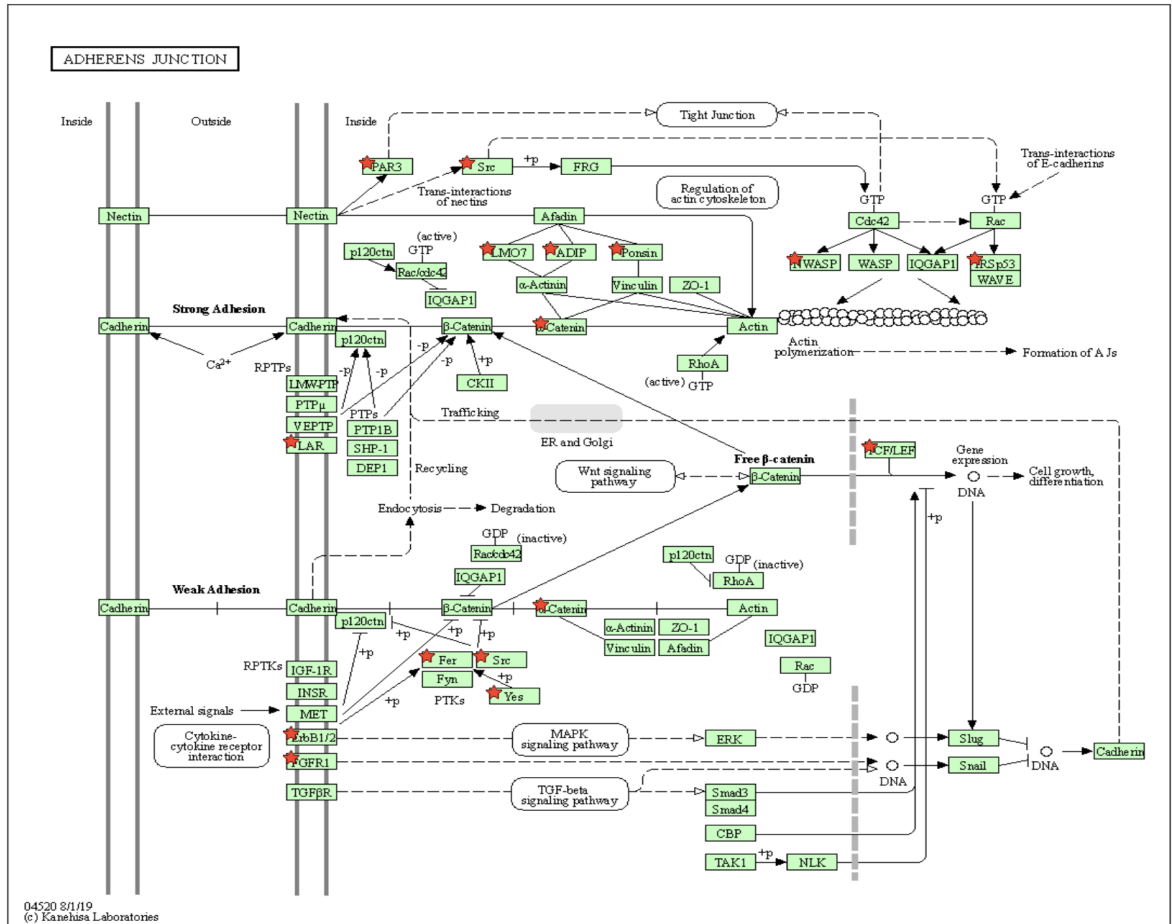
Supplementary Figure S2.4. Tpz-1 causes DNA fragmentation that interferes with evaluation of the CCRF-CEM cell cycle. **(a)** The effect of Tpz-1 on the CCRF-CEM cell cycle remains uncertain due to excessive DNA fragmentation in the sub-G0/G1 population after 72 h of exposure to 0.25xCC₅₀ (0.19 μM) or 0.5xCC₅₀ (0.37 μM). The distribution of cells between phases of the cell cycle cannot be distinguished. NIM-DAPI was used to stain and quantify the DNA content of each sample. 0.1% v/v DMSO and 100 μM H₂O₂ were used as vehicle and positive controls for cytotoxicity; untreated (UNT) controls were also included. **(b–d)** Representative histograms for DMSO, 0.5xCC₅₀ Tpz-1, and H₂O₂ treated samples. Statistical analysis was achieved by two-tailed Student's paired *t*-test, and the asterisk annotations in each graph represent the statistical significance of the treatments against the vehicle control; (*) *p* < 0.05, (**) *p* < 0.01, (***) *p* < 0.001.



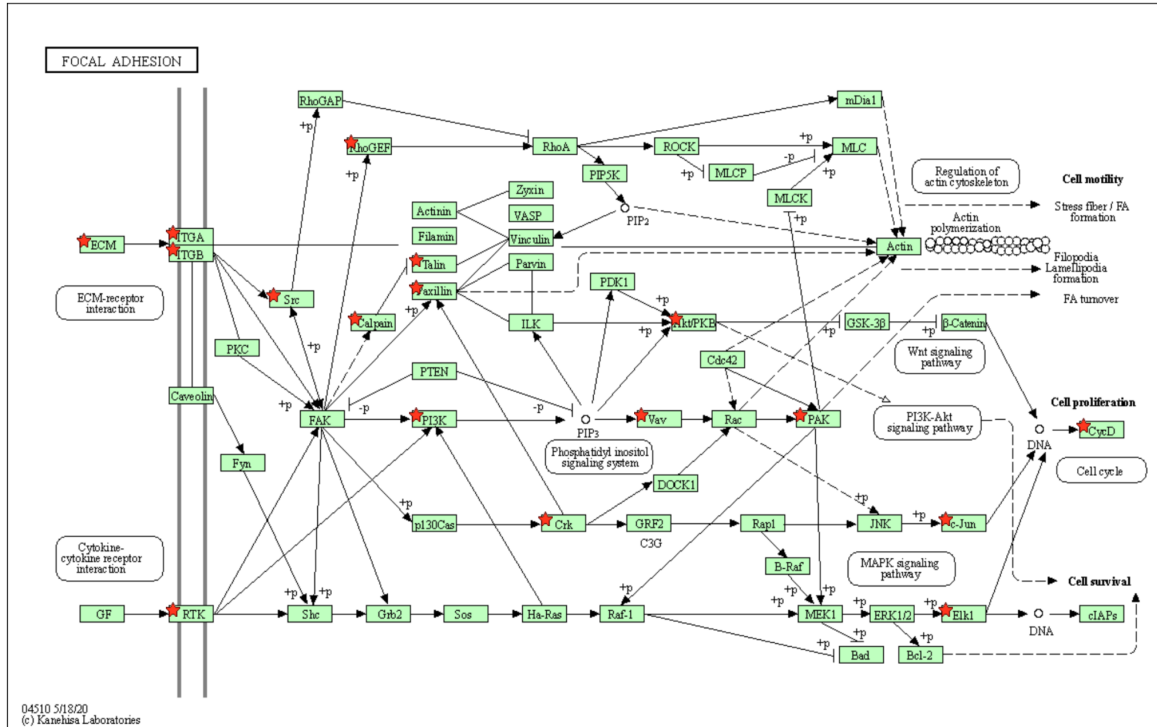
Supplementary Figure S3.2. KEGG 'RAP1 Signaling Pathway' diagram generated by DAVID analysis of genes downregulated by Tpz-1. Red stars indicated the significantly affected genes ($p = 5e-05$).



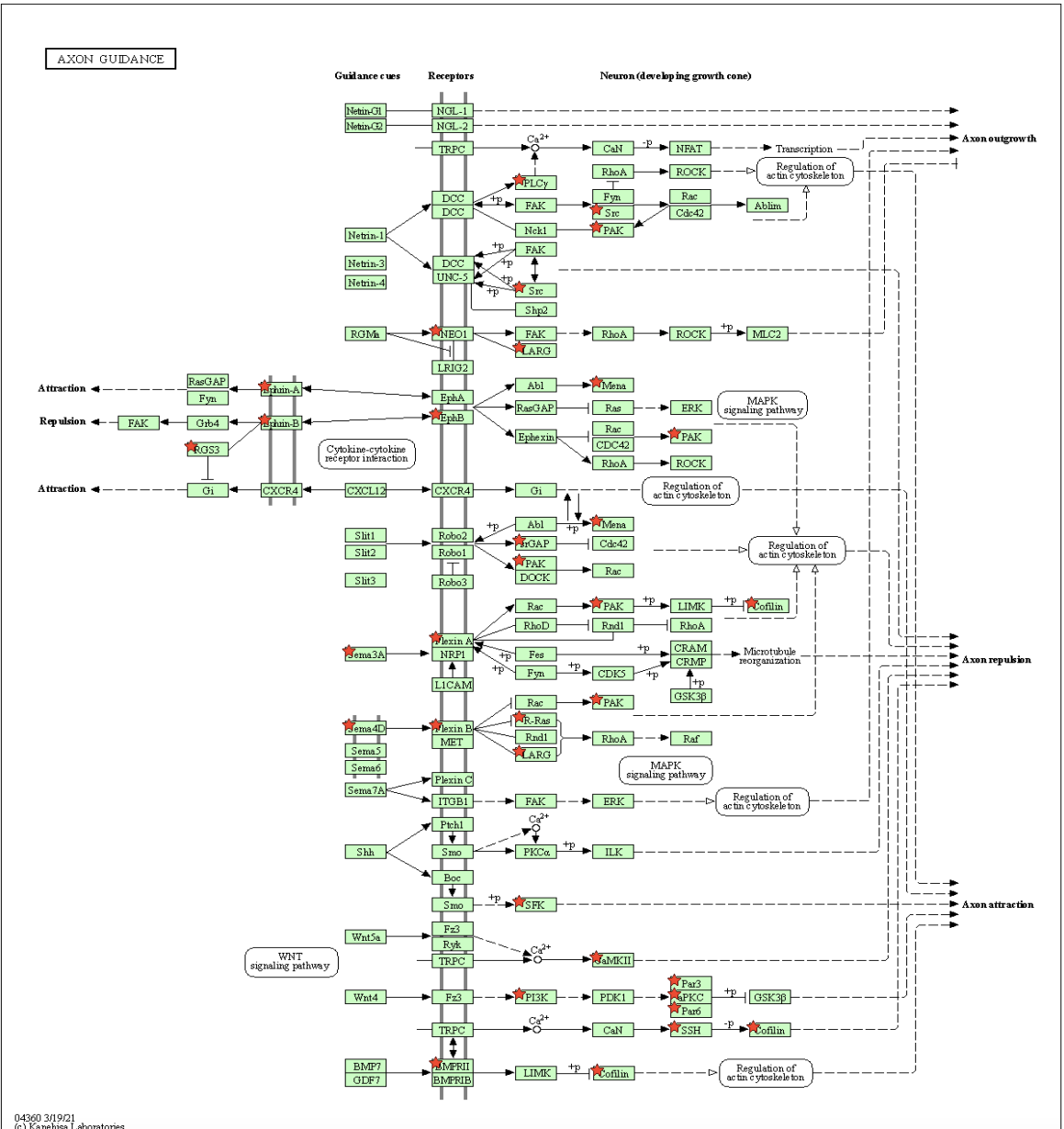
Supplementary Figure S3.3. KEGG 'ECM-Receptor Interaction' pathway diagram obtained from DAVID analysis of Tpz-1 downregulated genes. Red stars indicate the genes significantly downregulated after Tpz-1 treatment ($p = 5e-05$).



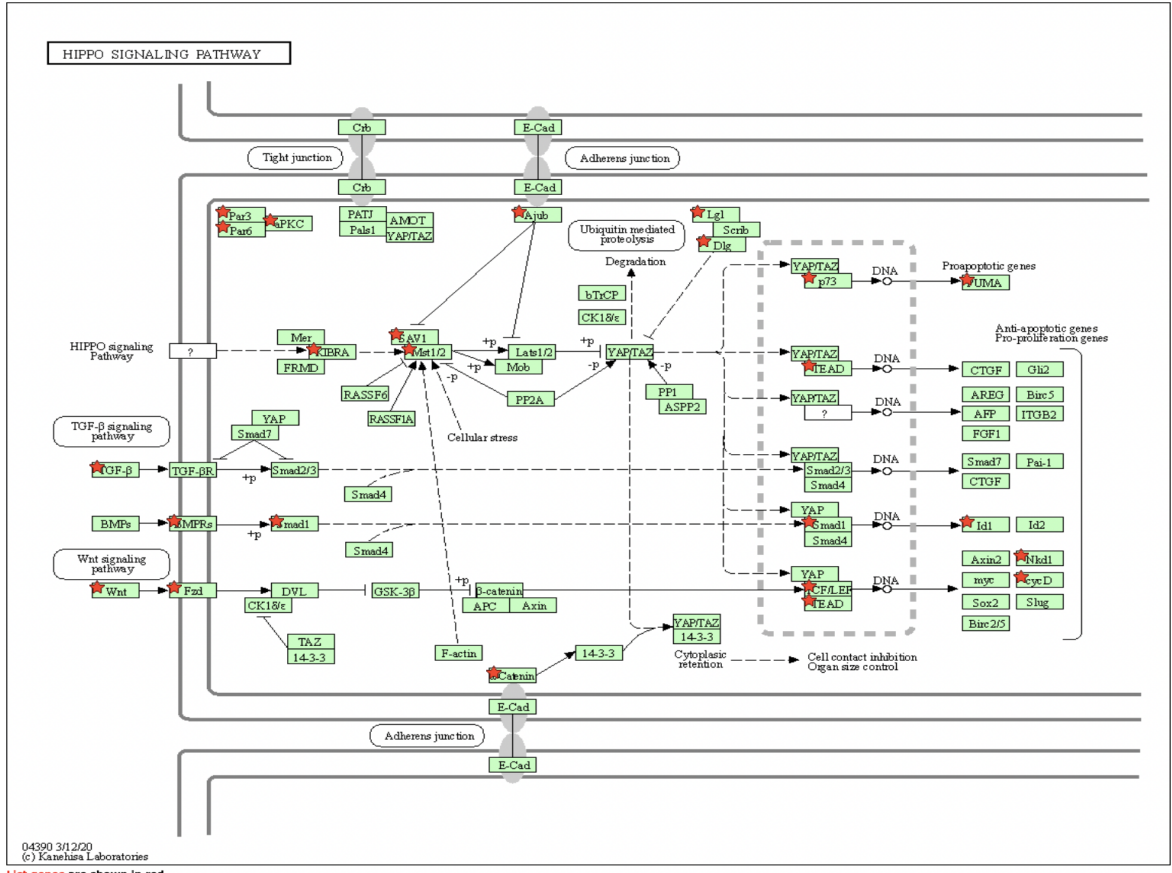
Supplementary Figure S3.4. KEGG 'Adherens Junction' pathway obtained via DAVID analysis of Tpz-1 downregulated genes. Red stars indicate the genes downregulated by Tpz-1 ($p = 5e-05$).



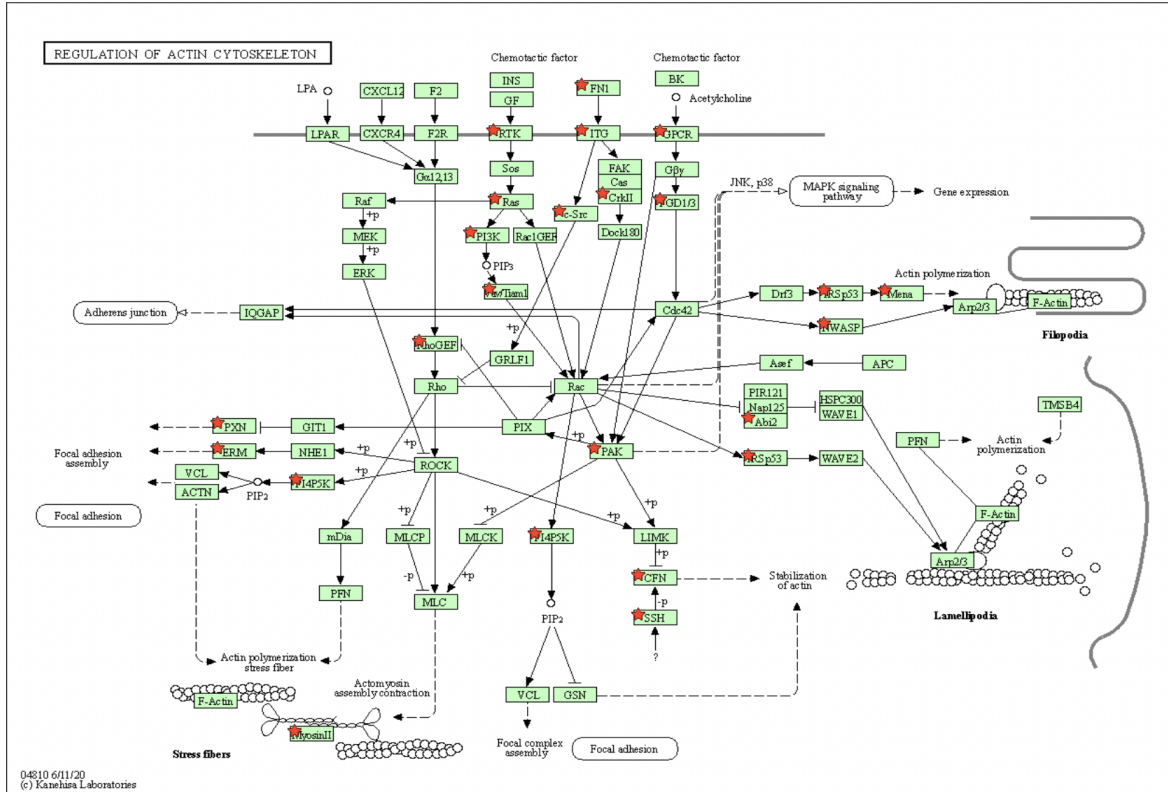
Supplementary Figure S3.5. KEGG 'Focal Adhesion' pathway generated by DAVID analysis of Tpz-1 downregulated genes. Red stars indicate the genes downregulated by Tpz-1 ($p = 5e-05$).



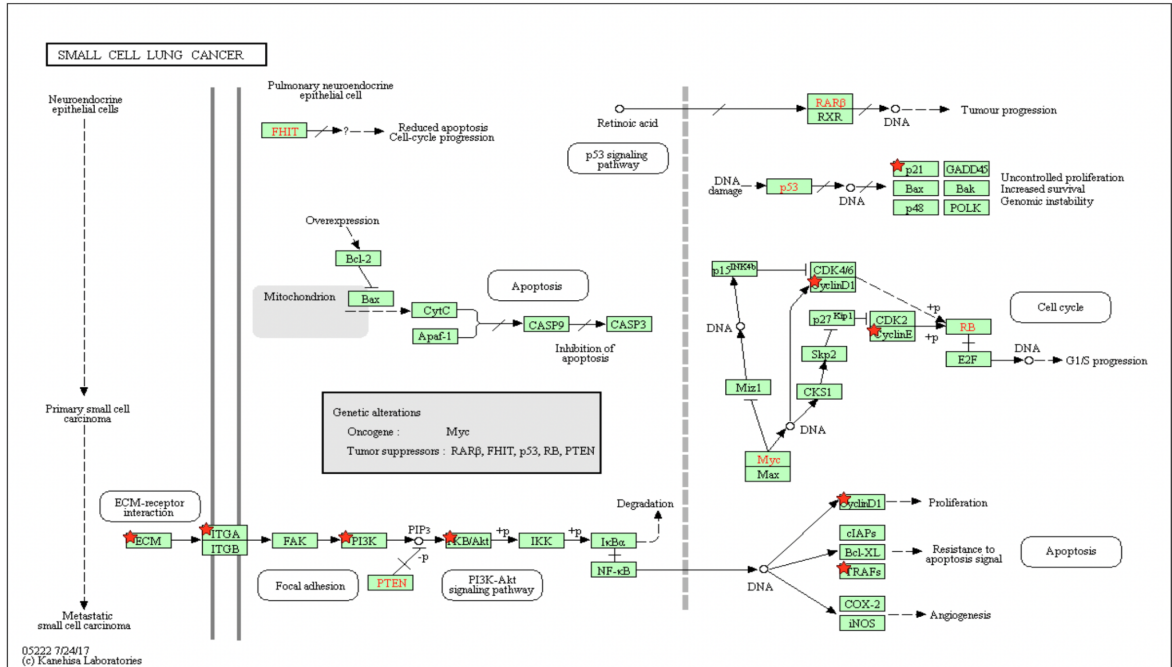
Supplementary Figure S3.6. KEGG 'Axon Guidance' pathway obtained from DAVID analysis of Tpz-1 downregulated gene list. Red stars indicate genes downregulated after Tpz-1 treatment ($p = 5e-05$).



Supplementary Figure S3.7. KEGG 'Hippo signaling pathway' obtained from DAVID analysis of genes downregulated by Tpz-1. Red stars indicate the affected genes ($p = 5 \times 10^{-5}$).

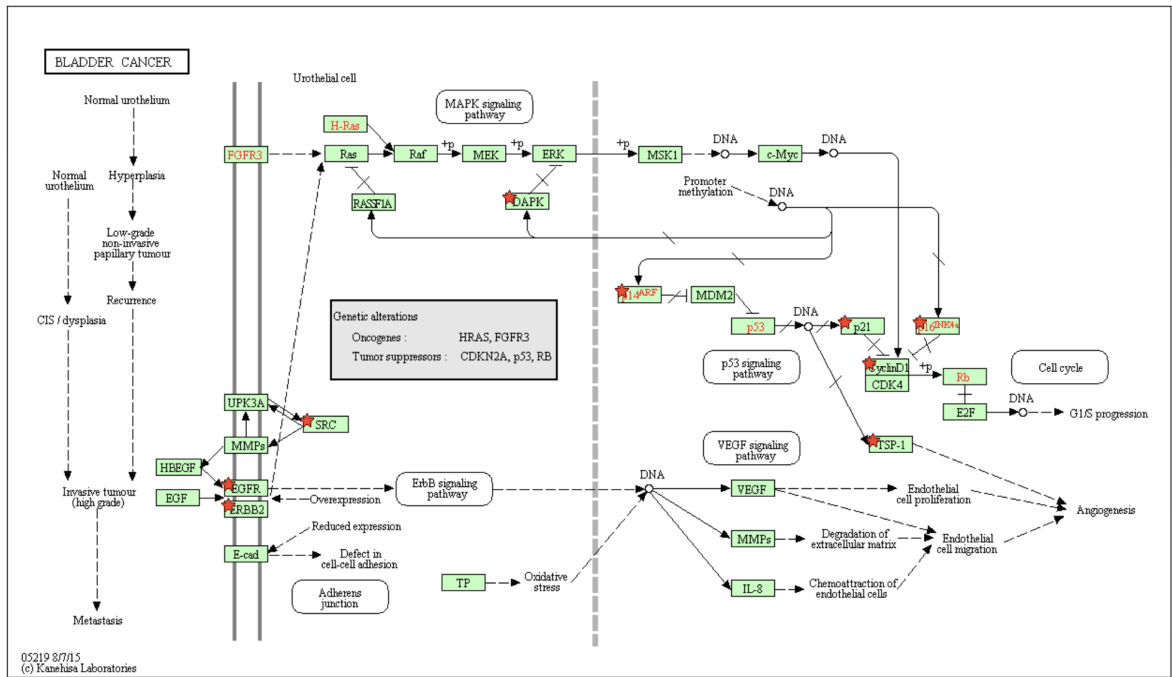


Supplementary Figure S3.8. KEGG 'Regulation of Actin Cytoskeleton' pathway obtained by DAVID analysis of Tpz-1 downregulated genes. Red stars indicate elements that were significantly downregulated by Tpz-1 ($p = 5e-05$).

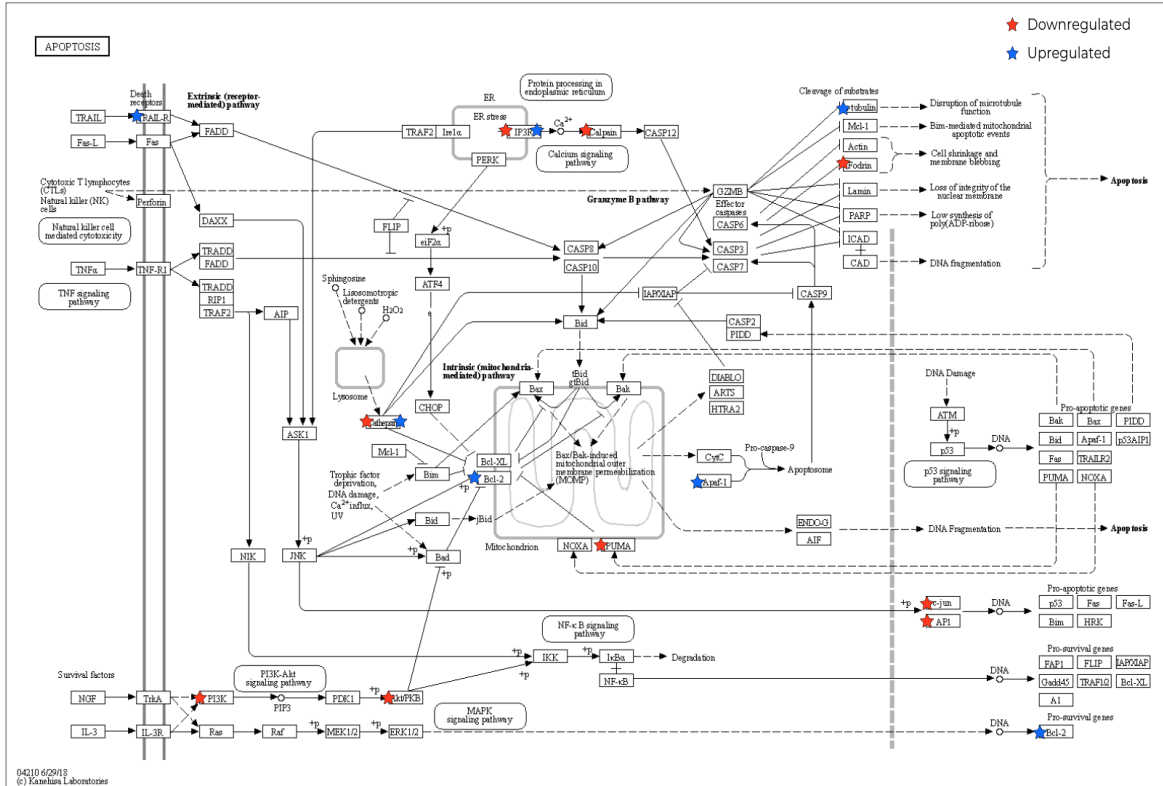


List genes are shown in red

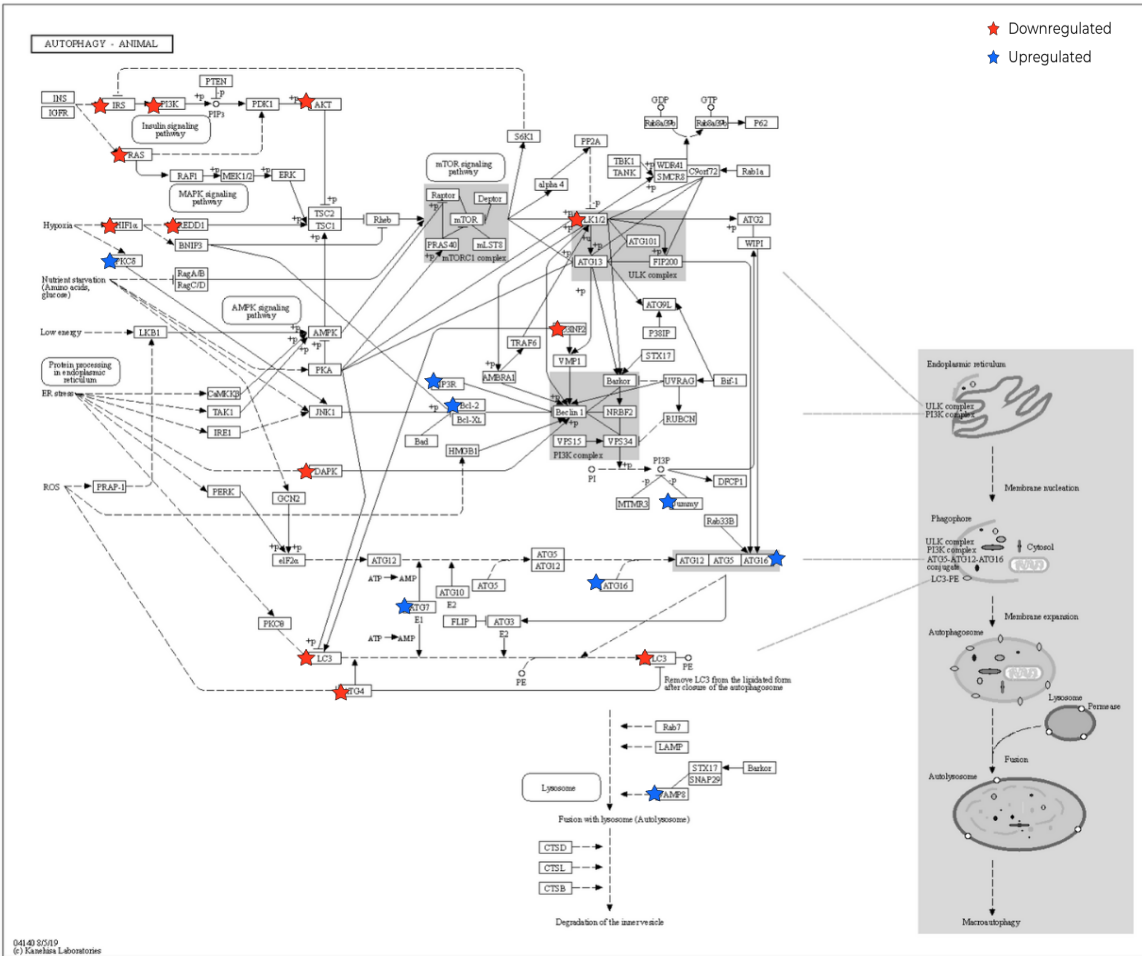
Supplementary Figure S3.9. KEGG 'Small Cell Lung Cancer' pathway obtained through DAVID analysis of Tpz-1 downregulated genes. Red stars indicate the genes affected by Tpz-1 ($p = 5e-05$).



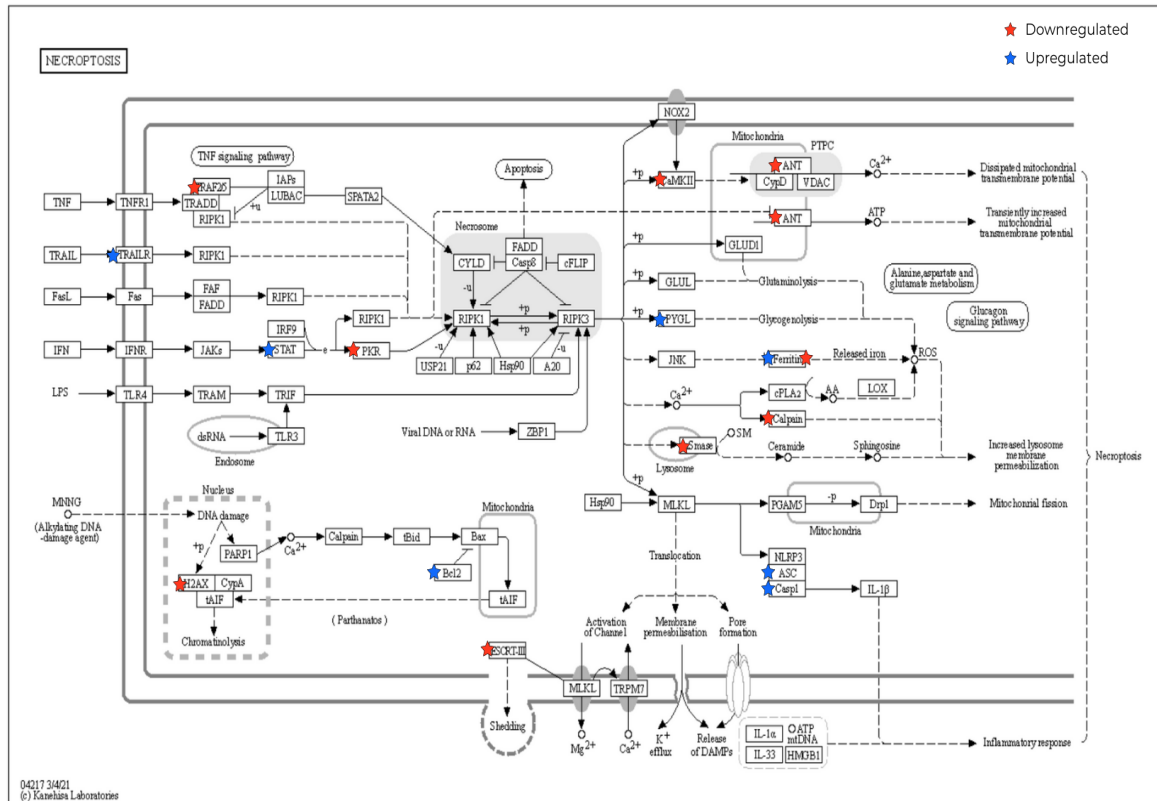
List genes are shown in red



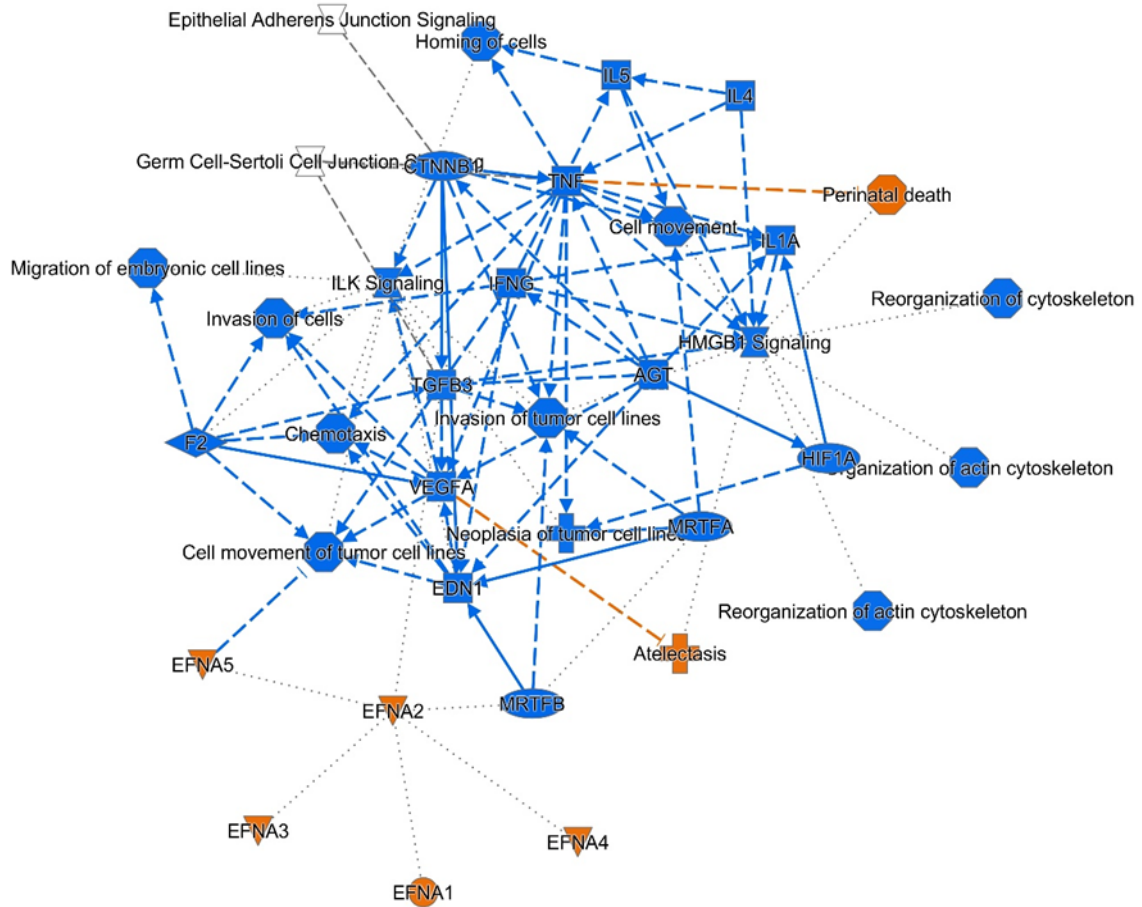
Supplementary Figure S3.12. KEGG ‘Apoptosis’ pathway. Red stars were overlaid to indicate the genes significantly downregulated by Tpz-1, and blue stars to indicate genes that were upregulated ($p = 5e-05$).



Supplementary Figure S3.13. KEGG 'Autophagy' pathway. Red stars were overlaid to indicate the genes significantly downregulated by Tpz-1, and blue stars to indicate genes that were upregulated ($p = 5e-05$).

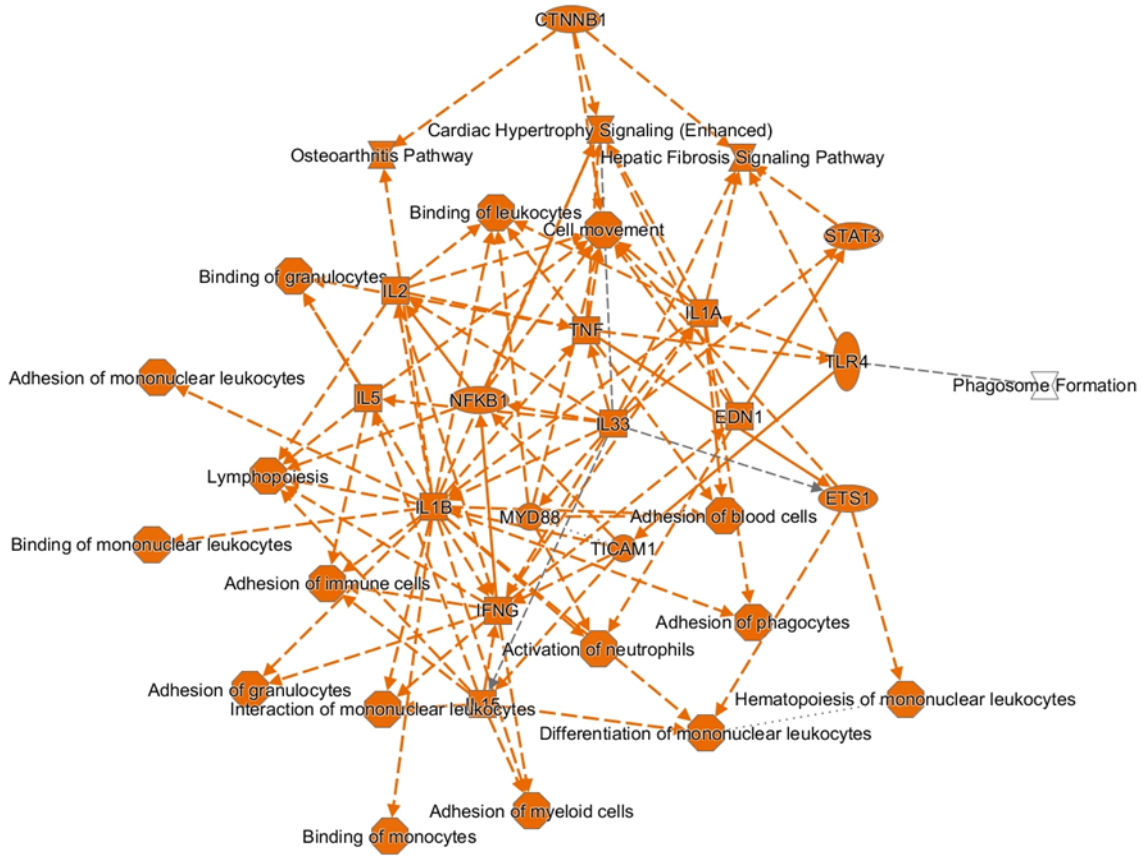


Supplementary Figure S3.14. KEGG 'Necroptosis' pathway. Red stars were overlaid to indicate the genes significantly downregulated by Tpz-1, and blue stars to indicate genes that were upregulated ($p = 5e-05$).



© 2000-2021 QIAGEN. All rights reserved.

Supplementary Figure S3.15. Graphical summary of IPA for top 100 genes downregulated by Tpz-1.



© 2000-2021 QIAGEN. All rights reserved.

Supplementary Figure S3.16. Graphical summary of IPA for top 100 genes upregulated by Tpz-1.

CURRICULUM VITA

Jessica Dyanne Hess received her Bachelor of Science degree in Chemistry from Virginia Commonwealth University in 2015. In 2017, she joined the Department of Biological Sciences at the University of Texas at El Paso as a master's student and transferred into the doctoral program in 2018. Under the guidance and supervision of Dr. Renato J. Aguilera, she has co-authored nine scholarly articles, two as first author, and is co-inventor on two provisional patents (pending) focused on anticancer small molecule formulations.

During her Ph.D., Ms. Hess enriched her training with a Certificate in Technical and Professional Writing and helped to foster the next generation of scientists through her role as a mentor and teaching assistant of general and organismal biology, immunology, and microbiology courses. Furthermore, she solely founded Cell Kulture Co. LLC in 2019 to creatively encourage public interest in science through her art.

Ms. Hess has achieved international recognition for her science and entrepreneurship. She has presented her research for the Thermo Fisher Scientific 'Gibco Cell Culture Hero' webinar series (2019), at an American Society of Cell Biology meeting poster session (2020), and was recipient of the nomination-based Thelma E. Morris Graduate Scholarship in Pathobiology (2020). She also won first place at The Mike Loya Center's student pitch competition (2020) and was featured in UTEP's Minero Magazine (Fall 2021). Most recently, Ms. Hess' graduate school success was celebrated with the Academic and Research Excellence and Best Dissertation in Biology awards from the UTEP College of Science for winter 2022. Upon graduation, Ms. Hess will pursue a

National Cancer Institute-funded T32 postdoctoral fellowship in DNA damage response and oncogenic signaling at the City of Hope in Los Angeles, California.

Contact Information: jessicahessphd@gmail.com

This dissertation was composed and typed by Jessica D. Hess.